AN INVESTIGATION OF A SUPERSONIC FLUID AMPLIFIER

by

Richard R. Scott

Final Report Prepared Under
Contract No. DA-01-021-AMC 15570(Z)
Harold R. Henry, Ph.D.
Project Director

Submitted to the U. S. Army Missile Command
Redstone Arsenal, Alabama

February 29, 1968
Bureau of Engineering Research
University of Alabama

AN INVESTIGATION OF A SUPERSONIC FLUID AMPLIFIER

by

Richard R. Scott

Final Report Prepared Under
Contract No. DA-01-021-AMC 15570(Z)
Harold R. Henry, Ph.D.
Project Director

Submitted to the U. S. Army Missile Command
Redstone Arsenal, Alabama

February 29, 1968
Bureau of Engineering Research
University of Alabama

Department of Mechanical Systems Engineering
College of Engineering
University of Alabama
University, Alabama 35486

U. S. Army Missile Command
Redstone Arsenal, Alabama
Attention: AMSMI-RGX

Re: Contract DA-01-021-AMC-15570(Z)

Gentlemen:

Enclosed are eight (8) copies of the final report under the subject contract entitled "An Investigation of a Supersonic Fluid Amplifier". This report has been submitted as a Doctoral Dissertation at the University of Alabama by Mr. Richard R. Scott.

An edited copy of the high speed films of the experiments was delivered to the Contract Supervisor in December, 1967 and is considered part of the final report.

If there are any questions concerning this report we will be glad to answer them.

Very truly yours,

Harold R. Henry

Harold R. Henry
Professor of Engineering Mechanics
and Project Director

Report Distribution:

(8) Contract Technical Supervisor
U. S. Army Missile Command
Redstone Arsenal, Alabama
Attention AMSMI-RGX

(1) Redstone Scientific Information
Center, Redstone Arsenal, Alabama
Attention AMSMI-RBL

(20) Defense Supply Agency, Headquarters
Defense Documentation Center for Scientific
and Technical Information,
Cameron Station
Alexandria, Virginia 22314

(1) U. S. Army Missile
Command
Procurement &
Production
Directorate
Attention AMSMI-IWC
(Mr. S.M. Bennett)

(1) Mr. G.W. Croker

(1) Mr. L.A. Woodman

An Investigation of a Supersonic Fluid Amplifier

by

Richard Royce Scott

ABSTRACT

Results of an analytical and experimental investigation of a supersonic fluid amplifier are presented. A power fluid was accelerated in a conical, convergent-divergent expansion nozzle with a 14^{o} half angle of divergence. The nozzle discharged into a two dimensional flow passage. Glass plates were used as two walls so that a schlieren light system could be used to observe the flow. High speed schlieren photographs (5000 frames/sec) were taken of the switching phenomena for power fluid supply pressures of 1200, 1000, 800, 600 and 250 psig.

For certain supply pressures the power flow can be switched from one to the other of two exit channels. Direction of the power flow is determined by a control jet issuing from one of the two control ports. The control ports were located opposite each other at the exit of the expansion nozzle and their geometrical axes were perpendicular to the axis of the nozzle.

An analysis is presented by which the bistable state of a supersonic amplifier can be described. One dimensional assumptions are made in order to determine the fluid properties before the fluid separates from the nozzle boundary. The area ratio and Mach Number

at separation are predicted by assuming that the particles moving along a characteristic streamline in the boundary layer flow into a stagnation region. The location of the stagnation region and the strength of the oblique shock initiated at that boundary determine whether the separated free stream boundary at that surface is deflected into the opposite exit channel or flows out the adjacent exit channel. The location of the stagnation region is predicted in terms of the specific heat ratio and the chamber to discharge pressure ratio. Results from both theoretical equations and experimental data are presented in graphical form.

An analysis is presented and an equation is derived to predict switching times. The analysis is based on a control volume located at the control port region. Experimental switching times determined from high speed schlieren film are tabulated for nitrogen and hydrazine at chamber pressures of 1200 and 1000 psig.

AN INVESTIGATION OF A SUPERSONIC FLUID AMPLIFIER

by

RICHARD ROYCE SCOTT

A DISSERTATION

Submitted in partial fulfillment of the requirements
for the degree of Doctor of Philosophy with
Major in Engineering Mechanics in the
Graduate School of the
University of Alabama

UNIVERSITY, ALABAMA

1968

ACKNOWLEDGEMENTS

The author wishes to express his appreciation to Dr. H. R. Henry for his direction of this work, and to Dr. S. C. Gambrell, Jr., Dr. D. C. Raney and Dr. J. L. Hill for their suggestions relative to preparation of the manuscript.

The author is indebted to the U. S. Army Missile Command for financial support of the project on which his dissertation was written, and to the University of Alabama for providing the computer facilities employed in preparing this dissertation.

Appreciation is also expressed to the students, Steve Richards, Jon Tromblee, Mickey Gamble and Ray Schofield, for their efforts on data reduction, programming and various other tasks necessary for the completion of this thesis.

TABLE OF CONTENTS

LIST OF FIGURES

LIST OF TABLES

LIST OF SYMBOLS

A	area
a	velocity of sound in an ideal fluid
B	lower model flow boundary
c	velocity of light in a vacuum
E_s	electric potential
F	force
f	region where the flow velocities are assumed zero or very slow
H	splitter tip position
h	enthalpy
I	an integral
j	position immediately preceeding shock in boundary layer
i_b	current in a wire
K	ratio of specific heats
ℓ	(see Figure II-7 for definition)
M	Mach number
n	index of refraction
$\vec{n}$	a unit vector
P	pressure
R	region of control volume
R_g	gas constant
S	surface of control volume
s	position immediately past shock initiation, in boundary layer

T	absolute temperature (^{o}R)
t	time
t_1, t_2	beginning and end of switching time, respectively
Δt	time to switch
U	upper model flow boundary
U_i	characteristic velocity
V	fluid velocity
V_n	velocity normal to control surfaces
V_{n_1}, V_{n_2}	components of velocity normal to a shock
$V_{t_1}, V_{t_2}, V_{t_3}$	components of velocity tangent to a shock
ω	flow rate
x, y, z	coordinate axis or coordinate distances
α	nozzle half angle
β	angle between the free stream boundary and the model boundary
γ	angle of control flow injection
$\Delta\theta_x, \Delta\theta_y$	(see Figure A-2 for definition)
δ	(see Figure II-7 for definition)
η	(see Figure II-7 for definition)
θ	angle between model center line and a typical fluid velocity
μ	(see Figure II-7 for definition)
ν	(see Figure II-7 for definition)
ξ	U_1^* / U_i

ρ	unit density of the fluid
σ	(see Figure II-7 for definition)
σ_1, σ_2	(see Figure A-1 for definition)
$\tau_2 - \tau_1$	time required for the pressure signal to reach its final value
φ	angle between shock and the model boundary
φ_1	maximum angle between shock and the model boundary

Subscripts

a	ambient properties
c	control port
en	entrance to exit channels
ex	outlet of exit channel
in	into region or surface
n	nozzle exit
o	chamber properties
out	coming from region or surface
t	nozzle throat
v	vent area of model

Superscripts

*	quantities in the boundary layer

I. Introduction

A. Analogy Between Electronic and Fluid Amplifiers

Fluid amplification has advanced rapidly to its present state since its conception in the late nineteen fifties. Some of the first contributions to the art and science were published in the proceedings of a symposium held in 1960 (15). Amplification is a process by which a fluid signal, either pressure or flow-rate, is used to control or direct a fluid stream whose pressure source or flowrate is usually greater than that of the signal. The process is similar to that occurring in an

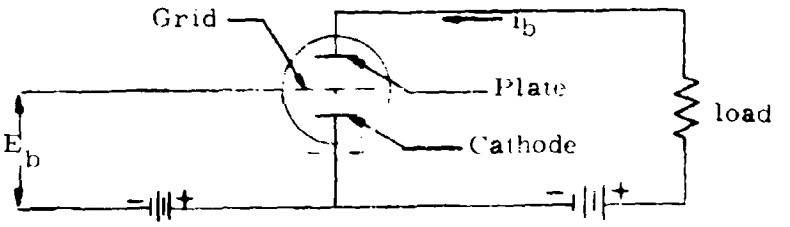

(a) Triode Vacuum Tube

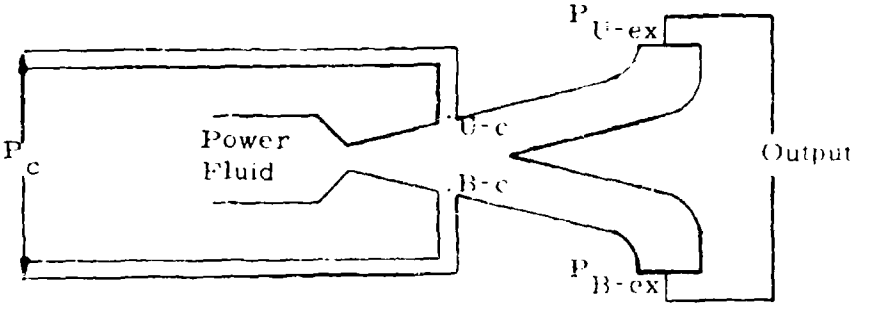

(b) Supersonic Fluid Amplifier

Figure I-1. Diagrams of Electrical and Fluid Amplifiers

electronic tube. Schematics of each process are shown in Figure I-1. In Fig. I-1(a) the cathode is heated and emits a flow of electrons to the plate. This current can be considered analogous to the power flow of the fluid amplifier. The electron flow from cathode to plate creates an electrical field. The insertion of the grid provides a means for changing the electrical field in the tube. When a voltage signal, E_s, is impressed on the grid circuit, then a small change in E_s will effect a large change in the cathode to plate voltage, such that the output voltage is an amplification of E_s.

Similarly in Fig. I-1(b) the power fluid of the fluid amplifier creates a pressure and momentum field between U-c and B-c. The control signal P_c can change the field and thus deflect the power jet, producing an amplification of the control signal.

The vacuum tube can be designed to amplify the voltage, current or power. Similarly the fluid amplifier can be designed to deliver either a pressure, flow or power amplification. Gain is defined as the ratio of output to input. Amplification is defined as the derivative of output with respect to input.

B. Discussion of Literature

Early work in the field of fluid amplification was in the area of subsonic amplification (29) and (30). As interest in the field grew, theories for different aspects of subsonic amplification were developed. Some of the applications include flow control valves with no moving

parts, logic circuits, proportional amplification, and guidance control (30) and (31).

One of the application areas in which intense interest has developed is that of missile guidance control systems (8). Of necessity, these are required to be reliable, small and powerful. The feature of no moving solid parts in fluid amplification systems contributes to their overall reliability. If in addition they can be made small and simultaneously powerful enough to perform the tasks desired, they can compete favorably with other means of guidance control. A system which employs a high pressure gas as the power source for the last or power amplifier could deliver the required control forces and yet be kept small. With these objectives the Army Missile Command has developed a control system which utilizes a supersonic power amplifier (8).

In addition to Dunaway (8) of the U. S. Army Missile Command, Holmes and Foxwell (13) have done important experimental work in determining the variables which affect supersonic fluid amplification. A paper by Shih (25) reports the results of a theoretical study of a two-dimensional supersonic fluid amplifier. Employing the method of characteristics Shih describes the pressures, velocities and free stream boundaries for various supply and control pressures when the power fluid is directed out a particular exit channel. This work and the experimental work mentioned above contribute to the understanding of the mechanics involved in the operation of the supersonic amplifier.

J. Yalamanchili has done both experimental (33) and analytical (32) work on a supersonic amplifier. The configuration investigated was analyzed from a free jet standpoint. Thus the model configuration and analysis are different than those presented here.

When one searches for references in supersonic amplification, papers on thrust vector control using secondary injection are certain to appear. This happens because there is considerable similarity between the two flow phenomena where the secondary jet is analogous to the control fluid signal. They both are used to deflect a larger stream and thus achieve a large response in relation to the signal used. An analysis of the interaction of injected fluid with the supersonic stream is presented in a paper by J. E. Broadwell (5) in which analytical results are compared with experimental results. Although thrust vector control by secondary injection and supersonic amplification may at first appear almost identical, they have two major differences. The first difference is that the power flow in the supersonic amplifier is usually overexpanded at the position where the control signal is applied. This overexpansion leads to separation in the nozzle. In thrust vector control, the power flow in the nozzle is intended primarily as the thrust of a rocket or missile. Since it is inefficient to either overexpand or underexpand the flow in the power nozzle, the flow is not overexpanded at the position of injection (26). The second major difference is that after the flow in a supersonic amplifier has been initially directed into an exit channel, rigid

boundaries continue to change the flow's direction. In the thrust vector control mechanism there are no boundaries which continually change the flow direction.

Since in supersonic amplification the flow is directed out one exit, separation from the opposite wall must be experienced. Flow separation can be divided into classes according to the manner in which it is caused. The three types of separation are spontaneous, semi-spontaneous and induced separations. Illustrations of each are given in Figure I-2.

Spontaneous shock-separation is defined as the type in which the shock, and flow downstream of the shock, are caused because of a downstream adverse pressure gradient imposed on the flow. An illustration of this type is the flow in an overexpanded nozzle shown in Figure I-2(a). A semi-spontaneous shock-separation (Figure I-2b) is caused by some obstacle in the flow, but the separation shock can still assume a free position and inclination angle. In both the spontaneous and semi-spontaneous cases, the separation shock is initiated at the boundary from which the flow separates. An induced shock-separation (Figure I-2c) is caused by an external shock impinging on a boundary layer and causing it to separate.

Three important papers of a theoretical nature which attempt to explain shock-separated boundary layers and thus separated flows are those by G. E. Gadd (12), M. Arens and E. Spiegler (2), and A. Mager (21). Gadd assumes that to separate a supersonic turbulent boundary

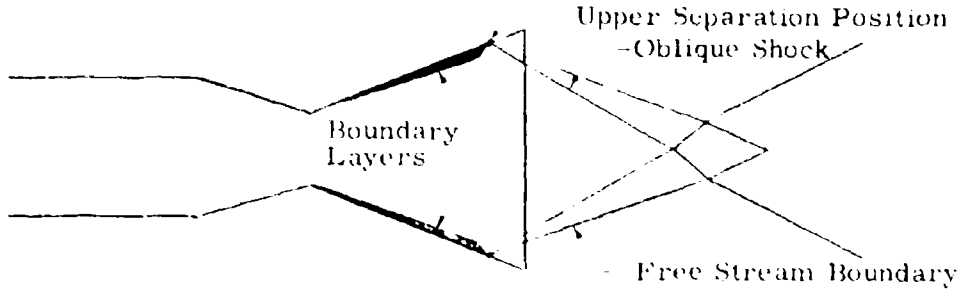

(a) Spontaneous Shock-Separation in an Overexpanded Nozzle

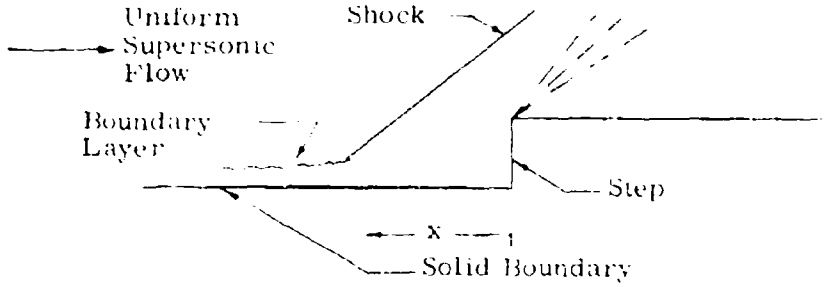

(b) Semi-Spontaneous Shock-Separation Due to Forward Facing Step

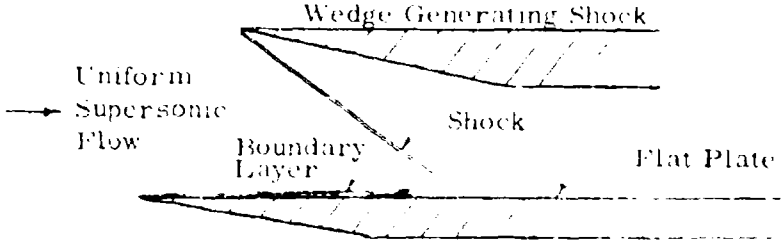

(c) Induced Shock-Separation Due to Shock Created Outside the Boundary Layer

Figure 1-2. Illustrations of Different Type Boundary Layer Separations.

layer where there is a shock-boundary layer interaction, a shock pressure ratio sufficient to stagnate a characteristic velocity U^* in the boundary layer is necessary. The shock Gadd is concerned with is one which is initiated outside the boundary layer (i.e., induced shock separation, see Figure 1-2(c)) and intersects the boundary layer some distance downstream of its generation. M. Arens and E. Spiegler use this idea in a theoretical development in which the shock is initiated in the vicinity of the boundary layer separation (spontaneous and semi-spontaneous). Experimental data published by various authors (3), (9) and (22) correlate well with the equations they derive. A. Mager describes a free or spontaneous separation by considering semi-empirical transformations between incompressible turbulent boundary layers and compressible turbulent boundary layers for the plane case. This theory compares well with McKenny's (22) two dimensional separation data in an over-expanded supersonic flow.

Arens and Spiegler show through plots of their derived equations and experimentally obtained data that their equations will predict separations for all the general cases shown in Figure 1-2. This appears reasonable since there is actually little difference among the three cases when the mechanics of flow in the boundary layer is used as a basis for comparison.

Other authors predict separation based on experimental observations. Defining P_1/P_a as the ratio of separation to atmospheric pressure, Frazer, Eisenklam and Wilkie (10) conclude that when a

jet discharges to an atmosphere of 14.7 psia the jet separates when $P_i/P_a = 0.36$. Summerfield (27) and McKenny (22) conclude that $0.38 \leq P_i/P_a \leq 0.41$ for chamber to ambient pressure ratios tested, and thus P_i/P_a is approximately constant. This may be true for the small range of pressure ratios ($13.4 \leq P_o/P_a \leq 22.4$) investigated. A larger range of chamber to ambient pressure ratios ($59 \leq P_o/P_a \leq 115$) indicates a definite dependence of the boundary layer separation on the free stream Mach Number (2) and (17).

C. Definitions and Description of Amplifier Characteristics

An amplifier is bistable if there are only two stable flow configurations which it will maintain. The power flow of an ideal bistable fluid amplifier can be switched from one to the other of these two stable flow configurations, which are, for the present study, from total flow out one exit to total flow out the second exit. If the switching constraint is removed before the power flow is fully switched, the power stream of the ideal amplifier will go to one of the two stable configurations. Often an amplifier does not have ideal bistable characteristics and a third flow configuration can be determined for which part of the power fluid leaves by one exit and the rest by the second exit. The flow in this third configuration is usually less stable than either of the "bistable" configurations, when the amplifier is operated in a supply pressure range for which flow out one exit channel can be maintained. The degree of stability for the third flow configuration can be seen to be smaller than that for flow out one exit

from the following qualitative reasoning. It is less difficult to stop a partial flow from one exit and thus force all the power fluid into a stable flow out the second exit than it is to stop the total power flow configuration. Thus an amplifier could be defined as bistable even though a third flow configuration can be determined, if this third configuration is less stable than the two "stable flow" configurations. Therefore the flow configuration which exists when the power fluid continues to flow out an exit, after all restrictions used to force the power fluid out that exit are removed, will be called a bistable flow configuration. The conditions necessary to maintain this stable state in the supersonic amplifier will be presented in Section II.

In addition to a study of conditions necessary to maintain the bistable state, the switching of the power fluid from one stable position to the other is also studied and results are presented herein. The switching time is defined as the time required to move the power stream from a stable position on one side of the amplifier to a stable position on the other side. The switching time is only part of the response time, which is defined as the time lapse necessary to observe full effects of the power stream at the output position after the control signal is applied. After the power stream is switched the fluid must flow to the output position. The time lapse between switching and arrival of power fluid at the output position is the transport time of the power stream. Schematically these times are shown in Figure I-3 and are essentially the same as in reference (18). As

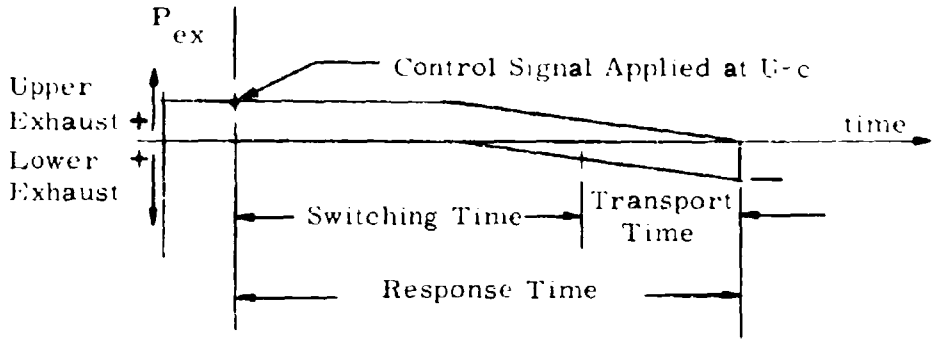

Figure I-3. Schematic of Amplifier Response Time

can be seen in Figure I-3, there is some time after the control signal is applied before there is a decrease in the output felt at U - ex and a response is felt at B - ex. Also it is seen that the switching time termination cannot be definitely identified on this diagram. This is because the portion of fluid from the power stream left in the upper channel after the power stream is switched is still felt at U - ex until it has flowed to the exit. This same time is necessary for the fully switched stream to be felt at B - ex.

Although the Army Missile Command had developed a supersonic fluid amplifier that operated, there were many questions connected with its operation still unanswered. Examples of these questions are: (1) why does the amplifier switch only in certain chamber pressure regions, (2) what are the effects of using a high temperature power fluid and (3) what are the effects of varying the magnitude and/or frequency of the control signal. In order to formulate a flow model from

which answers to questions of this type could be obtained, an experimental investigation of the switching phenomena was performed at the University of Alabama and Redstone Arsenal. Insight gained from the experimental results helped guide the development of a theoretical flow model. The purpose of this thesis is to present the experimental results, the theoretical flow model formulated to explain the experimental data, and describe the mechanics involved in supersonic fluid amplification. An understanding of the mechanics can be applied to other flow situations and in general used to improve amplifier design.

Figure II-1 (page 21) shows the flow model which was used for the experimental work. Details of the flow geometry are given in Section III. This configuration was chosen because the U. S. Army Missile Command's Inertial Guidance and Control Laboratories had a control system in which there was a similar amplifier and on which considerable preliminary experimental work had already been conducted. It was desired to establish a better basic understanding of this amplifier. Also it was known that this configuration performed reasonably well for certain ranges of supply pressures and control pressures.

D. Discussion of Basic Equations

Sonic flow is attained when the speed of a flowing fluid is of a magnitude such that a disturbance generated at a point in the stream cannot be propagated upstream of the point of disturbance. If the fluid reaches any higher speed, then the speed is referred to as supersonic. By applying the momentum and continuity equations to a plane

stationary disturbance in a flowing fluid, the speed which the fluid must attain to keep the disturbance from propagating upstream is

$$a = \sqrt{(\partial P/\partial \rho)} \quad . \qquad I\text{-}1$$

For a perfect gas ($P/\rho = R_g T$) and an isentropic process ($P/\rho^k =$ constant), I-1 becomes

$$a = \sqrt{K R_g T} = \sqrt{KP/\rho} \quad . \qquad I\text{-}2$$

The Mach number is the ratio of speed of flow to local speed of sound.

$$M = V/a$$

Thus M = 1 indicates sonic velocity.

The converging - diverging nozzle is used to accelerate compressible fluids to supersonic velocities. The supersonic flow will be reduced to subsonic flow if the high speed fluid passes through a normal shock. A shock in supersonic flow is a discontinuity, across which the stream properties (p, T, ρ, V) change. The "discontinuity" actually has a thickness on the order of 10^{-5} inches (24). The equations which govern the change in stream properties across a normal shock are well known and are developed in most gas dynamics texts (see for instance (20) and (24)). Figure I-4 shows two dimensional flow in a duct and an ideal normal shock. The equations which govern the changes in properties are listed for later reference. They are derived using the equations of continuity, momentum and energy,

for an ideal gas and steady flow.

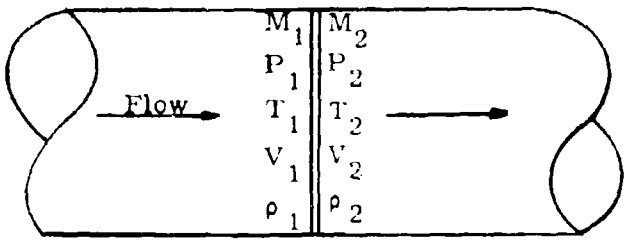

$M_1 > M_2$, $P_2 > P_1$

$T_2 > T_1$, $V_1 > V_2$

$\rho_2 > \rho_1$

Figure I-4. Normal Shock and Stream Property Changes Across the Shock

$$\rho_1 V_1 = \rho_2 V_2 \qquad \text{I-4}$$

$$P_2 - P_1 = \rho_1 V_1^2 - \rho_2 V_2^2 \qquad \text{I-5}$$

$$h_1 + \frac{1}{2} V_1^2 = h_2 + \frac{1}{2} V_2^2 \qquad \text{I-6}$$

From equation I-6 above, if one substitutes the definition of enthalpy and Mach Number one obtains:

$$M_2^2 = \frac{1 + \frac{K-1}{2} M_1^2}{K M_1^2 - \frac{K-1}{2}} \quad . \qquad \text{I-7}$$

The following equations are derived for an ideal gas from I-4, I-5 and I-6.

$$\frac{P_2 - P_1}{P_1} = \frac{2K}{K+1} (M_1^2 - 1) \qquad \text{I-8}$$

$$\frac{\rho_2}{\rho_1} = \frac{(K+1) M_1^2}{(K-1) M_1^2 + 2} \qquad \text{I-9}$$

$$\frac{T_2}{T_1} = 1 + \frac{2(K-1)(KM_1^2 + 1)}{(K+1)^2 M_1^2} (M_1^2 - 1) \qquad I-10$$

Equations I-7 through I-10 are the equations relating the properties of a stream across a normal shock.

The oblique shock occurs in supersonic fluid amplification as the stream is bent so that it is directed out one or the other of the amplifier output channels. Consider Figure I-5 which shows a supersonic stream flowing through an oblique shock. Figure I-5(a) shows a fluid

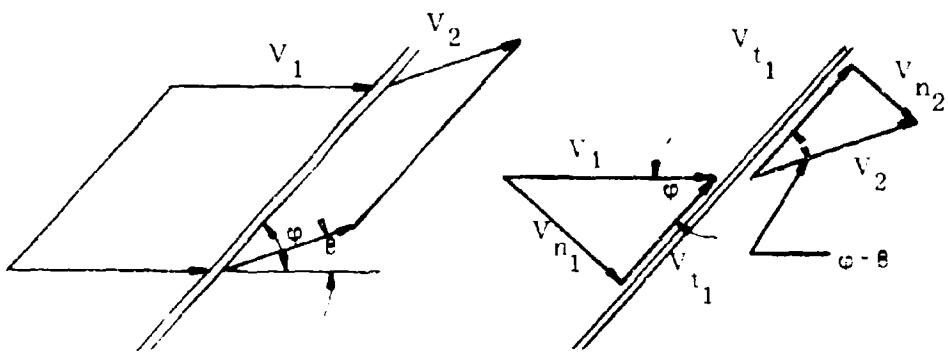

Figure I-5. Oblique Shock and Its Effect on a Streamline

stream of uniform velocity approaching an oblique shock wave inclined at an angle φ to the direction of flow. Across the oblique shock one streamline is shown inclined at an angle θ to the initial flow direction. Since the flow is uniform an analysis of what happens to one streamline will represent what happens to all the flow across the shock.

In Figure I-5(b) the velocity is divided into normal and tangential components on both sides of the shock wave. By using the continuity

and momentum equations parallel to the shock the following is obtained:

$$\rho_1 V_{n_1} = \rho_2 V_{n_2}$$

and

$$(\rho_1 V_{n_1}) V_{t_1} = (\rho_2 V_{n_2}) V_{t_2}$$

from which it is apparent that $V_{t_1} = V_{t_2} = V_t$.

When the continuity and momentum equations are applied across the shock in a normal direction, relations are obtained which are analogous to the normal shock relations. In the normal shock case we have $V_1/a_1 = M_1$, where V_1 is the normal component of flow. In the oblique shock, the initial normal component is $V_{n_1} = V_1 \sin \varphi$. The initial Mach Number now is $M_1 = V_1/a_1$ where $V_1 = V_{n_1}/\sin \varphi$. Thus

$$\frac{V_{n_1}}{a_1} = M_1 \sin \varphi .$$

To obtain the oblique shock relations M_1 is replaced by $M_1 \sin \varphi$ in equations I-7, I-8, I-9 and I-10. Similarly it can be shown that $\frac{V_{n_2}}{a_2} = M_2 \sin (\varphi - \beta)$. Thus, the equations relating properties across an oblique shock are:

$$M_2^2 \sin^2 (\varphi - \beta) = \frac{1 + \frac{K-1}{2} M_1^2 \sin^2 \varphi}{K M_1^2 \sin^2 \varphi - \frac{K-1}{2}} \qquad \text{I-11}$$

$$\frac{P_2 - P_1}{P_1} = \frac{2K}{K+1}\left(M_1^2 \sin^2 \varphi - 1\right) \qquad \text{I-12}$$

$$\frac{\rho_2}{\rho_1} = \frac{(K+1)\, M_1^2 \sin^2 \varphi}{(K-1)\, M_1^2 \sin^2 \varphi + 2} \qquad \text{I-13}$$

$$\frac{T_2}{T_1} = 1 + \frac{2(K-1)(KM_1^2 \sin^2 \varphi + 1)}{(K+1)^2 M_1^2 \sin^2 \varphi}\left(M_1^2 \sin^2 \varphi - 1\right). \qquad \text{I-14}$$

Consider now Figure I-5(b). From geometry $\tan \varphi = \frac{V_{n_1}}{V_t}$ and $\tan(\varphi - \beta) = V_{n_2}/V_t$. Using the continuity equation and eliminating V_t gives

$$\frac{\tan(\varphi - \beta)}{\tan \varphi} = \frac{V_{n_2}}{V_{n_1}} = \frac{\rho_1}{\rho_2} .$$

Using equation I-13, this becomes

$$\frac{\tan(\varphi - \beta)}{\tan \varphi} = \frac{(K-1)\, M_1^2 \sin^2 \varphi + 2}{(K+1)\, M_1^2 \sin^2 \varphi} .$$

Solving for $\tan \beta$, we obtain

$$\tan \beta = 2 \cot \varphi \frac{M_1^2 \sin^2 \varphi - 1}{M_1^2 (K + \cos 2\varphi) + 2} . \qquad \text{I-15}$$

The equations from I-11 to I-15 describe the properties of flow across an oblique shock which will be useful in describing the mechanics of

bistable flow and the switching of the stream from one exit channel to the other.

II. Development of Equations Describing Bistability and the Switching Phenomena

A. Regimes of Flow

The various regimes of flow which exist in a converging-diverging nozzle are determined primarily by the nozzle chamber pressure, the pressure of the ambient to which the nozzle exhausts, the nozzle geometry and the boundary layer. These regimes will be defined for an axisymmetric conical nozzle.

The flow regimes of importance for the nozzle geometry considered herein will be defined in terms of the pressure ratio (P_o/P_a). If $(P_o/P_a) = 1$ no flow occurs. If $(P_o/P_a)_1$ is defined as the maximum pressure ratio which cannot be exceeded if subsonic flow is to exist everywhere in the nozzle then $1 < (P_o/P_a) < (P_o/P_a)_1$ is the subsonic pressure ratio range. For $(P_o/P_a) = (P_o/P_a)_1$ the fluid velocity is sonic at the nozzle throat but subsonic from the throat to the exit. For $(P_o/P_a) \leq (P_o/P_a)_1$ there will be no shocks within the nozzle flow. Thus all flow in the nozzle can be considered one dimensional and isentropic when the boundary layer is neglected.

$(P_o/P_a)_2$ will be defined as the maximum pressure ratio for which normal shocks occur in the nozzle. Thus $(P_o/P_a)_1 \leq (P_o/P_a) \leq (P_o/P_a)_2$ is the flow regime for which normal shocks occur in the

flow. The supersonic velocity downstream of the nozzle throat is reduced to subsonic velocity by the normal shock at some position before the nozzle exit and the fluid then flows to the exit with subsonic velocity. When $(P_o/P_a) = (P_o/P_a)_2$ the normal shock reaches its farthest position, X_2, downstream of the throat. When $(P_o/P_a)_3$ is the pressure ratio for which oblique shocks exist at the nozzle exit then $(P_o/P_a)_2 < (P_o/P_a) \leq (P_o/P_a)_3$ is the regime for which oblique shocks exist within the nozzle. When the pressure ratio $(P_o/P_a)_4$ is reached the pressure within the flowing fluid at the nozzle exit (P_{ex}) is equal to the ambient pressure (P_a) to which the fluid flows. At this pressure all shocks vanish at the nozzle exit. Thus $(P_o/P_a)_3 \leq (P_o/P_a) < (P_o/P_a)_4$ is the regime for which oblique shocks exist at the nozzle exit. If (P_o/P_a) exceeds $(P_o/P_a)_4$ then $P_{ex} > P_a$ and the flow is called underexpanded.

The flow regime of interest in this investigation is that for which oblique shocks exist in the flow. The formation of these oblique shocks is associated with the nozzle boundary layer. This association is demonstrated with schlieren photographs by Shapiro (22) who shows that oblique shocks are replaced by a normal shock when the boundary layer is removed by suction.

Some characteristics and consequences of the oblique shock regime follow. The flow can no longer be approximated by one dimensional equations since the oblique shocks are two dimensional. The oblique shocks recompress the fluid, reduce the speed, and redirect

the fluid particles. The redirection causes the flow to separate from the nozzle boundary and is one of the mechanisms of interest in this investigation.

B. Discussion of Phenomena in the Oblique Shock Regime and Considerations of Conditions Necessary for Stable Flow

Two phenomena exhibited by the supersonic amplifier are of primary importance:

(1) the bistable flow for certain chamber pressure ranges, and

(2) the switching of the power flow from one exit to the other.

Bistability will be discussed first and a theory described by which it can be explained. This theory applies to other amplifiers with flow passages similar to those shown in Figure II-1. It was developed by observing the shock angles and free stream boundaries in high speed schlieren film, analyzing the numerical values of pressure at solid boundaries in the vicinity of the shocks, and utilizing knowledge of flow separation phenomena described in the literature.

Consider Figure II-2 in which φ_B is defined as the angle included between the bottom separation shock and the model boundary, and δ_B is the angle between the bottom free stream jet boundary and the model wall. φ_U and δ_B are similarly defined for the upper model boundary.

In Figure II-2 all the power fluid is leaving the model from the upper exit because the bottom shock, which begins at point 1_B, turns the flow which would otherwise go out the lower exit. When the

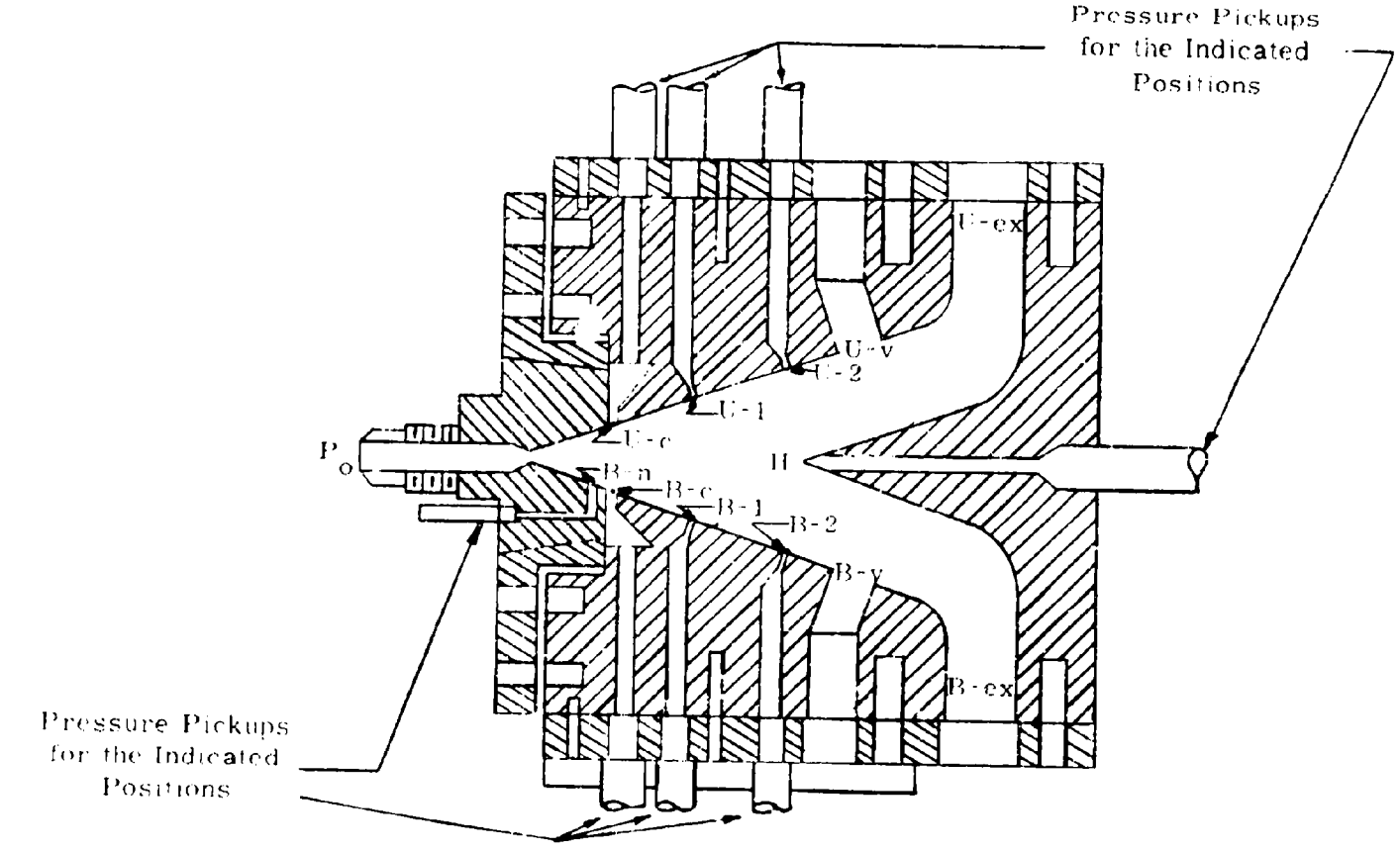

Figure II-1. Schematic of Test Amplifier Showing Pressure Tap Locations

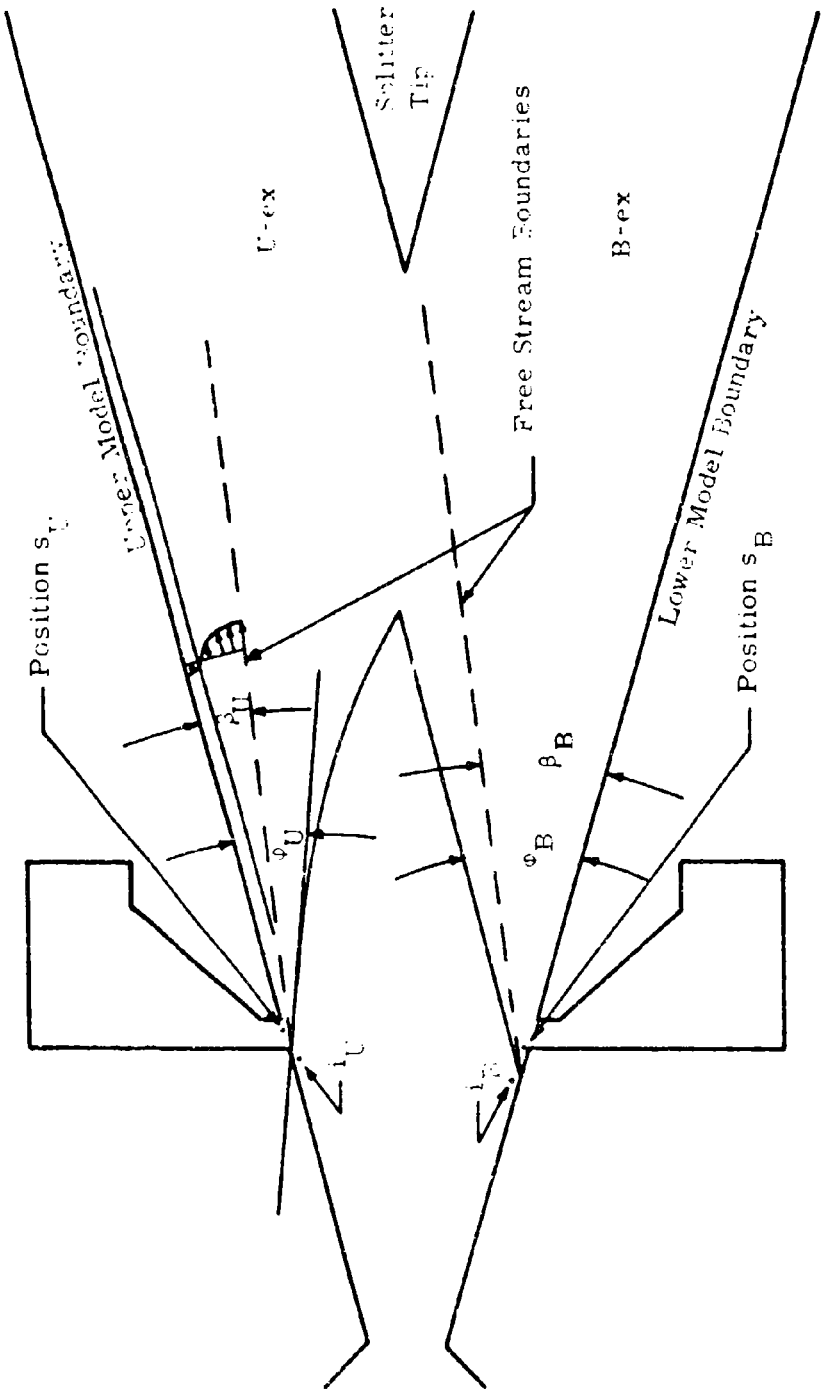

Figure II-2. Flow Model in the Flow Deflection Region

amplifier is operating in the bistable regime this condition will continue to exist after any control flow or restriction which forced the power flow out the upper channel is removed. The turning shocks beginning at positions i_U and i_B are stable because of the pressures maintained by s_U and s_B respectively. In the flow situation shown in Figure II-2 the pressure at s_B will be only slightly lower than the ambient into which the amplifier is exhausting. This is because the amplifier output legs discharge to the atmosphere and the entrainment occurring in the inactive leg causes only a small drop below ambient pressure.

The pressure at s_U will be lower than the pressure at s_B. This lower pressure exists because the power stream at position i_U has expanded farther than at i_B and the shock at the upper boundary is weaker than that at the lower. When the power stream almost fills the exit channel and the stream remains supersonic past the splitter tip then the outer wall region between s_U and U-ex, through which flow from the outside atmosphere can occur toward position s_U, is very small. Experimentally by graphite entrainment, flow toward position s_U has been observed in this region. This flow will increase the pressure maintained at position s_U and is detrimental to the bistable condition. The low pressure region at s_U can also be destroyed by flow from s_B around the power stream. When enough flow is present to raise the pressure at s_U to approximately the same pressure as at s_B the bistable condition will cease to exist. Thus

when the power stream fills the exit channel sufficiently to prevent flow from the ambient and from s_B around the power jet to point s_U, then a lower pressure is maintained at s_U than at s_B. The absolute values of these pressures determine where the respective shocks intersect the model boundary and the angle of the shocks which give the power fluid its direction as it leaves the amplifier nozzle.

In summary a list of necessary conditions for bistability (for example, all power flow out U-ex) is:

(1) The power stream must separate from the lower model boundary and be directed upward past the splitter tip so all power flow is out U-ex.

(2) To change the direction of the lower boundary streamline as indicated in Figure II-2 requires a shock.

(3) To cause the separation at s_B and the associated shock, which intersects the boundary at i_B and redirects the flow so that it just clears the splitter, it is necessary to maintain a unique pressure value at s_B for each P_o.

(4) Lastly, to prevent the shock angle φ_U from having the same magnitude as φ_B, and thereby causing similar upper and lower shocks, a lower pressure must be maintained at s_U. If the magnitudes of φ_U and φ_B are equal then the power jet will divide equally between the exit channels of this amplifier. To maintain the low pressure which exists because of the power stream overexpansion, the power stream must fill the amplifier channel at section $s_U - s_B$ to prevent fluid at

approximately ambient pressure from flowing around the stream to s_{U}. The power stream must also fill the upper exit channel and thus restrict flow from U-ex to s_{U} to maintain the low pressure at s_{U}.

The conditions which must be satisfied in order to maintain stability have been described qualitatively above. Equations describing the pressure ratios which must be maintained to satisfy the first three conditions will now be determined. Consider Figure II-3 which is the assumed flow model in the vicinity of separation. Point 1 is the position immediately following the shock and f is in the region where the flow velocities are assumed to be zero in the x direction and very small in the y direction.

In the one dimensional computations for nozzle flow all flow up to the oblique shock is usually assumed isentropic. In reality there is always a boundary layer and this is the reason for the existence of the oblique shock. In the boundary layer the velocity of the fluid near the wall is less than the free stream velocity. For the present case where the stream is overexpanded (i.e., the exit pressure is less than atmospheric) the momentum of the fluid near the wall is small and the velocities are subsonic because of the boundary layer, it can be seen that the higher atmospheric pressure will cause an adverse pressure gradient and a reverse flow near the boundary at the exit. Thus the velocity of the forward boundary layer flow will be zero at some place upstream of the exit. The slowing of these particles causes a pressure rise which reaches a maximum at the region where

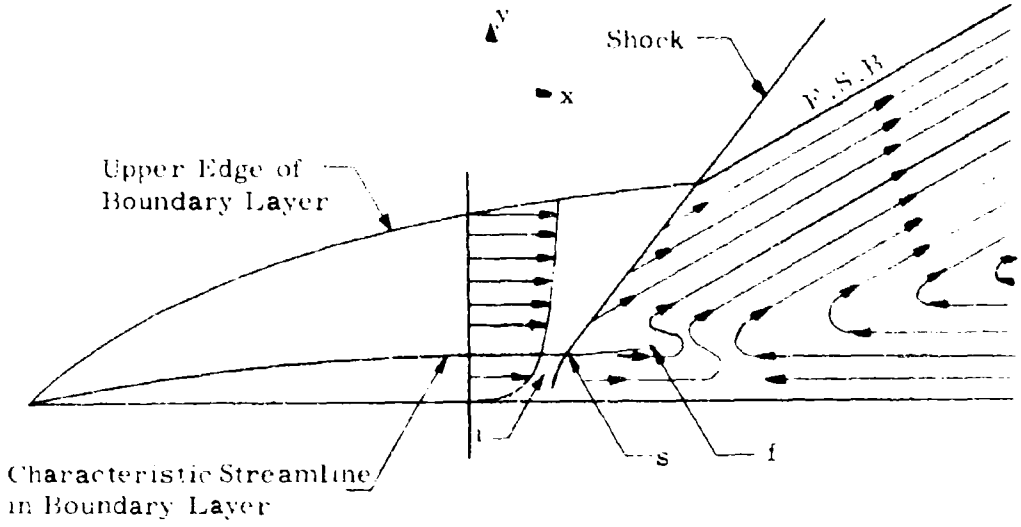

Figure II-3. Flow Separation Model

The assumptions made in developing the bistable flow equations are:

1. The particles in the vicinity of f are essentially at rest.

2. The stagnation process from region s to f occurs isentropically

3. The disturbance created in the vicinity of the region of i, s and f is propagated into the supersonic flow as an oblique shock.

4. A constant stagnation temperature is assumed in a boundary layer cross section.

the particles are essentially stagnated. This stagnated region acts as a disturbance in the flow which is propagated from the boundary layer into the supersonic stream as an oblique shock wave. Following the work of Arens and Spiegler (12), equations will be derived describing the pressure rise in the boundary layer necessary to maintain the oblique shock.

The oblique shock wave is the means by which the pressure of the stream boundary is brought up to the pressure of s. As a good approximation when the fluid reaches f the pressure can be taken as ambient pressure when the output legs discharge to the atmosphere. When a supersonic streamline crosses the shock, the direction of the fluid particles will be changed because of the properties of the oblique shock shown in Section I.

By definition of the Mach Number, the ratio between any two Mach Numbers can be expressed as

$$\frac{M_1^*}{M_1} = \frac{a_1}{a_1^*}\frac{U_1^*}{U_1} = \frac{U_1^*}{U_1}\sqrt{\frac{T_1}{T_1^*}}$$

where the superscript * indicates quantities in the boundary layer. Assuming that the stagnation temperature across the boundary layer is constant, then

$$\frac{M_1^*}{M_1} = \frac{U_1^*}{U_1}\sqrt{\frac{1 + \frac{k-1}{2} M_1^2}{1 + \frac{k-1}{2} M_1^{*2}}} \quad , \qquad \text{II-1}$$

Equation II-1 can be solved for M_1^* as follows:

$$M_i^* = \frac{\frac{U_i^*}{U_i} M_i}{1 + \frac{k-1}{2} M_i^2 \left[1 - \left(\frac{U_i^*}{U_i} \right)^2 \right]} \quad 1/2 \quad , \qquad \text{II-2}$$

Thus if the relation between U_i and U_i^* is known, then for any free stream Mach Number M_i, the Mach Number M_i^* may be found. The velocity and Mach Number on a characteristic streamline within the boundary layer are important parameters in the following theory of separation. Depending upon how this streamline is chosen it is apparent that U_i^* could have any value between the free stream velocity and zero. Gadd (11) shows that when a characteristic streamline is chosen such that $U_i^*/U_i = 0.6$ the results of the separation theory correspond well with experimental results for free stream Mach Numbers up to and in the neighborhood of $M_i = 4$. Assuming that this relation holds approximately between $M_i = 4$ and $M_i = 5$, M_i^* can be calculated from equation II-2. When the magnitude of M_i^* is calculated using these assumptions, it appears from the data taken from the present study that the characteristic streamline crosses a normal shock in going from region i to s for values of M_i between four and five. As M_i decreases there will be some value of M_i for which $M_i^* = 1$. For any $M_i^* < 1$, the particles flowing along the characteristic streamline will be assumed to be brought to the essentially stagnation pressures of region f isentropically.

Assuming that the fluid particles which have crossed the normal shock are then brought to the pressure of the stagnation region f

isentropically, one equation may be developed to describe the pressure rise between region i and f. With these assumptions then we may write the pressure ratio P_f/P_i as

$$\frac{P_f}{P_i} = \frac{P_f}{P_s}\frac{P_s}{P_i} \quad . \qquad \text{II-3}$$

From Figure II-3 we can see that P_f/P_s is the pressure rise due to the isentropic velocity reduction of the particles flowing along the characteristic streamline and P_s/P_i is the rise due to the normal shock. These ratios are

$$\frac{P_s}{P_i} = 1 + \frac{2k}{k+1}\left(M_i^{*2} - 1\right) \qquad \text{II-4}$$

and

$$\frac{P_f}{P_s} = \left[1 + \frac{k-1}{2} M_s^{*2}\right]^{\frac{k}{k-1}} \quad . \qquad \text{II-5}$$

Since it is more convenient to deal with the final equations in terms of M_1, the inviscid free stream Mach Number, equation II-2 will be used to eliminate M_i^* from equations II-4 and II-5. Equation I-7, the relation between Mach Numbers across a normal shock, will be utilized in expressing M_s^* in terms of M_1. Equations II-4 and II-5 can then be expressed in terms of M_1 and combined to give the pressure ratio P_f/P_1 as,

$$\frac{P_f}{P_1} = \frac{\left[\left(\frac{k+1}{2}\right) M_1^2 \xi\right]^{\frac{k}{k-1}}}{\left[1 + \frac{k-1}{2}(1-\xi) M_1^2\right] \left\{\frac{M_1^2}{2}\left[(k+1)\xi - \frac{(k+1)^2}{k+1}\right] - \frac{k-1}{k+1}\right\}^{\frac{1}{k-1}}} \qquad \text{II-6}$$

where $\xi = U_1^*/U_1$. Equation II-6 was derived by Arens and Spiegler (2), as was an equation for which the assumed velocity along the characteristic streamline was subsonic and thus the complete compression to P_1 was an isentropic process. Equation II-6 accounts for both normal shock compression and the subsequent compression after the particles flowing along the characteristic streamline have crossed the normal shock indicated in Figure II-3. If $M_1^* = 1$, equation II-4 reduces to $P_s/P_1 = 1$ and the ratio P_f/P_1 is achieved through an isentropic process. Thus equation II-6 predicts the approximate pressure ratio to stagnate the particles flowing along the characteristic streamline whether they cross a shock or not.

In the inviscid free stream the flow is primarily isentropic. Until the cross-section at 1 is reached, the Mach Number is given by

$$M_1^2 = \left(\frac{2}{k-1}\right)\left[\left(\frac{P_o}{P_1}\right)^{\frac{k-1}{k}} - 1\right]$$

or

$$M_1^2 = \left(\frac{2}{k-1}\right)\left[\left(\frac{P_o}{P_f}\right)^{\frac{k-1}{k}}\left(\frac{P_f}{P_1}\right)^{\frac{k-1}{k}} - 1\right]. \qquad \text{II-7}$$

With equations II-6 and II-7 it is possible to write a computer program by which values of P_f/P_1 and M_1 may be calculated for a given P_o/P_a. Results of these computations are presented in graphical form in section III.

When M_1 is known, then the area ratio A_1/A_t may be calculated for the separation position by the following equation.

$$\frac{A_1}{A_t} = \frac{1}{M_1}\left[\left(\frac{2}{k+1}\right)\left(1 + \frac{k-1}{2} M_1^2\right)\right]^{\frac{k+1}{2(k-1)}} \qquad \text{II-8}$$

Values of the oblique shock angle φ and the free stream boundary are also calculated from equations I-12 and I-15. These calculations are performed in the free stream flow where the disturbance in the boundary layer has caused the oblique shock to be propagated. The value of the oblique shock angle φ is determined by the pressure jump across the shock and the Mach Number before crossing the shock. As the pressure P_f is increased or decreased it can be seen that φ will also increase or decrease in a similar manner. It will be shown in Section III that the experimental relation between φ and the control pressure is similar to that indicated by the above equations. It is assumed that an artificial ambient in the vicinity of the control port which causes P_f is approximately equal to the control pressure. Calculated values of φ are compared to experimental values of φ whenever possible in section III.

C. Discussion of Switching Theory and Derivation of an Equation for Switching Time

Since the basic purpose of the bistable fluid amplifier is to obtain a fluid flow from one of two exits, then there must be some means of switching the power fluid from a stable flow configuration out one exit to the second exit. This switching is the second important phenomenon in bistable fluid amplification, and is accomplished by a secondary fluid flow called the control flow or control signal. The following development discusses the variables which affect the power stream's position and their relation to the time involved in switching.

Consider Figure II-4. A control volume is shown enclosed with dashed lines. The control volume is chosen such that the [illegible]nt boundary is the plane which passes through the surface connecting the downstream control port boundaries, and the o[illegible]r boundaries are the diverging walls of the expansion nozzle. Lines 1 and 1' which diverge from the model's lower and upper boundaries by φ_{lB} and φ_{uB} respectively represent the lower and upper projections of the continuous shock surface between 1 and 1'. The shock occurs all around the power jet in the manner of a "warped conical" shock. The line indicated by 5 represents the intersection of the conical shock with the nozzle. The lines indicated by 2 and 2' are the lower and upper projections of the "warped conical" free stream boundary which diverge from the lower and upper model boundaries by β_{lB} and β_{uB} respectively. The upper and lower control port entrances into the

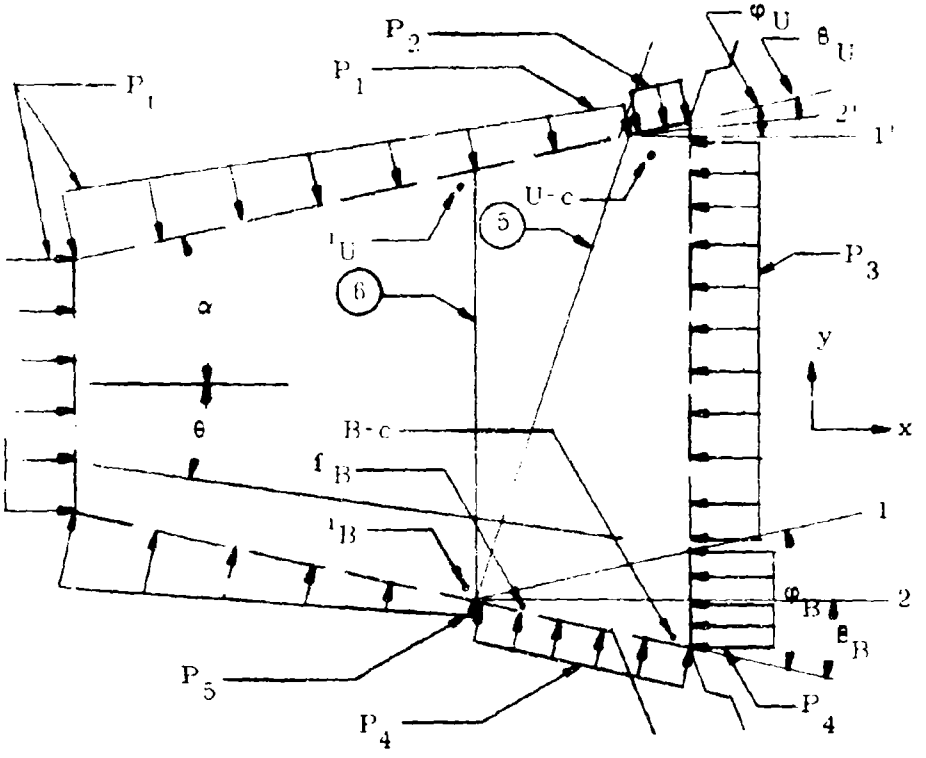

Figure II-4. The Control Volume With Pressures, Shocks and Free Stream Boundaries Indicated.

control volume are located at U-c and B-c respectively. The appropriate pressures acting on the boundaries are also shown.

This control volume was chosen because, included within it and on its boundaries are the total causes of switching and the boundary conditions can be approximated by reasonable assumptions. We will assume that the chamber pressure is high enough so that the control port cross-section downstream of the power jet separation is essentially still filled by the power jet. It is also assumed that the power

jet fills the upper exhaust channel, for the configuration shown in Figure II-4. When the power jet fills the flow channel between the control ports U-c and B-c then a low pressure region will exist in the vicinity of U-c because of the power stream overexpansion. The supersonic flow effectively isolates region U-c from high pressure sources that would raise the pressure of U-c because fluid cannot flow around the power stream to U-c and pressure waves cannot reach U-c, from or downstream of B-c, across the supersonic stream. Thus unless this steady power fluid flow situation is disturbed by a control signal flow from port U-c the low pressure at region U-c will not change. With these conditions, the assumption that the actual switching phenomenon is governed by occurrences in and on the boundary of the control volume is justified by the following argument. If the pressure ratio P_o/P_a is high enough to cause unseparated supersonic flow to the cross-section indicated by line ⑤, then schlieren photographs indicate that supersonic velocities will continue to the splitter tip H shown in Figure II-1. Then the flow conditions at the control volume exit will only be affected by changes in the oblique shocks and these are considered adequately in the control volume.

The control volume of Figure II-4 is shown for the case where the power fluid is diverted out the upper exhaust channel. The chamber pressure is a value for which the flow is stable and the conditions shown are those which apply just before the power fluid is to be diverted to the lower channel by an injection of control flow at

U-c. These conditions can be determined by using an isentropic, one dimensional analysis for the inviscid free stream flow and the bistable analysis for the boundary layer-shock interaction presented herein.

When injection is first begun at U-c the flow separates near the control port. As the control pressure P_{U-c} increases, the shock angle φ_{U-c} increases. The increase in pressure in this region causes the upper free stream boundary to be deflected toward the splitter tip. Conditions required by the steady state shock-boundary layer interaction analysis show that the point of intersection of the free stream boundary with the nozzle boundary will move toward the nozzle throat. Now if the control pressure in the U-c region is increased only to the pressure which exists between streamline 2 and the lower boundary and if the equal pressures on the top and bottom of the jet are maintained, a symmetrical flow separation will occur with resulting fluid flow from both exits. If the upper control pressure is increased slightly above this ambient pressure an asymmetrical separation will occur with resulting fluid flow from both exits. If the upper control pressure is increased slightly above this ambient pressure an asymmetrical separation will be created if the higher pressure fluid at U-c cannot flow around the power stream to the position B-c. This asymmetrical separation will cause more than half of the power stream to be diverted into the lower exit channel

When the control pressure at U-c is large enough to divert a sufficient quantity of power fluid into the lower channel so that the exit flow begins to restrict the reverse atmospheric flow from B-ex to B-c, then the pressure in the region B-c will begin to decrease, leading to a decrease in the lower shock strength, and the power stream will complete its switch to the bottom exit channel. To achieve the asymmetrical separation the pressure to which the conical expansion nozzle flows at the upper boundary must be greater than the pressure at the lower boundary. This higher pressure is achieved with the control signal. Once the power stream fills the lower channel then the pressure exposed to the upper portion of the jet by entrainment from the atmosphere into the mixing region is enough greater than the low pressure near the lower wall that the control flow is no longer needed to hold the jet in a stable position.

We wish to determine the variables which affect the mechanics of switching and their relation to the switching time. Since switching is an unsteady process which involves pressure forces and momentum change, we introduce the unsteady momentum equation applicable to a control volume.

$$\sum \vec{F} = \frac{\partial}{\partial t} \int_R \rho \vec{V} dR + \int (\rho \vec{V})\vec{W} \cdot \vec{n} dS \qquad \text{II-9}$$

Specializing equation II-9 for the y direction, we obtain:

$$\sum F_y = \frac{\partial}{\partial t} \int_R \rho V_y dR + \int_S V_y d\omega_{out} - \int_S V_y d\omega_{in} \qquad \text{II-10}$$

where ω is the mass rate of flow.

In applying equation II-10 to the control volume it is advantageous to first consider Figure II-4. The flow to the plane indicated by line (6) is steady for any model if P_o/P_f is constant. Plane (6) is the cross-section passing through the farthest upstream point of the "warped conical" shock. Consider Figure II-5(a), which is an enlarged view of the control volume included between plane (6) and the control volume downstream exit surface, plane (7). The reduced control volume shown as regions R_1, R_2 and R_3 are enclosed by the surfaces S_4, S_5, S_1, S_2 and S_3. These surfaces are connected as shown in Figure II-5(b). Regions R_1, R_2, and R_3 are anular regions which are defined as the undeflected, deflected, and mixing regions respectively. Surfaces S_1, S_2, and S_3 are the exit surfaces associated with regions R_1, R_2, and R_3. These surfaces are shown inside their boundaries in Figure II-5(b). This view of the nozzle illustrates how the regions and surfaces are connected.

Surface S_5 is the projection of the strong portion of the conical shock when the flow is all out either the top or bottom exit. The lines 1 and 1' are projections of the strong and weak portions respectively, of the "warped conical" shock, shown in a general position. Note that when the power fluid flows out one exit, i.e., the upper exit then a strong and weak shock exist at the upper and lower nozzle exit boundaries respectively, and vice-versa for all flow out the lower exit.

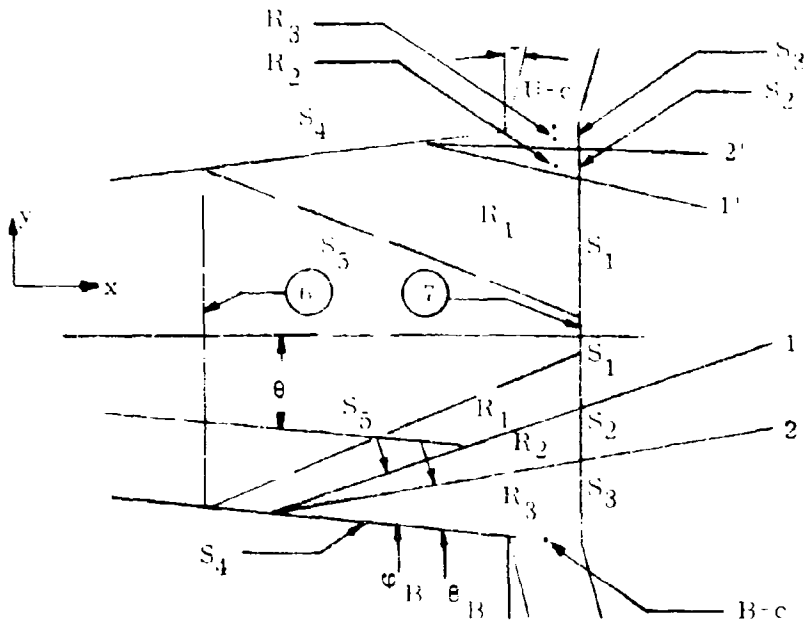

(a) Nozzle Side View Illustrating the Upper and Lower Shock Projections

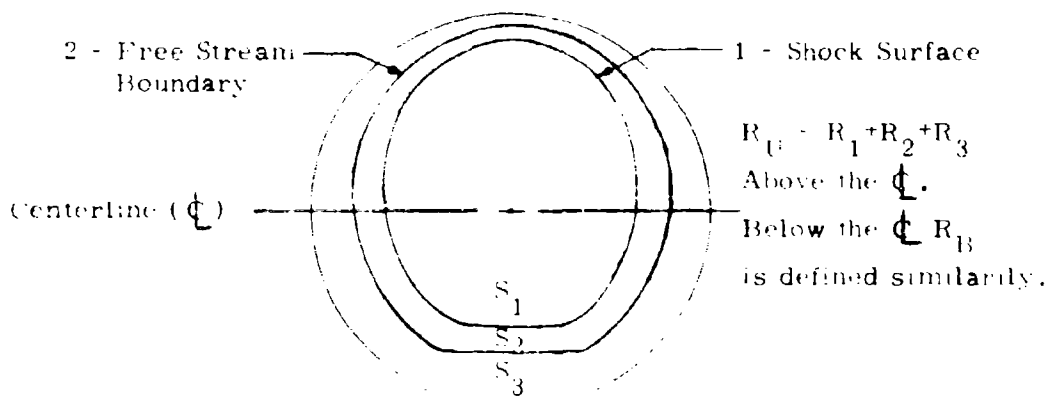

(b) Exit View of Conical Nozzle Which Shows the Free Stream Boundary and Shock Surfaces at the Nozzle Exit

Figure II-5. An Enlarged View of the Reduced Control Volume.

To get a time for switching from one channel to the other, one can integrate equation II-10 with respect to time. Integrating from the beginning to the end of the power stream switch, t_1 to t_2, gives,

$$\int_{t_1}^{t_2} \sum F_y dt = \int_{t_1}^{t_2} \frac{\partial}{\partial t} \int_R \rho V_y dR dt + \int_{t_1}^{t_2} \int_S V_y d\dot{m}_{out} dt - \int_{t_1}^{t_2} \int_S V_y d\dot{m}_{in} dt \quad . \qquad \text{II-11}$$

[1] [2] [3] [4]

It will be assumed that the same mechanics are involved at the upper flow boundary when the power stream switches from the upper to lower exit as occurs at the lower when the power stream switches from lower to upper. Equation II-11 will therefore be applied to the switching phenomena with the power stream initially going out the upper exit. When the flow switches from the upper to lower exit the "warped conical" shock translates and rotates until 1' is the projection of the strong shock and 1 is the weak shock.

In equation II-11 terms [1], [2], [3], and [4] will be designated as I_1, I_2, I_3, and I_4. Considering I_2 first it may be expressed as:

$$I_2 = \int_R \left[(\rho V_y)_{t_2} - (\rho V_y)_{t_1} \right] dR \qquad \text{II-12}$$

where the volume indicated by R is shown by R_1, R_2 and R_3. Region R is defined in this manner because each individual volume will be

considered individually when equation II-11 is applied.

Consider term [1] of equation II-11. There are pressure forces acting on the surfaces of the control volume and these include forces due to the control signal. Consider regions R_U and R_B of Figure II-5 and it is evident that the forces acting on the surface S_{5-U} and S_{5-B} cancel because of the axial symmetry of the undisturbed supersonic flow in the nozzle. The vertical forces on surfaces S_1, S_2 and S_3 are zero. During switching the surface pressures on S_{4-U} and S_{4-B} are continuously changing. This is due to the translation and rotation of the upper and lower shocks and the changing control pressure. Although the forces produced by these pressures are oppositely directed on the control volume, the integral of their magnitudes may not cancel during the switching time.

The forces $F_c(t)$ produced by the control signals in general may vary with time as indicated schematically in Figure II-6. The force resulting from the control signal can be divided into three regimes,

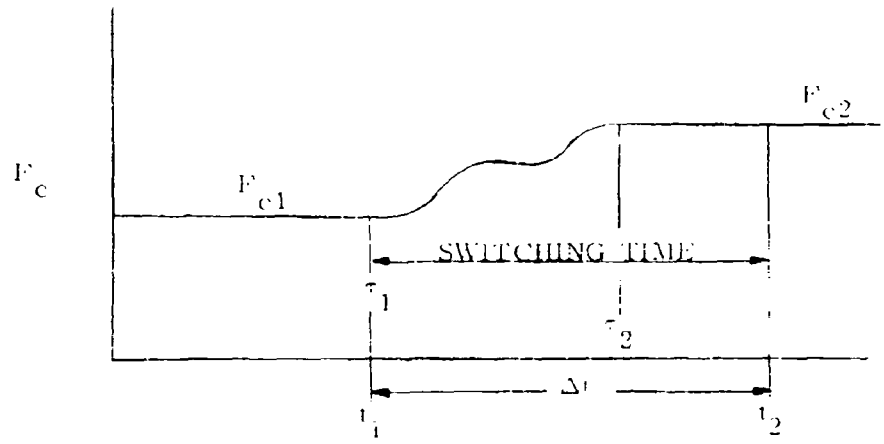

Figure II-6. Variation of Force Produced by Control Signal

the off control, control signal building, and the full or final control signal. When $t<\tau_1$ then equation II-11 becomes:

$$\int_{t}^{t_1} \sum \vec{F}\, dt = \int_{t}^{t_1}\left[\int_{S} \rho\, \vec{v}(\vec{v}\cdot\vec{n})ds\right] dt$$

which is the equation for steady flow since the stream momentum and forces are not changing with respect to time. When $\tau_1 \le t \le \tau_2$ then

$$\int_{t_1}^{\tau_2} F_c\, dt = \int_{\tau_1}^{\tau_2} f(t)\, dt \qquad \text{-13(a)}$$

where $f(\tau)$ is the function which describes the manner in which the control signal builds. For $\tau_2 < t < t_2$ then

$$\int_{\tau_2}^{t_2} F_c\, dt = F_{c2}(t_2 - \tau_2) \qquad \text{II-13(b)}$$

For $t > t_2$ then a steady flow situation exists similar to that for $t < \tau_1$. The integrals of the forces in the y direction acting on the stream during switching are then,

$$I_1 = \int_{t_1}^{t_2} F_{S_{4\text{-}B}}\, dt + \int_{t_1}^{t_2} F_{S_{4\text{-}U}} + \int_{t_1}^{t_2} F_c\, dt \qquad \text{II-14}$$

The integrals over surface $S_{4\text{-}U}$ and $S_{4\text{-}B}$ depend on the way the shock translates and rotates during switching. Integrals II-13(a) and II-13(b) must be considered when evaluating the third integral in

equation II-14, which will be defined as the total force over both control port areas.

Now consider term (1) of equation II-11. Using the relation $dm = \rho V_n$ we obtain, letting S_{5-C} be the control port area,

$$I_{41} = \int_{t_1}^{t_2} \int_{S} \rho V_y V_n \, ds_{in} \, dt = \int_{t_1}^{t_2} \left[\int_{S_{5-C}} \rho V_y V_n \, ds_{in} + \int_{S_{5-B}} \rho V_y V_n \, ds_{in} + \int_{S-C} \rho V_y V_n \, ds_{in} \right] dt \quad \text{II-15}$$

These are the primary momentum influxes.

For some streamline located by θ (see Figure II-7) from the model center line the quantities passing through the surface S_{5-B} are, $V_y = -V \sin \theta$, $V_n = V \sin \delta = -V \sin (\alpha - \varphi_1 - \theta)$ so,

$$I_{41} = \int_{t_1}^{t_2} \left[\int_{S_{5-B}} -\rho V^2 \sin \theta \sin (\alpha - \varphi_1 - \theta) \, ds_{in} \right] dt .$$

Using the Mach Number definition and noting that the influx of momentum across S_{5-B} is independent of time we obtain,

$$I_{41} = -\frac{\Delta t}{2} \int_{S_{5-B}} KPM^2 \left[m \sin 2\theta + n \cos 2\theta - n \right] ds_{in} \quad \text{II-16(a)}$$

where $m = \sin(\alpha - \varphi_{max})$ and $n = \cos(\alpha - \varphi_{max})$. A similar development can be made for surface S_{5-1}. The relations,

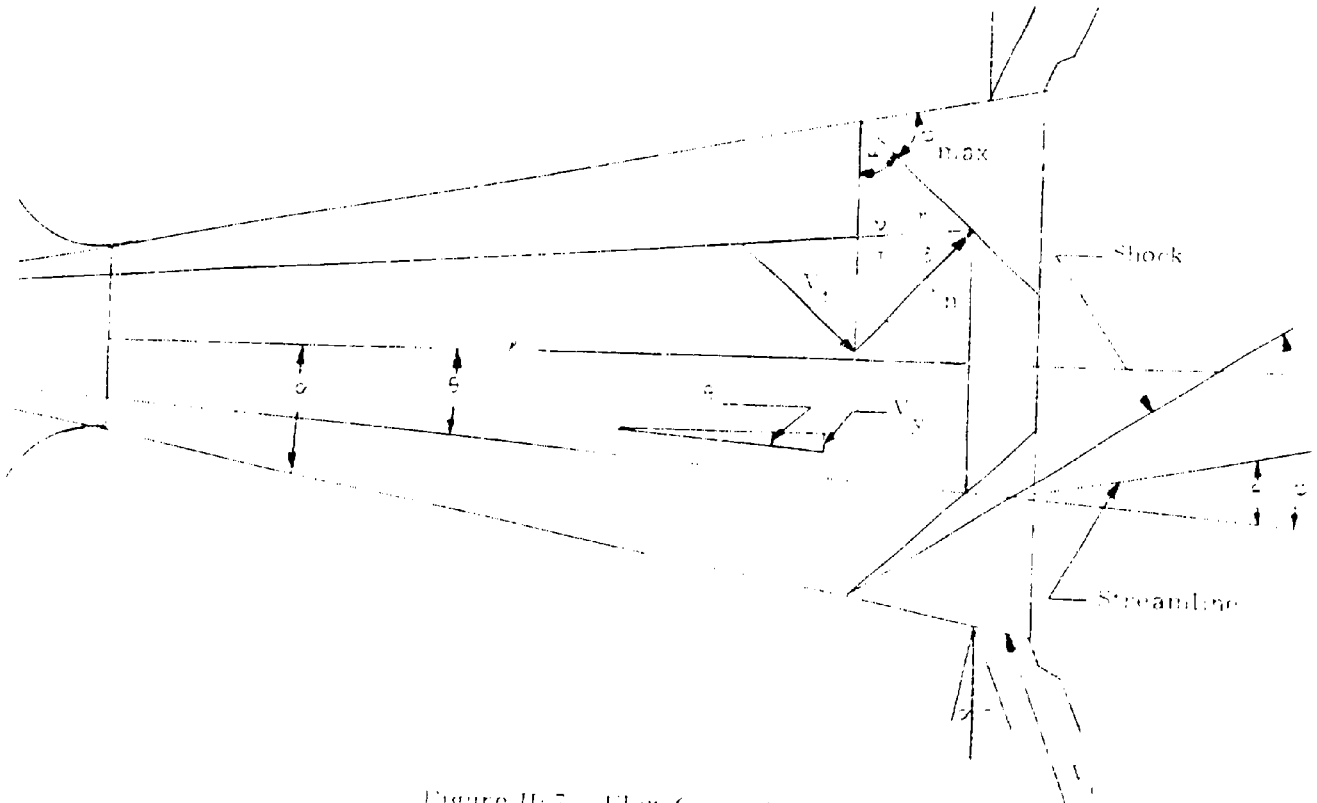

Figure II-7 Flow Geometry

$$A/A_t = \frac{1}{M}\left[\frac{2}{K+1}\left(1 + \frac{K-1}{2} M^2\right)\right]^{\frac{K+1}{2(K-1)}} \qquad \text{II-16(b)}$$

$$M^2 = \frac{2}{K-1}\left[\left(\frac{P_o}{P}\right)^{\frac{K-1}{K}} - 1\right] \qquad \text{II-16(c)}$$

and

$$\ell = \frac{D_t\left(\sqrt{A/A_t} - 1\right)}{2 \tan \alpha} \qquad \text{II-16(d)}$$

provide a relationship between ℓ and the pressure P. The variable ℓ is defined in Figure II-7. Integrals over S_{5-U} and S_{5-B} cancel if the model is symmetrical since the vertical velocity components are equal but opposite.

The last manner in which momentum flux can cross the surfaces into the control volume is across S_3. Across S_{3-U} and S_{3-B} there is flux both in and out of the region because of entrainment from ambient into the so-called mixing region. As shown in Figure II-3, there is momentum flux into the region from the atmosphere. This mass must also leave, so the atmospheric flow enters and leaves R_3 between the free stream boundary and model boundary. The total momentum flux into the mixing region is then,

$$I_{42} = \int_{t_1}^{t_2}\left[\int_{S_{3-B}} \rho V_y V_n ds_{in} + \int_{S_{3-U}} \rho V_y V_n ds_{in}\right] dt \quad ,$$

II-17

This mixing is difficult to define explicitly and simplifying assumptions will be made in dealing with it.

Term [3] will now be considered in relation to the surfaces S_1, S_2, S_3, S_4 and S_5. There is no momentum flux out of surfaces S_5 or S_4. The integrals I_3 for these surfaces thus are zero. The momentum flux out R_B through S_3 and R_U through S_3 is between the free stream boundary and model boundary and is given by,

$$I_{31} = \int_{t_1}^{t_2}\left[\int_{S_{3-B}} \rho V_y V_n ds_{out} + \int_{S_{3-U}} \rho V_y V_n ds_{out}\right] dt \quad . \qquad \text{II-18}$$

This integral is due to the second portion of the mixing region Integrals I_3 and I_4 over surface S_3 is the integral of momentum flux due to the reverse flow from the atmosphere and some small portion of the power fluid from the boundary layer mixing and flowing out of region R_3 together. For surface S_{2-B} and S_{2-U} term [3] is,

$$I_{32} = \int_{t_1}^{t_2}\left[\int_{S_{1-B}} \rho V_y V_n ds_{out} + \int_{S_{1-U}} \rho V_y V_n ds_{out}\right] dt \qquad \text{II-19(a)}$$

which is the flux out of the control volume after crossing the shocks 1 and 1'.

For surface S_{1-U} and S_{1-B} term [3] is

$$I_{33} = \int_{t_1}^{t_2}\left[\int_{S_{1-U}} \rho V_y V_n ds_{out} + \int_{S_{1-B}} \rho V_y V_n ds_{out}\right] dt \quad . \qquad \text{II-20}$$

When shock 1 rotates toward the lower boundary a portion of the lower control volume will contain fluid which has not crossed the lower shock. This is easy to observe when the apparent shocks are in the intermediate position shown in Figure II-5. The integral of momentum flux over surfaces S_{1-U} and S_{1-B} in equation II-20 include all the flux leaving the control volume exit which doesn't cross the apparent shocks.

Time t_1 has been designated as the beginning of the switching phenomenon. Between times t_1 and t_2 the shock angles φ_B and φ_U are changing. Consider the integrals over S_1, S_2 and S_3. It can be seen that the values of the integrands of these integrals vary with time because of the movement of the shocks through the control volume.

The control volume is determined by P_o/P_f and K according to the location of the shocks as given by equation II-6, II-8 and II-16(d). When the control volume is determined computations can be performed to find the switching time of the power fluid from

$$\int_{t_1}^{t_2} \left[F_{S_{4-B}} + F_{S_{4-U}} + F_c\right] dt = \int_R \left[(\rho V_y)_{t_2} - (\rho V_y)_{t_1}\right] dR$$

[1] [2]

$$-\int_{t_1}^{t_2}\left[\int_{S_{3-B}} \rho V_y V_n ds_{in} + \int_{S_{3-U}} \rho V_y V_n ds_{in}\right] dt$$

[3]

$$-\int_{t_1}^{t_2}\left[\int_{S_{5-U}} \rho V_y V_n ds_{in} + \int_{S_{5-B}} \rho V_y V_n ds_{in} + \int_{S-C} \rho V_y V_n ds_{in}\right] dt$$

[4]

$$+\int_{t_1}^{t_2}\left[\int_{S_{3-B}} \rho V_y V_n ds_{out} + \int_{S_{-U}} \rho V_y V_n ds_{out}\right] dt$$

[5]

$$+\int_{t_1}^{t_2}\left[\int_{S_{1-B}} \rho V_y V_n ds_{out} + \int_{S_{1-U}} \rho V_y V_n ds_{out}\right] dt$$

[6]

$$+\int_{t_1}^{t_2}\left[\int_{S_{1-U}} \rho V_y V_n ds_{out} + \int_{S_{1-B}} \rho V_y V_n ds_{out}\right] dt \quad . \quad \text{II-21}$$

[7]

The numbered terms are those developed previously and are defined as: [1] the forces acting on the control volume in the y direction, [2] the change of momentum within the control volume from the initial to final flow configurations, [3] induced influx of momentum across surfaces S_3, [4] primary influx of momentum due to the power fluid and control fluid, [5] the efflux of entrained fluid and a small portion of the power fluid, [6] power fluid efflux whose direction has been changed by the shock system, and [7] power fluid efflux whose direction is not changed in the control volume.

Equation II-21 is derived in a general form and may be used to calculate switching times in different amplifiers of a similar geometry

In applying the equation each term must be evaluated for the particular model under consideration.

In solving this equation for a switching time it may be noted that when the shocks have reached a steady state position the power stream has switched. Thus if one knew the time required for the shocks to assume their final position one would have the switching time. The time Δt does not appear explicitly in equation II-21 therefore a numerical scheme of computation utilizing a computer is, in general, necessary to obtain a solution for Δt.

III. Description of Experimental Apparatus and Methods

A. Apparatus Description, Theory and Arrangement

As mentioned in Section I the purpose of the experiments was to provide qualitative and quantitative information so that insight into the mechanics of amplifier operation could be gained. To obtain this information two separate data recording systems were utilized for most of the tests described in this section. The first of these consisted of a schlieren system and a high speed camera which recorded the shock system within the flow photographically. The second data recording system consisted of pressure transducers, amplifiers and an oscillograph which recorded various pressures of importance within the amplifier. These data recording systems, in some instances, furnished information regarding the same phenomenon in two completely different manners. For example, from observing the high speed schlieren film it can be determined when control flow is being supplied at a particular port and also by which exit the power fluid leaves the amplifier. This information can also be obtained by observing the values of pressure recorded at the control ports and exit channels.

The power fluid was either nitrogen, supplied through a manifold and pressure reducing valves from standard storage bottles, or

hydrazine, supplied from a hot gas generator. The nitrogen bottle reservoir was located outside the test bay which housed the equipment shown in Figure III-1. The hydrazine generator was located inside the test bay close to the model.

The schlieren photographs were obtained utilizing a six inch schlieren system manufactured by the Aerolab Supply Company of Hyattsville, Md. The components used in these experiments can be identified in Figure III-1 as the light source, two mirrors and knife edge. This schlieren system and a Hycam high speed camera were used to record the shocks and flow system in the amplifier. The light was supplied as a line source, and diverged to completely cover the first mirror which had a large radius of curvature. The light source was placed at the focal point of the first mirror so that the reflected light rays leaving the mirror were parallel. The reflecting surface of the second mirror was just covered by the light received from the first mirror since the rays leaving the first mirror were parallel. The second mirror focused the light and reproduced the light source image at the knife edge which was arranged parallel to the image and then adjusted to intercept approximately one half the light. Across the knife edge the light column diverged. The location of the camera was adjusted such that the image projected on the film would just cover the film. Thus the six inches shown between the knife edge and camera would be different for different cameras.

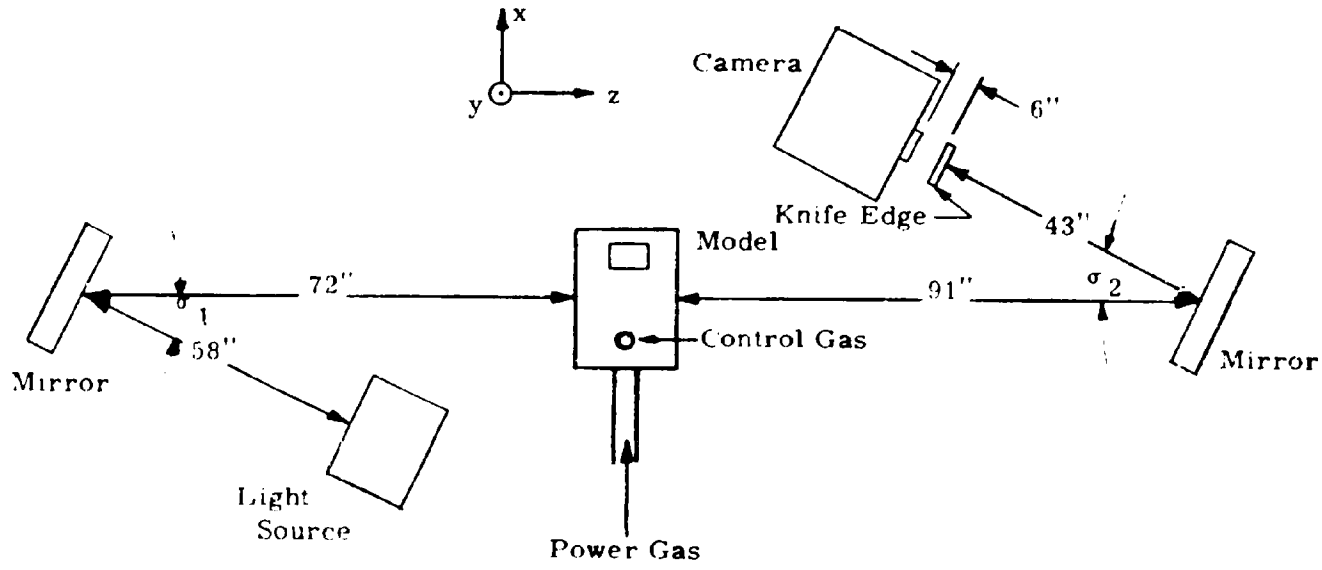

Figure III-1. Schlieren Light and Camera System

Care was taken to align the model and light system such that the model's test section lay in the x-y plane and the light coming from the first mirror was perpendicular to the x-y plane. The angles α_1 and α_2 were kept less than 15°. The light source and knife edge were located on opposite sides of the parallel light to reduce asymmetry of the image (19).

The schlieren system makes density gradients visible in terms of intensity of illumination. A light ray passing through a flow field will be deflected if there is a density gradient normal to the light path. This deflected ray may either pass or be intercepted by the knife edge, which thus determines if the illumination is increased or decreased at the position on the screen which this ray should illuminate. Consider Figure III-2(a) where the gas flow is two dimensional and the circle with a dot indicates that the light is coming out of the page as it leaves the test section. Now if there is a density gradient in the y direction in the vicinity of the ray it will be deflected up or down depending on the gradient. The boundary layer could be distinguished from the supersonic flow field, for example. If a normal shock exists as shown, and since there is a large gradient across it, the light rays passing through it will receive a $\Delta\theta_x$ deflection in the vicinity of the shock wave. The gradients observed depend on the orientation of the knife edge. If the knife edge is located along the x axis then light rays given a $\Delta\theta_y$ deflection are passed or intercepted according to whether $\Delta\theta_y$ is positive or negative.

The light rays are deflected by the density gradients because the index of refraction varies approximately linearly with the density. The index of refraction is defined as $n = c/v$ where c is the velocity of

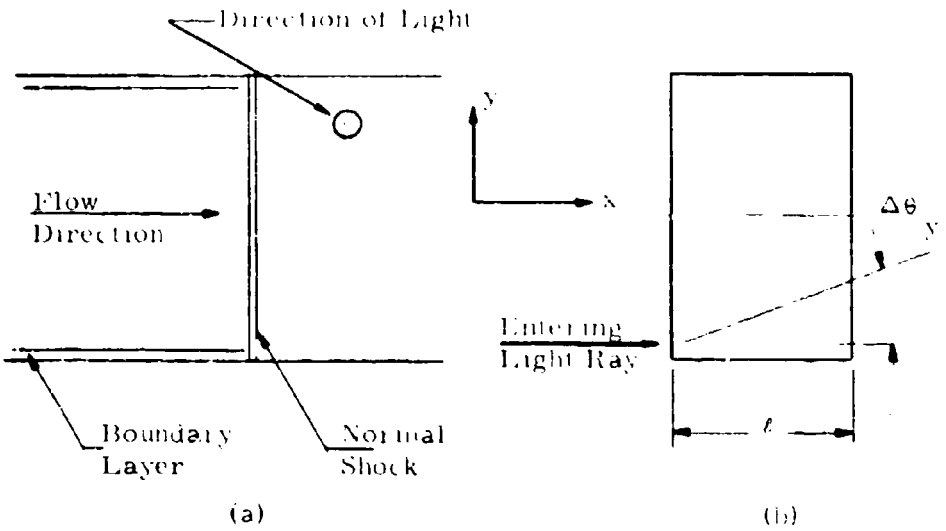

Figure III-2. Effects of Density Gradients on Light Rays.

light in a vacuum and v is its velocity in the medium of index n. The index of refraction for ordinary gases is given by

$$n - 1 = k_1 \rho \qquad \text{III-1}$$

where k_1 is a constant.

The changes in light intensity can be measured to get numerical values for the changes in density by using a light sensitive meter. This procedure was not used in this project.

The camera used to make the high speed moving pictures of the switching operation was a model K20S4E Hycam high speed camera

It was manufactured by Red Lake Laboratories at Santa Clara, California. A Milli Mite Signal Generator was used in conjunction with the camera to determine the speed with which the event occurs to an accuracy of ± 5%.

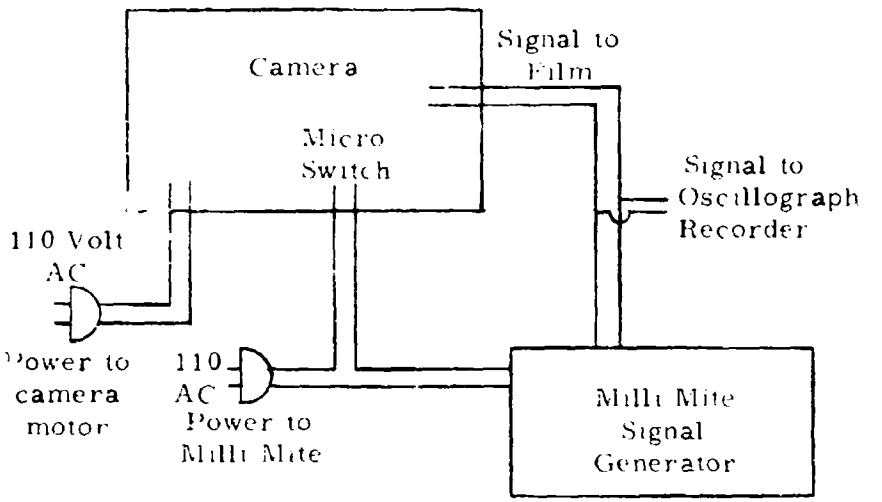

Figure III-3. Electrical Circuit of Camera and Timing Signal.

A diagram of the electrical wiring connected with the camera, Milli Mite signal generator and oscillograph recorder is shown in Figure III-3. With this arrangement the camera and oscillograph recorder both experienced the results of the electrical signal, produced by the signal generator, at the same time. The signal produced reached a maximum voltage at the rate of one thousand times per second. A small light bulb in the camera was energized by this signal. The bulb was positioned such that some of the film frames, which are recording the event taking place, have a small area

exposed to the light from the bulb. The number of frames exposed to the signal depends on the film speed in the camera.

The signal which energized the bulb was also utilized in actuating a galvanometer in the oscillograph. Actuating the galvanometer caused "pips" to be produced on the oscillograph paper on which the pressure time record was being recorded. The parallel wiring system shown in Figure III-3 made it possible to use the same voltage signal to energize both timing light and galvanometer.

As shown in Figure III-3 the electrical power to the signal generator was controlled by a microswitch inside the camera. The micro switch closed after one hundred feet of a two hundred foot roll of film had been used. The signal generator was then energized and began to produce the signal which energized the timing light and galvanometer. In practice this arrangement sent a strong signal to the oscillograph recorder, which needed very little power to operate the galvanometer producing the "pips" on the oscillograph paper. The signal to the camera was not strong enough, immediately after the generator began operation, to energize the timing light bulb. A better wiring arrangement might have been one which sent the output of the generator through the camera micro switch before the camera was turned on. This would have allowed the generator to warm up so that its maximum output could be delivered when the switch was closed.

Since timing marks were not distinguishable on the film a portion of the film at a known frame rate was used to obtain shock angles during the switching process. This film strip was determined from a speed vs time calibration graph. All the high speed test film was run with the camera controls set at an indicated 5000 frames/second. A calibration curve was obtained from film that had been run at this camera setting and also had the timing light marks. This curve indicates that approximately fifty feet of a 200 foot roll of film ran at the constant speed of 5000 frames per second. This section of the two hundred foot roll of film was used to obtain the shock-angle vs time curves of Section IV.

To observe the developed film, a 16 mm projector was used. The projector could be operated at the standard speed of 32 frames/second or the film could be advanced frame by frame. To obtain data such as shock angles, free stream boundaries, separation position and the intersection of free stream boundaries with shocks, the film was viewed frame by frame. These values were recorded for all the schlieren cinematographic data obtained, and are presented graphically when possible in the experimental results section.

Shocks and free stream boundaries were very faint in some cases when hydrazine was the power gas. The gas was very hot and in the small test room the accumulated gases and induced density gradients on the outside of the model reduced the visibility of phenomena which were occurring in the model. Since personnel could not be in the

vicinity of a hot gas test, the knife edge could not be adjusted during the test to improve the initial setting. The pressure recording system began with pressure pickup, using Consolidated Electrodynamics Corporation (CEC) pressure transducers. The electrical signal generated was then amplified with a carrier amplifier to the desired value. This signal was then applied to a galvanometer which rotated according to the applied voltage. A small mirror directed a high intensity light onto light sensitive paper. This paper was driven at a constant speed so that a pressure-time curve was obtained.

Table III-1 gives the type and important characteristics of the equipment used in the pressure recording system.

Table III-1. Type Pressure Recording Equipment Employed

	Range (psi)	Natural Frequency (cps)	Per cent Accuracy
Pressure transducer CEC 4-326-0003	0 to 25 and 0 to 50	10,000	
Pressure Transducer CEC 4-326-0006	0 to 500 and 0 to 1500	10,000	
Galvanometer CEC 7-323		1 000	±5%
CEC 7-326		5,000	±5%
Carrier Amplifier 1-127, 20KC		3,000	±1%

*frequency response flat at 3000 cps within ± 1%

The complete pressure recording system was calibrated at the beginning of each test day. This was a static calibration and was

accomplished in the following manner. All transducers in the 0 to 25 and 0 to 50 psig range were attached to a pressure manifold, which had a bourdon tube pressure gage as the pressure measuring standard. Air pressure was applied to the manifold, and thus all gages were calibrated simultaneously. Pressure was applied in 5 psig increments until 15 psig was reached and in 5 in Hg vacuum until 20 in Hg was reached. When each static pressure was obtained, the oscillograph recorder was started and a short segment of paper obtained which contained the deflection from zero represented by the particular pressure applied to the individual transducers. A calibration sheet similar to Figure III-4 was made from these deflections where the spaces between each deflection are subdivided linearly.

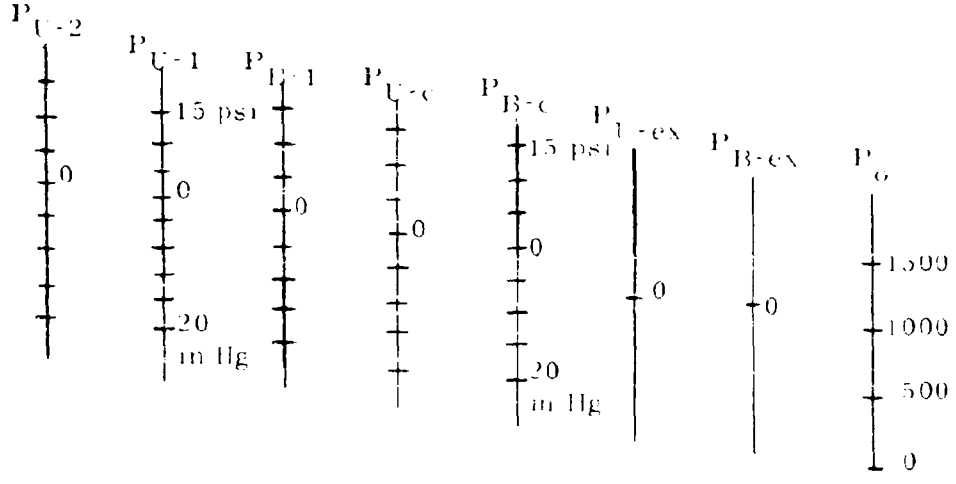

Figure III-4. Typical Pressure Transducer Oscillograph Calibration Chart

In Figure III-5 the positions of pertinent flow dimensions of the model are indicated and in Table III-2 dimensions of importance are tabulated. In Table III-3 the significant model areas and area ratios are tabulated. Figure III-6 shows a drawing of the model assembled for testing.

Table III-2. Model Dimensions

All dimensions are in inches.
Throat diameter - 0.0745 ± 0.0001
Diameter at exit of round nozzle - 0.323 ± 0.002
Vertical dimension of the flow path at control port - 0.350 ± 0.003
Thickness of flow channel - 0.314 ± 0.0005
Top exit - 0.314 ± 0.0005 by 0.420 ± 0.003
Bottom exit - 0.314 ± 0.0005 by 0.420 ± 0.003
Entrance to top channel - 0.314 ± 0.0005 by 0.430 ± 0.003
Entrance to bottom channel - 0.314 ± 0.0005 by 0.430 ± 0.003
Diameter of static pressure openings - 0.040 ± 0.0005
Diameter of pipe leading to model throat - 0.190 ± 0.002
Control port throat - 0.314 ± 0.005 by 0.048 ± 0.002

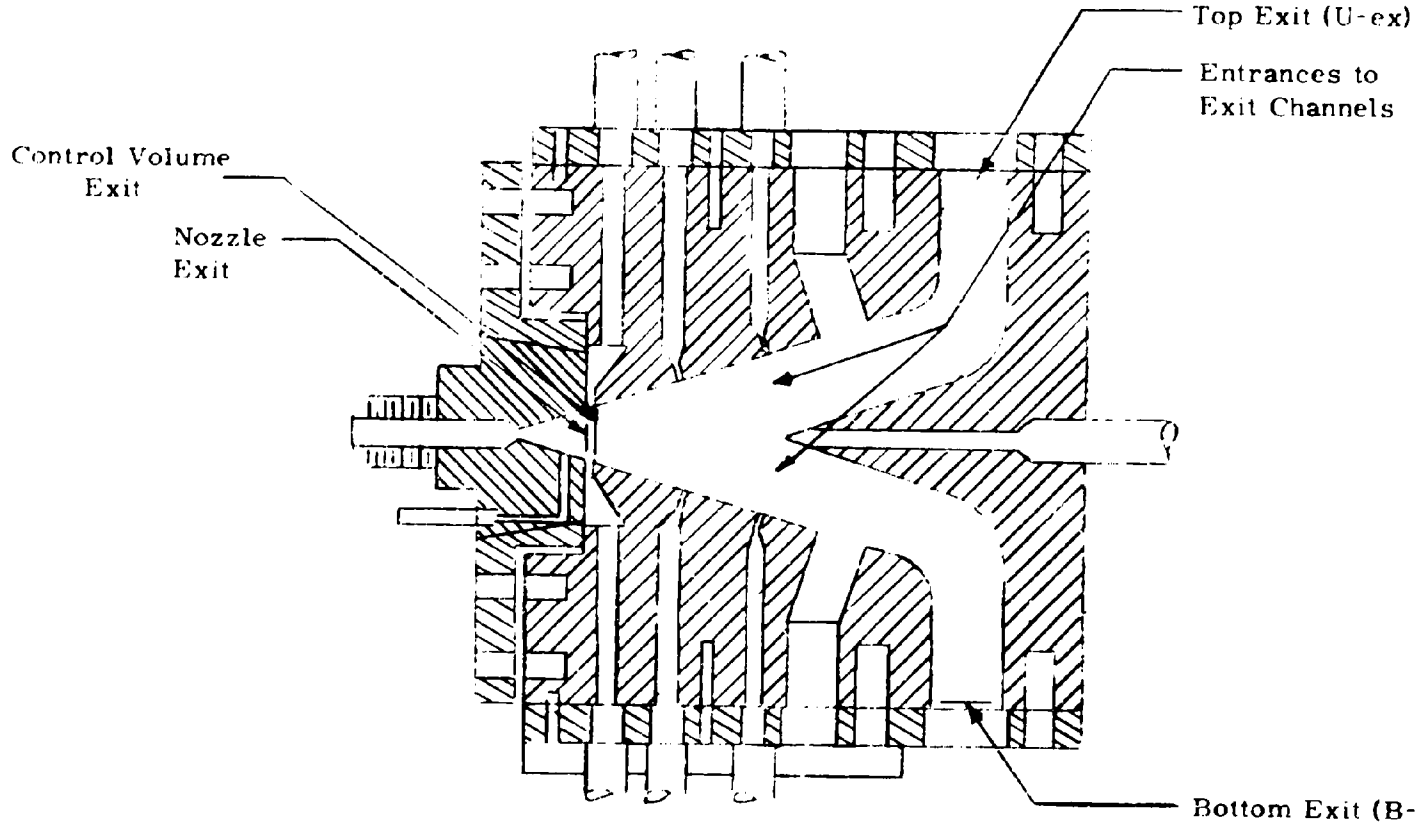

Figure III-5. Flow Positions of Importance

Table III-3. Model Areas and Area Ratios

Area of control port (A_c)	$0.314 \times 0.048 = 1.51 \times 10^{-2}$ in^2
Area of nozzle throat (A_t)	$\frac{\pi}{4}(0.0745)^2 = 4.35 \times 10^{-3}$ in^2
Area of nozzle exit (A_n)	$\frac{\pi}{4}(0.323)^2 = 8.20 \times 10^{-2}$ in^2
Area of channel exits (A_{ex})	$0.420 \times 0.314 = 1.32 \times 10^{-1}$ in^2
Area of entrance to channels (A_{en})	$0.430 \times 0.314 = 1.35 \times 10^{-1}$ in^2
Nozzle half angle	14.0°

B. Model Description

In performing the experimental work care was taken to follow procedures which made the results of the experiment repeatable and ameanable to analysis. The purpose of this section is to describe the model, each experiment and the methods and procedures employed in performing these tests.

The expansion nozzle from the stagnation chamber to position U-c and B-c was axisymmetrical and conical with a nominal expansion ratio (A_n/A_t) of 19 and a half angle of expansion of 14°. At the control ports the cross section is discontinuous. The channel from this position to either exit is rectangular. Position II is the splitter tip which is the beginning of the separate output channels. The different positions for which pressure measurements were recorded in the tests are B-c, B-1, B-2, U-c, U-1, U-2, and II. The pressure

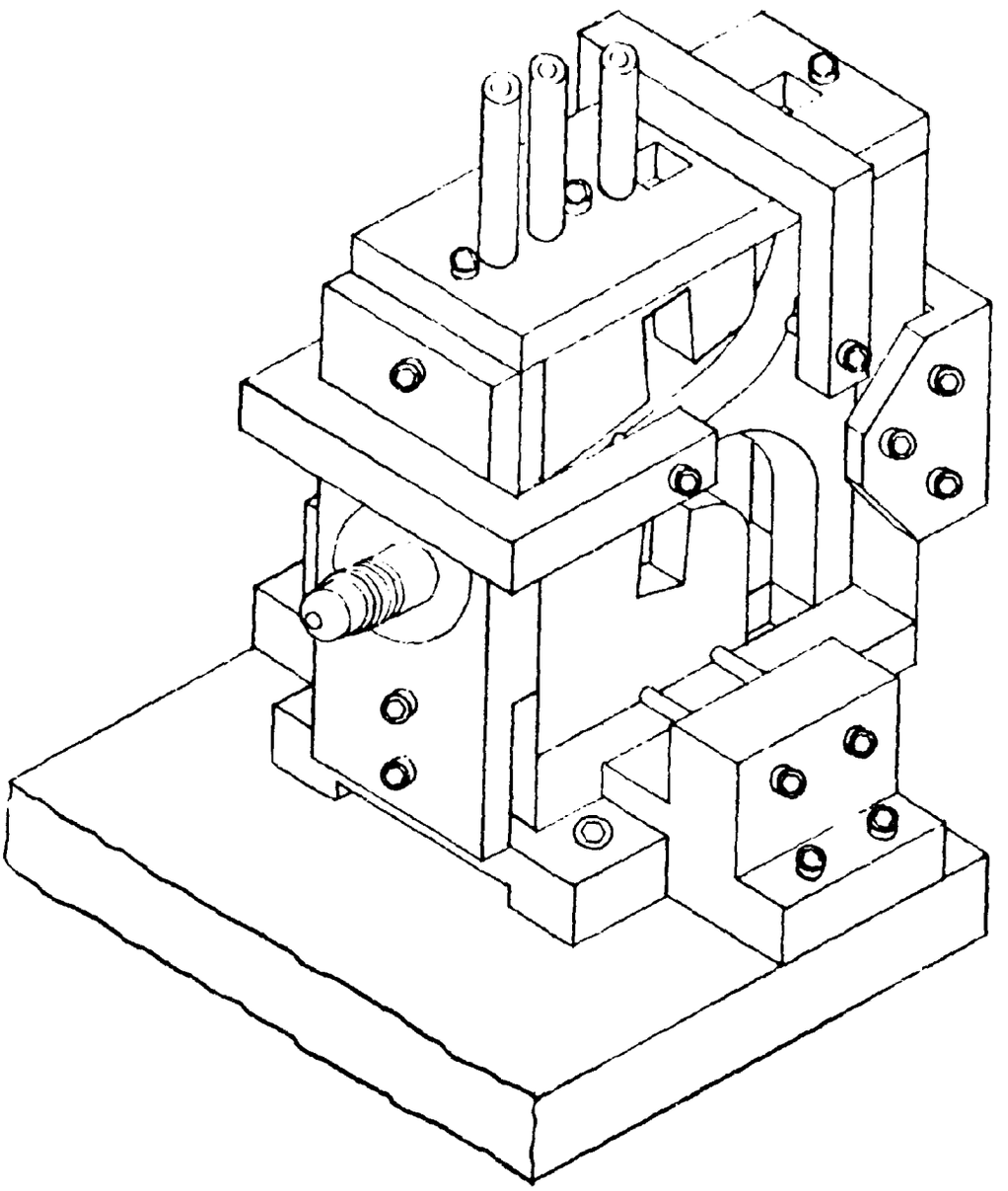

Figure III-6. Model Assembled for Testing

pickup at position B-n was installed, after the main experiments had been performed, to determine additional information in this vicinity when the amplifier was operated in its bistable region with no control flow.

The flow cross-section from the control position to each channel exit was visible because glass was used as the flow channel side walls. The upper and lower channel sections and the splitter section were sandwiched between one half inch thick glass walls. With flow visualization methods it was then possible to observe the flow and shock patterns. Positions B-v and B-v were originally intended to be vents to the atmosphere but were closed because they only serve a purpose when the amplifier supplies the control signal for another stage.

There were seven tests, or series of tests, performed using the model shown in Figure III-6. Before assembling for each test the model was checked visually to insure that the thin rubber gaskets which seal the flow channels to the glass side walls were not damaged. After each test the model was disassembled in order to clean the glass walls, and this frequently resulted in damage to the thin gaskets. When the model was reassembled it was realigned using two metal positioning blocks inserted into the upper and lower exits. With the glass pressed firmly against the two blocks in the exit channels the appropriate securing screws were tightened. This care insured that the flow channels remained essentially the same for each test and that

atmospheric air did not leak into the low pressure flow regions.

Nitrogen was always used as the control signal gas and was used as the power fluid except for two tests in which hydrazine was used as the power fluid. Results of the tests are given in Section IV.

Test series 1 - Amplifier Bias Determination

Description of test conditions - No control flow was used.

Purpose of tests -Ranges of supply pressure were investigated to determine whether the model exhibited tendencies to flow out either the upper or lower channel exits.

Test procedure - The power fluid was increased both slowly and rapidly to determine if $\partial P_o / \partial t$ would cause any bias. Pressures were recorded manually when significant and the reason for the significance was also recorded.

Test series 2 - Determination of Bistable Range

Description of test conditions - With no control flow or pressure signal applied the pressures at B-n, B-c, B-1, U-c, B-ex and U-ex were recorded as the chamber pressure, P_o, was slowly increased.

Purpose of tests - This test was performed to (1) demonstrate the bistability of the amplifier and (2) to obtain a record of the pressures created at the positions B-n, B-c, B-1, and U-c and (3) to determine the amplifier's bistable range. Pressures at B-ex and U-ex identify the outlet flow exit.

Test procedure - (1) The oscillograph was started and (2) the power

fluid (nitrogen) supply pressure was slowly increased as the experimenter closed the bottom exit (B-ex) with his hand to force the flow out the upper exit (U-ex). When the P_o was reached for which the power flow would continue to flow out U-ex without the aid of the experimenter's hand, the hand was removed. P_o was increased slowly from this pressure, for which flow was steady, stable and leaving the model from U-ex, until the flow split. This same procedure was followed when the flow was forced out B-ex.

Test series 3 - Oil Flow Pattern on Glass Side Walls

Description of test conditions - Patterns were observed both with and without control flow. No pressures were recorded except P_o.

Purpose of tests - By observing the manner in which the flow near the glass walls forced the oil to flow on the glass walls some characteristics of flow in the main stream could be ascertained.

Test procedure - The power flow was directed out an exit by using a control flow, or by hand, and oil was injected in the other exit channel. The flow patterns on the glass walls were observed and recorded by hand. This procedure was performed in the bistable range with and without control flow.

Test series 4 - Slow Speed Switching, Cold Power Gas

Description of test conditions - Solenoid valves were used to actuate the control signal. Pressures were recorded at positions U-c, U-1, U-2, U-ex, B-c, B-1, B-2, B-ex, P_o, and H. High speed (5000

frames per sec) schlieren motion pictures were taken of the switching phenomena. The power gas (nitrogen) stagnation temperature was essentially the same as ambient (these are referred to as cold gas tests).

Purpose of tests - The schlieren motion pictures and the pressure data were recorded during a switching process. Later the pictures were observed at a greatly reduced speed and also analyzed as stationary frames so a better understanding of the switching phenomena could be formed.

Test procedure - The schlieren light system was arranged as shown in Figure III-1 and the high speed camera adjusted and loaded with film. The solenoid valves were wired through a single switch so that one of the valves was open while the other was closed and vice-versa. Thus with the equipment preliminaries satisfied, the high pressure nitrogen source was regulated down until the desired chamber pressure, for which the test was to be run, was achieved. Next the solenoid valve switch was operated by hand at the rate of two or three cycles per second. After the model was operating, the oscillograph recording mechanism was started and immediately thereafter the camera and timing system (see Figure III-3) were started. When a two hundred foot roll of film had been run through the camera the power gas, control gas and pressure recording system were turned off. The film was identified and stored for reduction at a later time. This procedure was performed for chamber pressures of 1200, 1000,

800, 600 and 250 psig.

Test series 5 - High Speed Switching, Cold Power Gas

Description of test conditions - A flueric oscillator, was used to produce the control signal in this test so that there were no mechanical operations occurring anywhere in the control flow path. Pressures were recorded at the same positions in this test as in test 4, and schlieren motion pictures were obtained in an identical manner. Again the test was essentially a cold gas test

Test procedures - The schlieren light system and camera system procedures were identical to those outlined in test 4 Test 5 was run for chamber pressures of 1200, 1000, 800, and 600 psig.

Test series 6 - Slow Speed Switching Hot Power Gas

Description of test - The solenoid valves of test 4 were used to actuate the control flow. Pressure existing at the same positions as in test 4 were again recorded and high speed schlieren photographs were again taken. The power gas was produced with a hydrazine generator. Liquid hydrazine (N_2H_4) was forced into a steel pressure chamber heated initially with an electrical coil to approximately 1200^{O} F. This temperature caused the hydrazine to vaporize and decompose into NH_3, H_2 and N_2 in percentages which vary according to the gas temperature. The decomposition of the gas released energy which increased the temperature of the gas leaving the generator to approximately 1700 to 1800^{O} F at a pressure of about 1400 psig

Test procedure - The light system arrangement was identical to that in tests 4 and 5. The camera system was identical except a remote control switch was added to the camera. After all final adjustments in the vicinity of the model were made all personnel left the area of the model since the hydrazine gas is extremely dangerous. The hot gas generator was started by a qualified operator inside the control room. The control flow was also actuated to prevent overheating some part of the model. When the desired chamber pressure to the model was achieved and the hot gas generator was operating in a steady state condition the pressure recording was begun and the camera started. When the 200 feet of film had run through the camera (less than two seconds) the hot gas generator and pressure recording system were stopped. Film and pressure data processing procedures were the same as in test 4. Tests were performed for chamber pressures of 1250, 1150, 1000, 800 and 600 psig

Test series 7 - High Speed Switching Hot Power Gas

Description of test - The oscillator described in test 5 actuated the control flow in this test. As in test 6 the schlieren and camera system adjustments were completed and all personnel cleared from the test area. The hot gas generating system as described in test 6, was used in this test

Test procedure - Because of time limitations only one test was completed using hot gas and the oscillator. This was performed at a chamber pressure of 1000 psig. The procedure in test 7 was essen-

tially the same as that of test 6 except for the different method of actuating the control flow.

Except for minor adjustments, tests 4, 5, 6 and 7 were all conducted in the same area without any change in the light or camera system.

IV. Analysis of Results

A computer program incorporating the bistable analysis of section II, was written to determine the quantities φ, ϵ, X_1, A_1/A_t, M_1 and P_1/P_t by varying the ratio P_o/P_t. These quantities have been calculated for the amplifier described in Section II with values of k 1.40, 1.36, 1.32, 1.28, 1.24, 1.20. The program uses an iterative process to solve for values of P_o/P_t which satisfy equations II-6, II-7 and II-8. Results from experiments described in Section III are presented and compared to theoretical values in the following developments when applicable.

Test Series 1 - Amplifier Bias Determination

No consistent bias was observed. For supply pressures above 200 psig the flow approximately split between the two exits. If foreign matter was deposited along one boundary the flow tended to go out the opposite exit. $\partial P_o/\partial t$ did not affect the exit by which the power fluid left the model.

Test Series 2 - Determination of Bistable Range

When power supply pressures of approximately 550 psig were reached the power fluid would flow out either the upper or lower exit without further assistance from any source. If the supply pressure was increased after a stable supply pressure was reached, stable flow out either exit continued until the supply pressure reached about 1350 psig. The lower limit is repeatable within $\pm$ 50 psig while the upper limit tends to vary approximately $\pm$ 100 psig. Figure IV-6 shows the

pressure variations in each control port vicinity with the supply pressure when the power fluid was initially forced out the upper exit for three separate tests. Similar results were obtained when the power flow was forced out the lower exit.

Test Series 3 - Oil Flow Pattern on Glass Side Walls

The oil flow patterns observed on the glass walls were essentially the same with or without control flow. When control flow was used the effects of its vertical velocity were apparent in the control port region.

Many different camera techniques were tried in attempts to record the flow patterns photographically. These attempts were not successful because the cameras and photographic equipment available were not adequate.

Although photographs of the flow patterns were not obtained the patterns observed helped in formulating the flow separation model shown in Figures II-3 and II-4. The line in the figure indicated by (5) appeared as a thin circumferential ring of carbon around the nozzle boundary. As the supply pressure was increased this carbon ring approached the exit of the conical nozzle.

When the power flow was directed out the upper exit, carbon particles on the glass walls indicated this. Air from the atmosphere was detected entering the lower exit as it flowed past the experimenter's hand, which was held in this vicinity. Graphite particles indicated that this reverse flow was entrained by the power stream and left the model by the upper exit.

Test Series 4 - Slow Speed Switching, Cold Power Gas

Solenoid valves were used as the control flow actuators so that it could be certain that control flow came from only one control port. Since the power that actuated the solenoid valves was controlled manually with a toggle switch, switching speed was on the order of two or three cycles per second. The high speed film data indicates long periods of steady state operation, which is confirmed by the oscillograph data.

Data obtained during the switching of the power jet are not analyzed because the solenoid valves bounce off their seats when closing. This is apparent from the film because of the oscillation of the power jet and also from the variations of the control pressure signal recorded by the oscillograph. Since the $\partial P_c / \partial t$ was not always positive during switching, when using the solenoid valves, the shock angles versus time data were not taken from the film. Values of P_o / P_c versus the strong shock angle, reduced from portions of the film and oscillograph records when the model operated at steady state, are plotted on Figure IV-8.

Test Series 5 - High Speed Switching, Cold Power Gas

The flueric oscillator supplied a control signal such that the value of P_c increased approximately linearly with time. P_c usually reached a value between one third and one half of the total switching time, that was held until the switching was complete. Figures IV-10, 11, 13 and 14 show plots of P_c and shock angles versus time for the various

supply pressures. Both P_c and ϕ are plotted versus the same time scale in each figure. It can be seen that P_c reached a steady value before the shock angles stop changing. Figures IV-16 and 17 show photographic switching sequences for supply pressures of 1200 and 1000 psig.

The information presented in Figures IV-10, IV-11, IV-16 and IV-17 is representative of the data which was helpful in formulating the flow model and equations to describe steady state flow and the switching process. These figures are discussed further when specific points are discussed in connection with the flow model and equations.

Test Series 6 - Slow Speed Switching, Hot Power Gas

The objective of these tests was to determine the same type information as recorded in Test Series 4. Again the solenoid valves displayed poor seating characteristics. Thus since the clarity of the photographic data was also very poor this data was not analyzed.

Test Series 7 - High Speed Switching, Hot Power Gas

Only one high speed switching test at a supply pressure of 1000 psig was completed satisfactorily. Data from the oscillograph record is plotted in Figure IV-12. A photographic switching sequence similar to those of Figures IV-16 and IV-17 are not shown here because all clarity of details is lost when going through the necessary reproduction processes. Results of this test are compared to the flow model and the cold gas tests when possible in the following discussion.

Figure IV-1 shows the area ratio at separation as a function of P_o/P_f which was chosen as the independent variable since this ratio, for any particular model geometry, is known to affect the separation position. As P_o/P_f increases, the separation region moves closer to the nozzle exit. This phenomenon was observed experimentally by the author and Mr. B. J. Clayton of the U. S. Army Missile Command when running test series 3 during which an oil-graphite solution was injected into the amplifier and P_o/P_f was varied by varying P_o. The stagnation region in the nozzle was visible because of the light circumferential ring of carbon formed on the nozzle boundary. Referring to Figure II-3 one can see that both upstream and downstream of the separation region there is flow near the boundary and toward the region. Thus the separation region is the only region where the carbon particles can remain at rest.

It can be seen from Figure IV-1 that for any value of P_o/P_f the area ratio at separation, A_1/A_t, increases as k decreases. The estimated value of k for gaseous anhydrous hydrazine is 1.29, and there is uncertainty in this value. The uncertainty is due partially to the unknown dissociation and its affect on the value of k. Assuming the average value of $k = 1.29$ then hydrazine will separate farther downstream of the nozzle throat than will nitrogen under the same conditions. One thus can deduce that each has its P_o/P_f range of operation. It can also be seen that the difference in A_1/A_t between different k values increases as P_o/P_f increases. With X_1 defined as

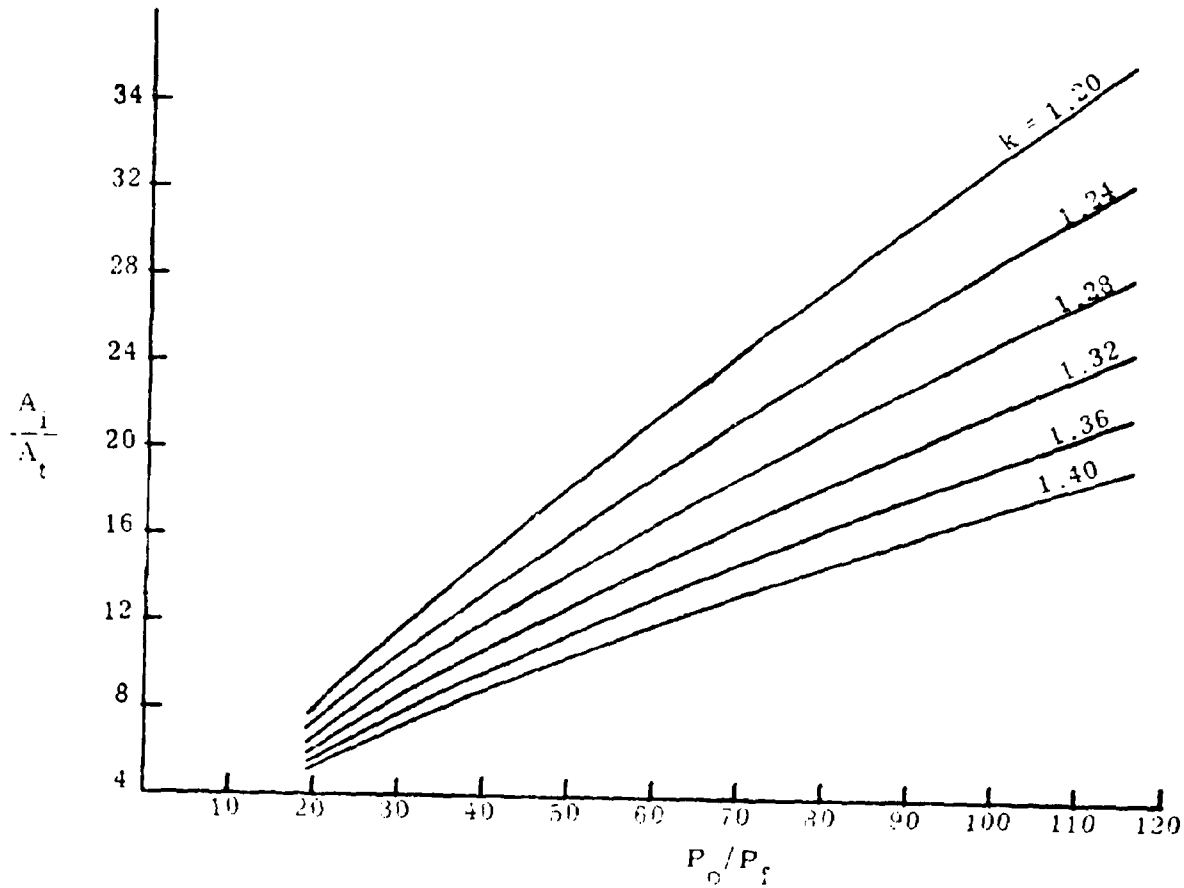

Figure IV-1. Area Ratio at Separation Versus the Chamber to Ambient Pressure Ratio.

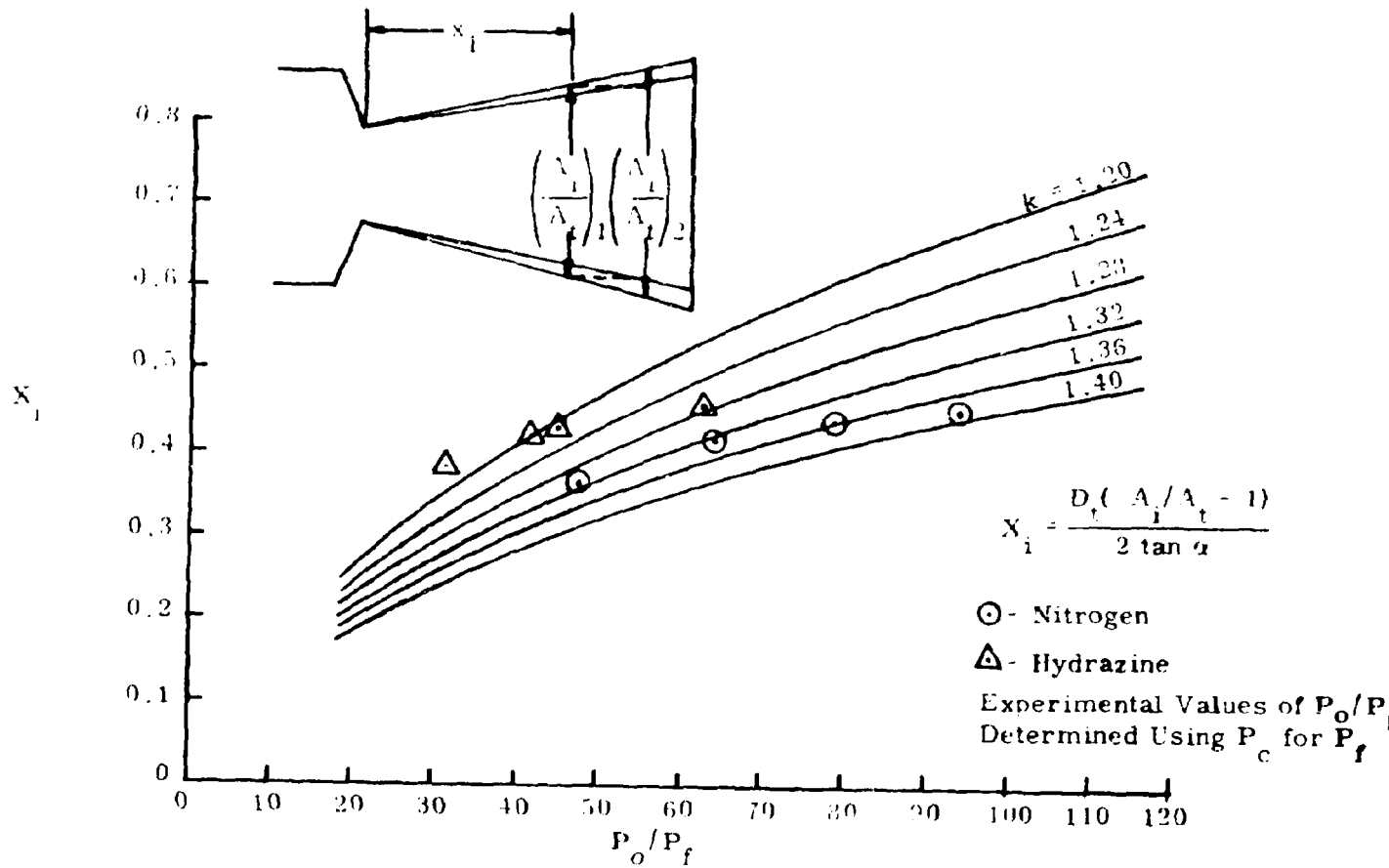

Figure IV-2. Distance Between the Throat and Separation Position Versus the Chamber to Ambient Pressure Ratio.

the distance from the nozzle throat to the separation position a plot of X_1 against P_o/P_f would be expected to yield a trend similar to that in Figure IV-4. The calculated curves of Figure IV-2 confirm this. The experimental X_1 values plotted on the same graph indicate a similar trend although it can be seen that a line connecting the nitrogen and hydrazine points would cross the curves for different k values. A change in P_o/P_f may affect the temperature and percent dissociation of hydrazine and thereby cause a resulting change in k which is indicated in Figure IV-2. This type variation indicated by the experimental points for nitrogen is not expected. The variation between calculated and experimental values could be due to the reduction in cross section of the inviscid flow region caused by boundary layer growth. This reduction was neglected in the bistable theory development. The figure insert on Figure IV-2 shows how the boundary layer build-up can cause error in the calculated and experimental values of X_1 and M_1. Although calculations using the bistable theory indicate the flow should separate at X_1 the growth of the boundary layer reduces the effective area for flow and thus the actual separation position is at X_2.

The experimental values of X_1 were obtained graphically in the following manner. Using projections of the schlieren film, a line, tangent to the shock at the nozzle exit, was projected to the nozzle boundary. The distance from this intersection to the nozzle throat, measured parallel to the model axis, was the experimental X_1.

Figures IV-16 through IV-22 show reproductions of photographs made from the 16 mm film. Film of this type was used to obtain the values of X_1, φ_B and φ_U. Since the experimental value of X_1 for nitrogen and $P_o/P_f = 93.5$ lies close to the k = 1.40 curve but departs from this curve as X_1 decreases, it can be seen that the accuracy of the shock projection method decreases as the intersection position moves nearer the nozzle throat.

Figures IV-3 and IV-4 indicate the calculated Mach Number in the vicinity of the separation region and also the values of P_o/P_f and P_i/P_f respectively, at which the flow separates. Both figures indicate that as P_f is lowered the separation Mach Number increases for a given fluid. At high altitudes this might require an increase in control signal pressure to insure amplifier operation.

Figure IV-5 shows the relation between the pressure ratio P_o/P_f and the angle the oblique shock makes with the model's boundary. These angles are calculated downstream of the separation position and outside the boundary layer. From these curves it can be seen that φ decreases as P_o/P_f increases. Thus, even if the separation region is fixed, there is some $(P_o/P_f)_{max}$ for any amplifier for which the angle φ is too small to direct the free stream boundary past the splitter tip. As P_o/P_f decreases φ increases and will become normal to the free stream boundary for some value $(P_o/P_f)_N$. For $\varphi = \varphi_N$ we know that the streamline direction is unchanged and for $\varphi = \varphi_N - \Delta\varphi$ the direction of the free stream boundary is changed

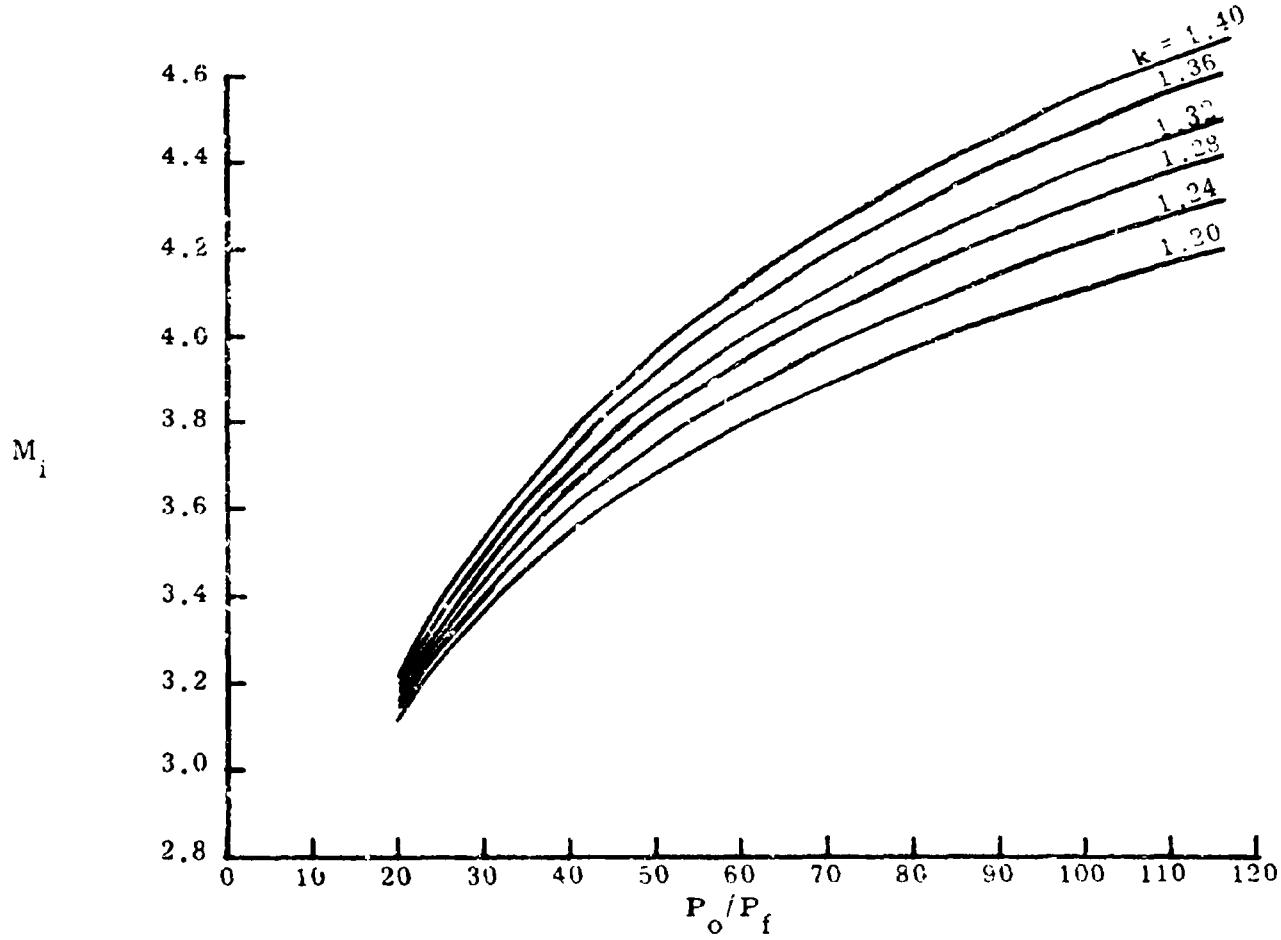

Figure IV-3. Mach Number Variation Versus Chamber to Ambient Pressure Ratio.

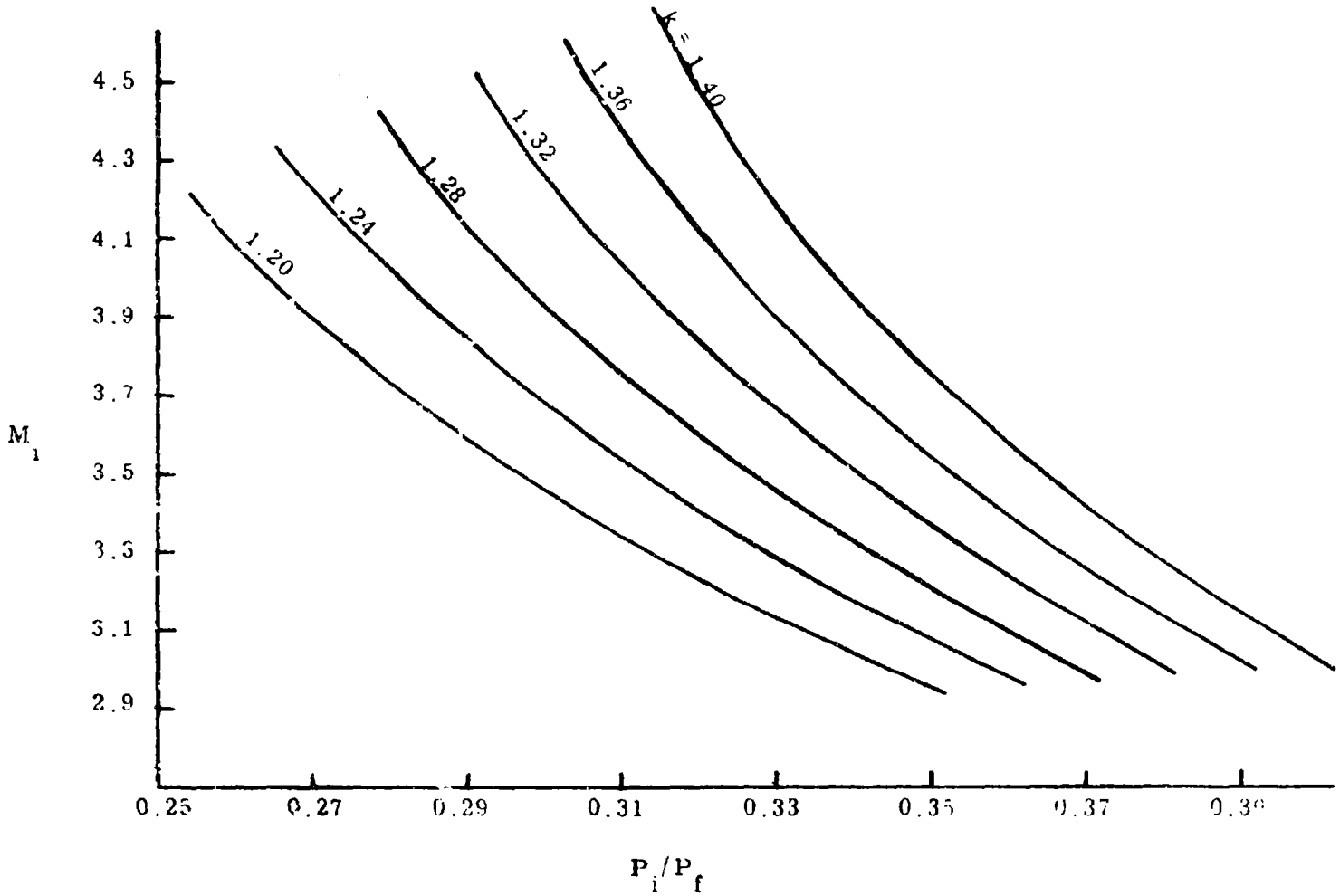

Figure IV-4. Separation Mach Number Variation Versus Ratio of Separation to Ambient Pressure.

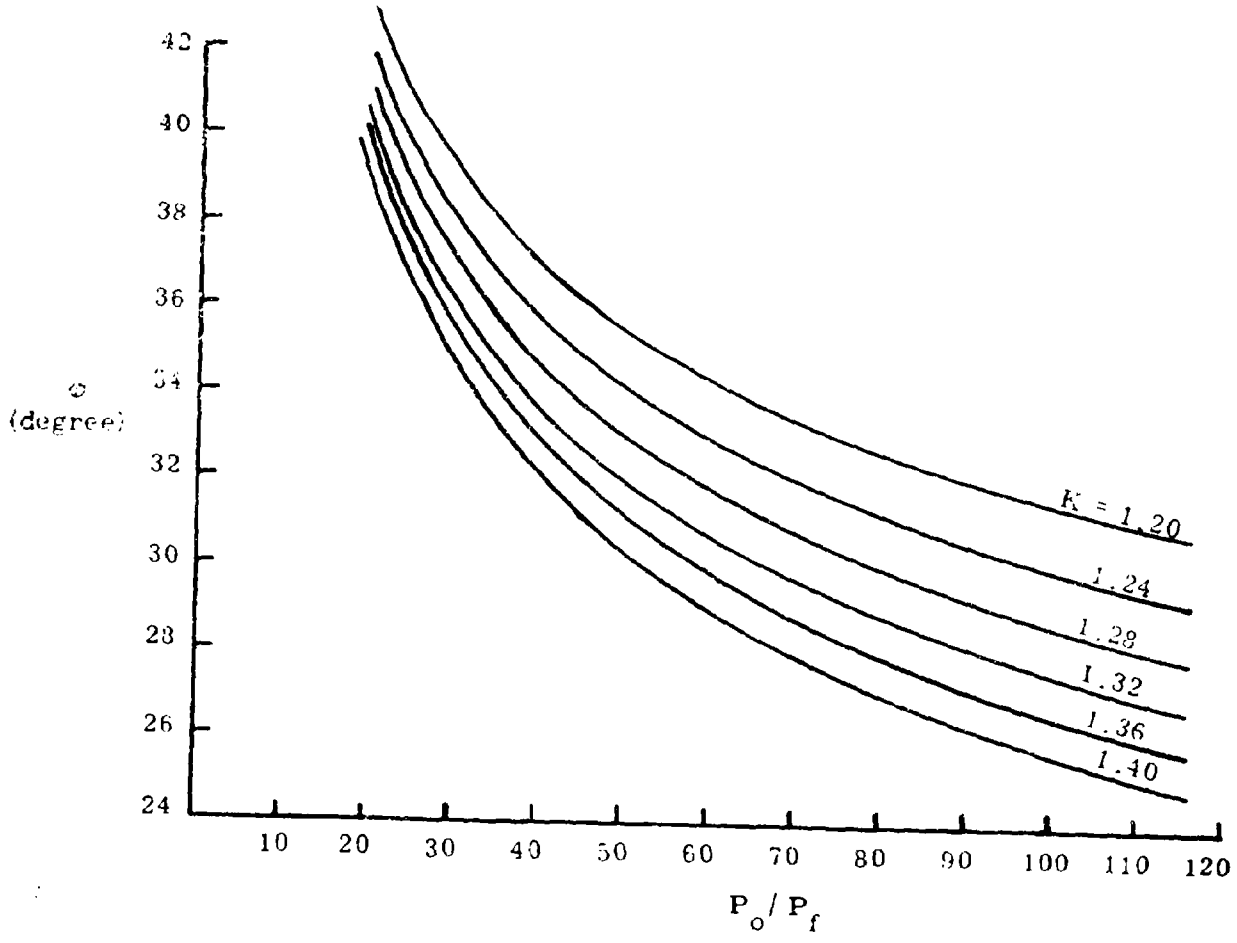

Figure IV-5. Shock Angle Versus the Chamber to Ambient Pressure Ratio.

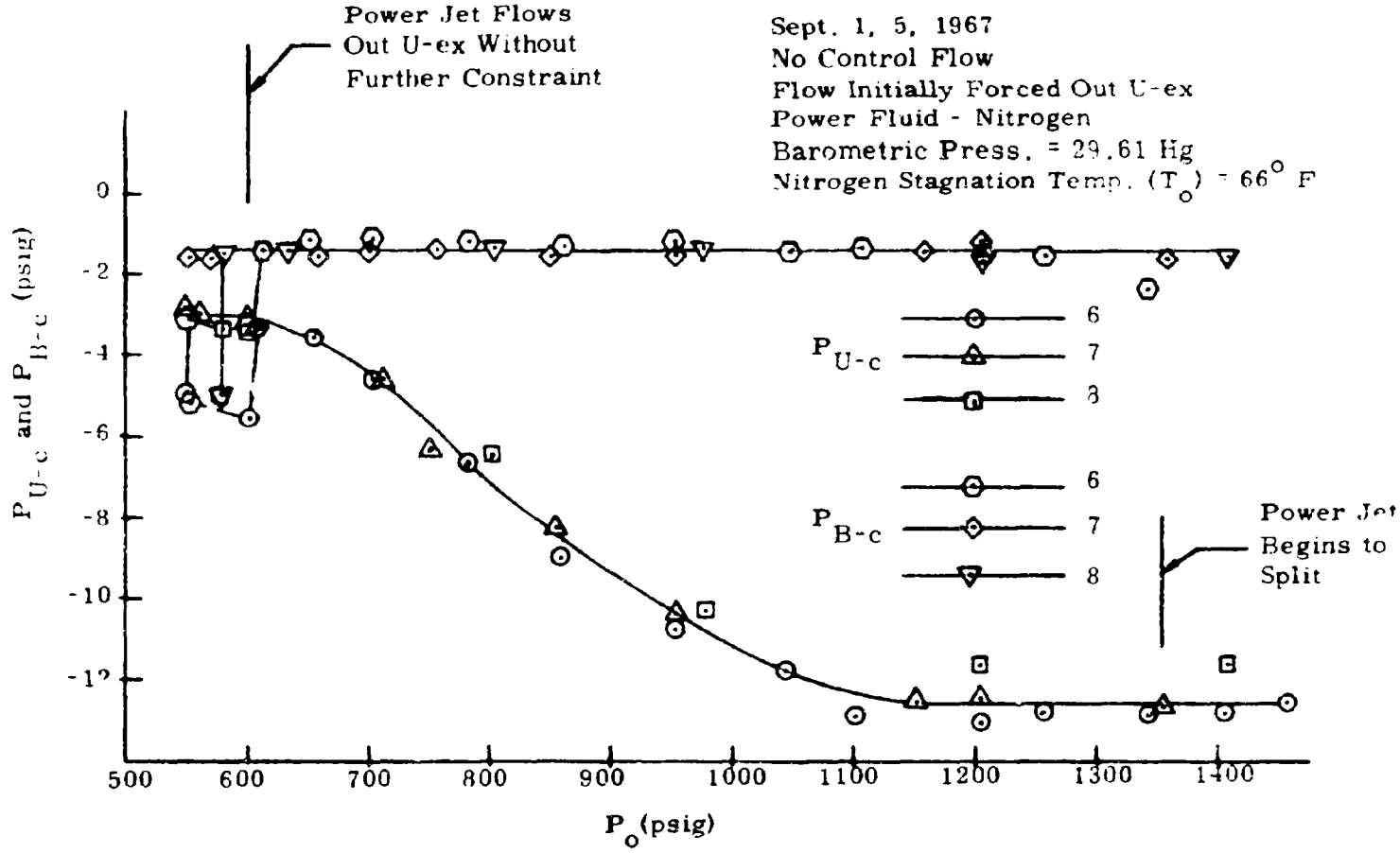

Figure IV-6. Control Port Pressure Variation as P_o is Gradually Increased

only slightly. Thus, for the values of (P_o/P_f) there is some lower limit $(P_o/P_f)_{min}$, for which the amplifier will be bistable. Figure IV-6 shows experimentally that (for P_{atm} = 14.4 psia)

$$(P_o/P_f)_{min} \approx (P_o/P_c) = 614.4/13.0 = 47.2$$

and

$$(P_o/P_f)_{max} = 1414.4/13.0 = 109$$

where P_c is measured in the vicinity of region f. These values would vary for different amplifiers.

Rough calculations of θ for bistability for geometrical considerations alone require that $\theta_{min} = 21^o$. This value of θ_{min} was calculated for the following conditions: $\alpha = 14.0^o$, $P_o/P_c = P_o/P_a = 1414/14.4$, the separation position is determined using the bistable analysis and the splitter tip position is located 1.25 inches from the separation position. It is also assumed for this calculation that the free stream boundary approximates a straight line from separation to the splitter tip. θ obtained from results of the bistable analysis in Section II predict values in the neighborhood of 16.58. Since it has been observed experimentally that flow in the amplifier is stable for $P_o/P_a = 1414/14.4$, then it can be seen that the bistable analysis predicts a smaller range of P_o/P_a than that for which flow in the amplifier is bistable.

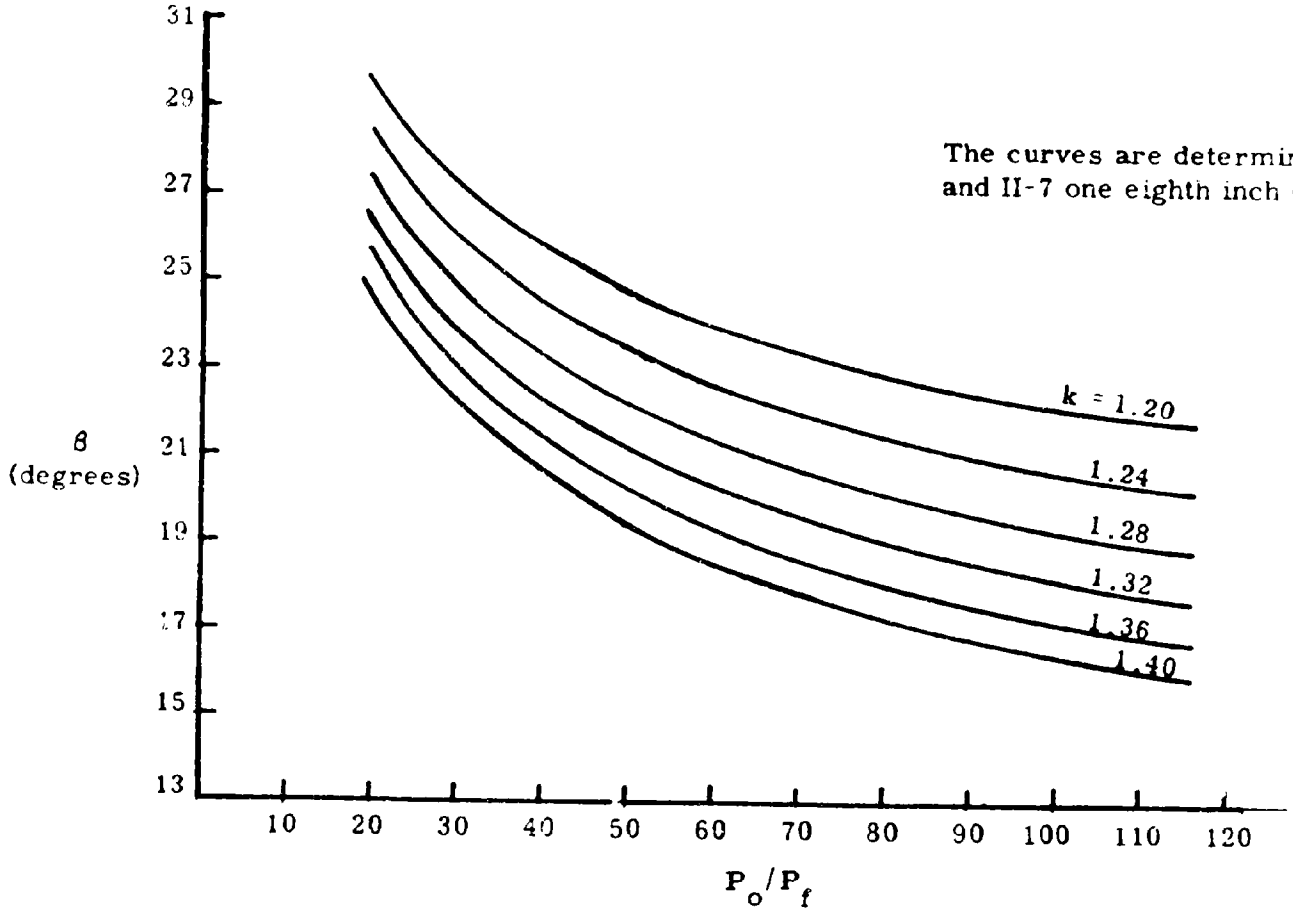

The curves are determined by equations [illegible], II-6 and II-7 one eighth inch downstream of separation.

Figure IV-7. Variation of the Free Stream Boundary With the Ratio of Chamber to Ambient Pressure.

Probably the major cause of the disagreement in the calculated and experimentally observed θ values is that no consideration was given to the reduction of cross-sectional area available for flow due to boundary layer growth in the bistable analysis formation. In his dissertation Duffy (7) determines the boundary layer thickness along the wall of a 15^{o} half angle conical nozzle by theoretical approximation and also experimentally. His plots of data indicate that the boundary layer increases approximately linearly from the throat. Assuming the boundary layer he obtains with an air supply pressure of 1000 psig is similar to the one obtained with nitrogen, and the streamline between the boundary layer and inviscid flow is the deflected free stream boundary then $\theta_{min} = 17^{o}$ is obtained, which is much closer to the calculated value of $\theta = 16.58$. These calculations indicate that the boundary layer growth is a significant mechanism in bistability.

No geometrical considerations restrict P_o/P_1 such that it must be above some value $(P_o/P_1)_{min}$ to maintain stable flow as the splitter tip placement requires a P_o/P_1 below a $(P_o/P_1)_{max}$. The fixed position of the model's control ports, together with the fact that control flow will flow around a power stream which does not fill the flow area, prevented a meaningful experimental investigation of the phenomenon in this P_o/P_1 region with this amplifier.

Figure IV-8 shows the general agreement of experimentally determined values of P_o/P_1 and with the $K = 1.40$ curve determined

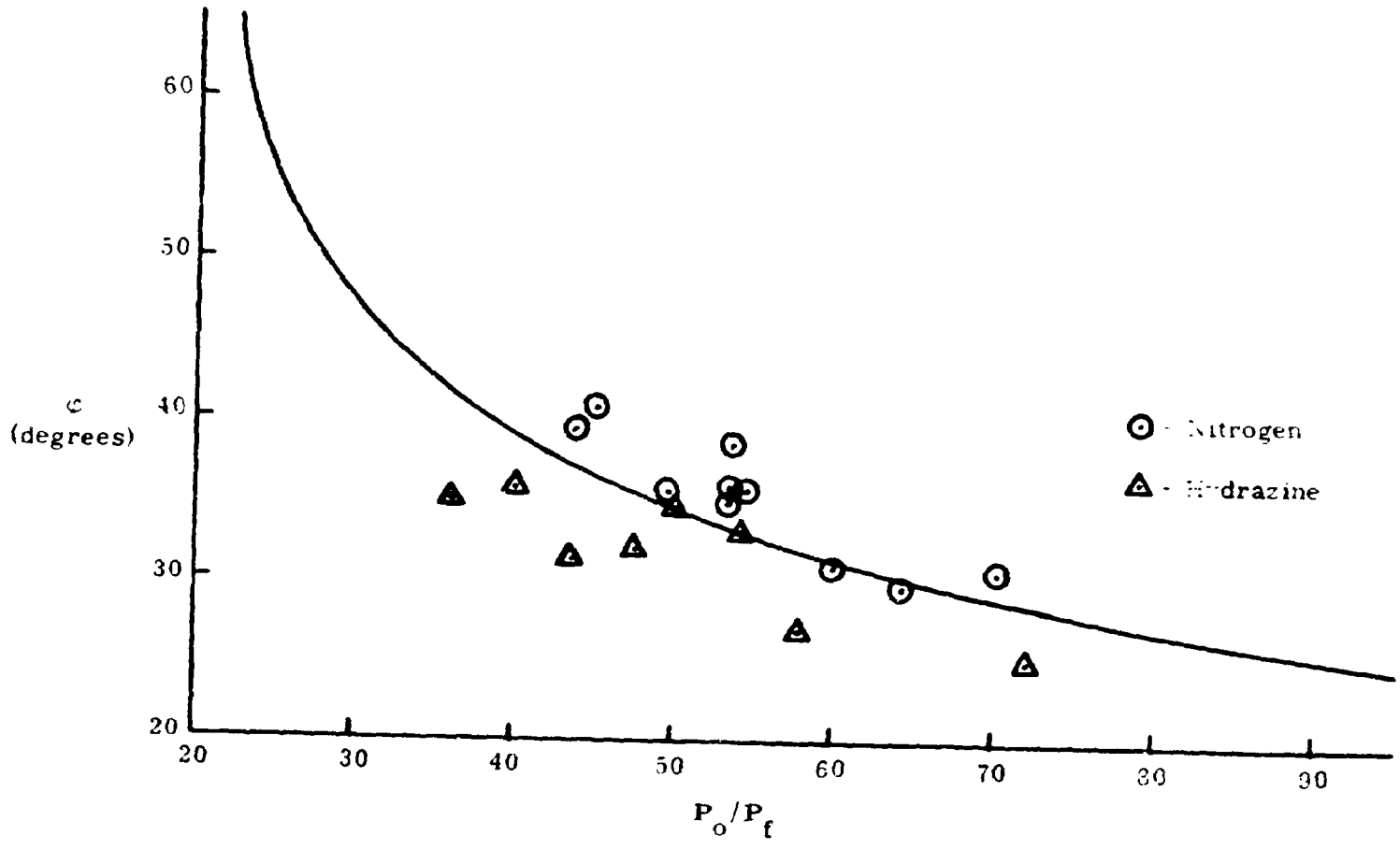

Figure IV-8. Experimental Values of P_o/P_c vs. Shock Angle at Control Volume Exit.

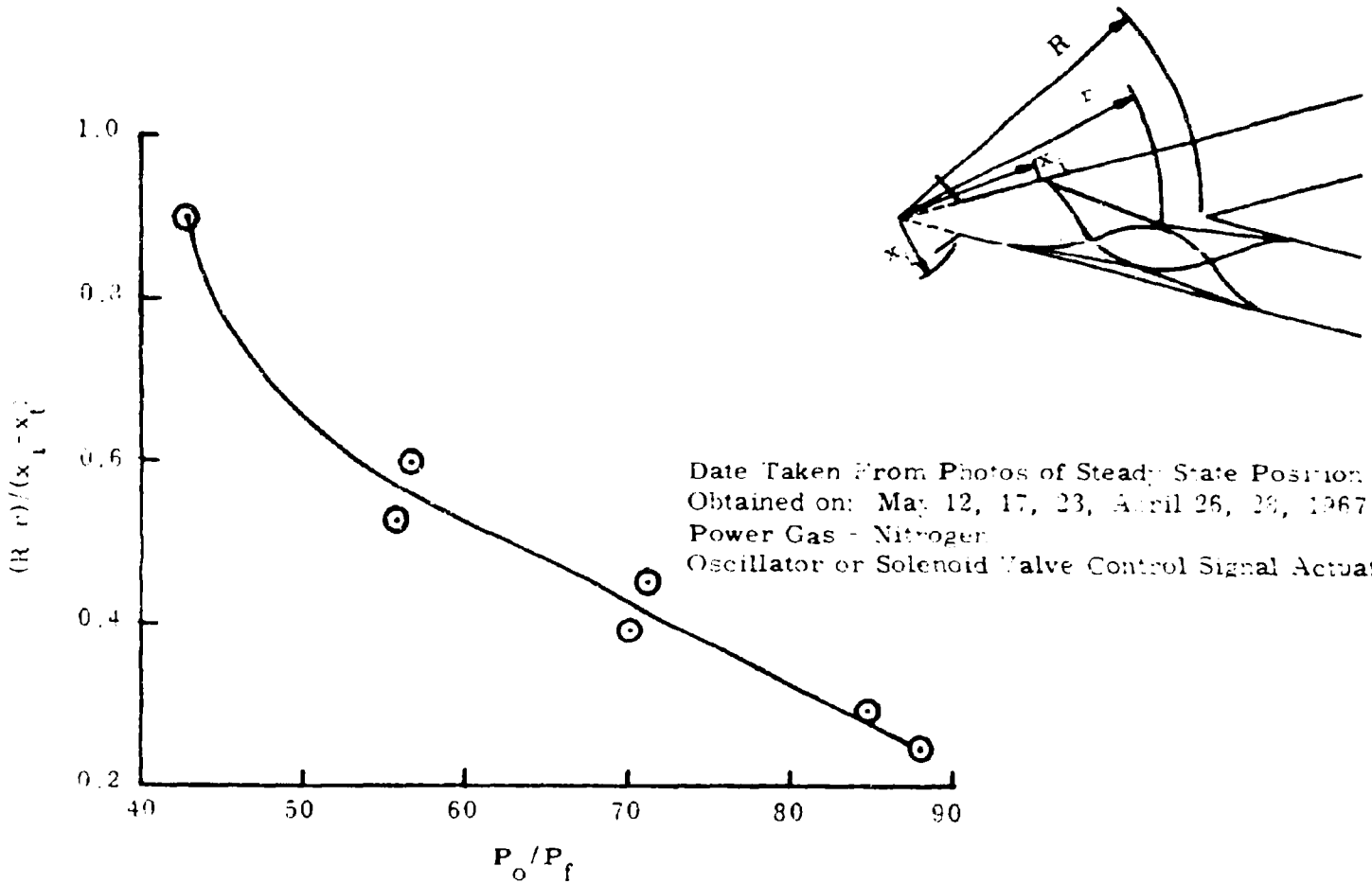

Date Taken From Photos of Steady State Position
Obtained on: May 12, 17, 23, April 26, 28, 1967
Power Gas - Nitrogen
Oscillator or Solenoid Valve Control Signal Actuator

Figure IV-9. Shock - Free Stream Boundary Intersection Variation With P_o/P_f.

from the bistable theory of Section II. P_c is the stagnation pressure of the control signal and this control signal corresponds to the shock angle designated as φ_{max}, and is the second coordinate determining the experimental points.

Figure IV-9 shows the plot of experimental values of P_o/P_f versus $(R-r)/(X_t-X_i)$. R-r is the distance between the first free stream boundary-shock intersection and the splitter tip. $X_t - X_i$ is the distance from the nozzle throat to the separation region. This information could be of help in determining splitter tip positions for similar amplifiers.

Figures IV-10, 11, 12, 13, and 14 show the experimental values of the upper (φ_U) and lower (φ_B) shock angles during the time when the power stream is switching. These five figures also show a representative partial cycle of the control pressures recorded at U-c and B-c. Full cycle plots of $P_{U\text{-}ex}$, $P_{B\text{-}ex}$, $P_{U\text{-}1}$ and $P_{B\text{-}1}$ are included. Since syncronization between film and oscillograph data was not achieved, a representative pressure cycle was chosen to show the relation between control pressure rise and the shock angle magnitude during switching. In all cases the beginning of switching is defined as the time when the shock angle with the smallest magnitude begins to increase. It is defined in this manner because when a control flow is used to switch the power stream the smaller shock angles increase as the control pressure increases. For example, if the power stream switches from the lower to the upper exhaust channels, then the lower

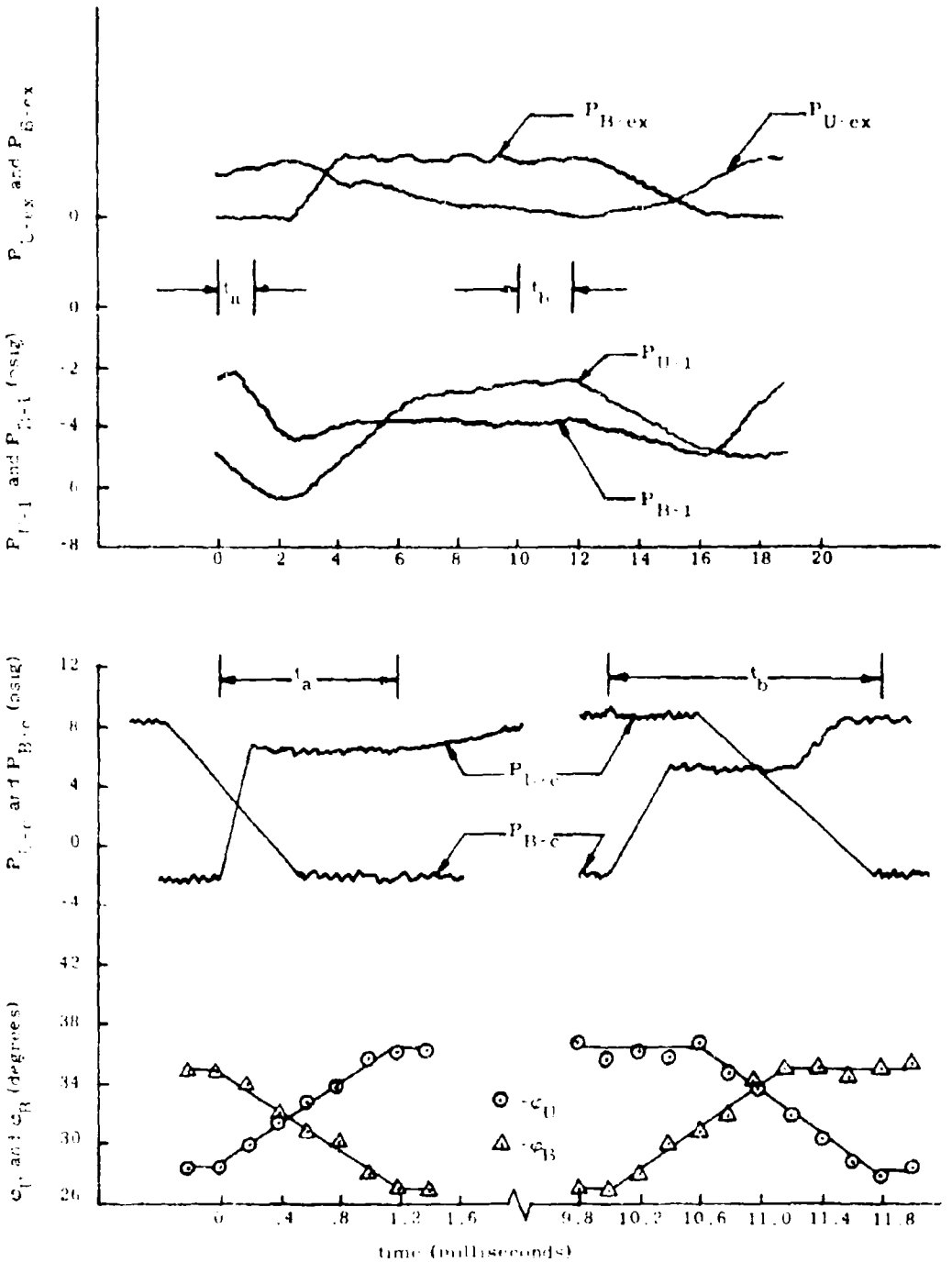

Figure IV-10. Pressures and Shock Angles Versus Time, P_o = 1200 psig, Power Gas = Nitrogen, Oscillator Control

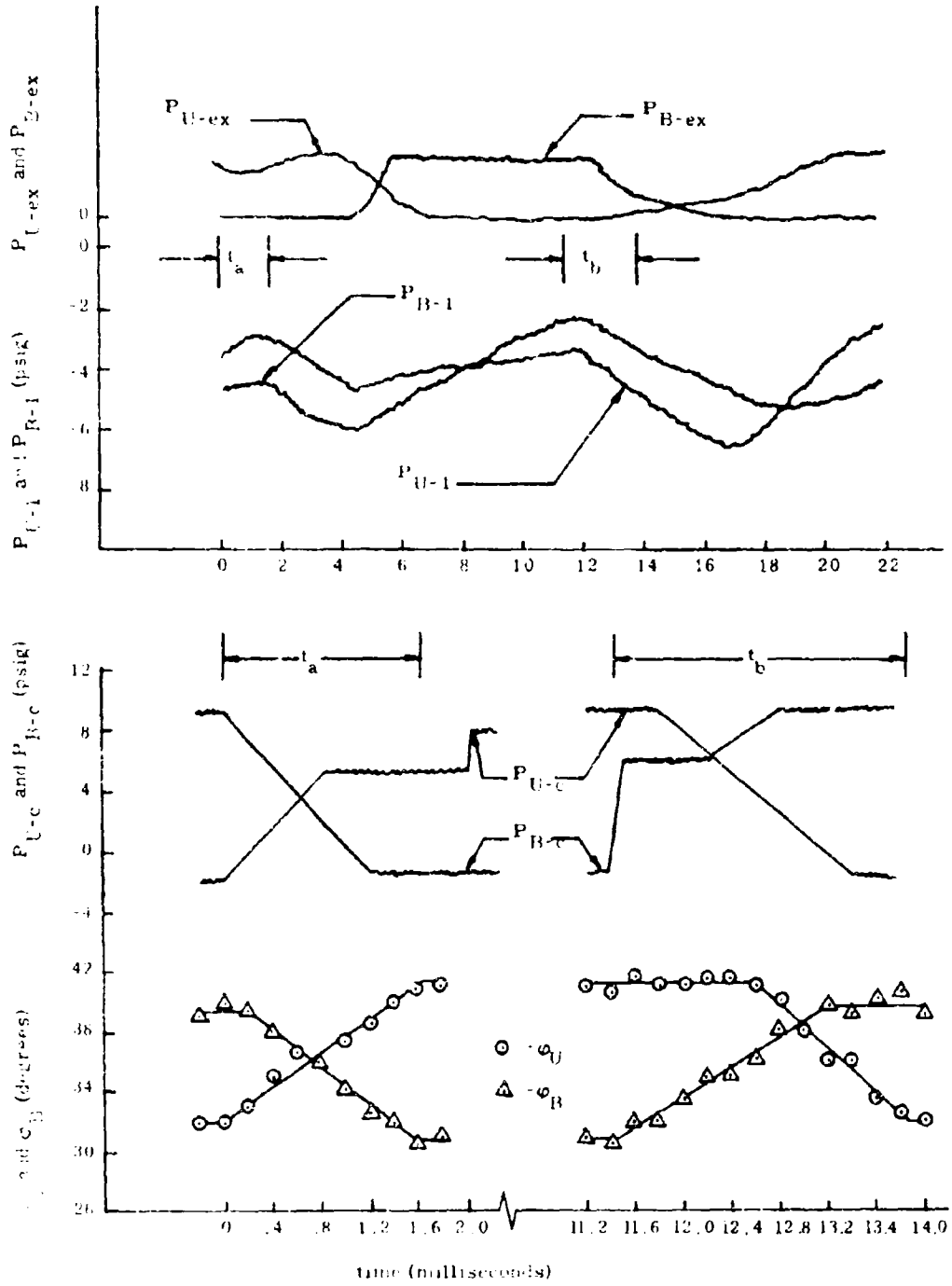

Figure I. 11. Pressures and Shock Angles Versus Time. P_o = 1000 psig, Power Gas - Nitrogen, Oscillator Control

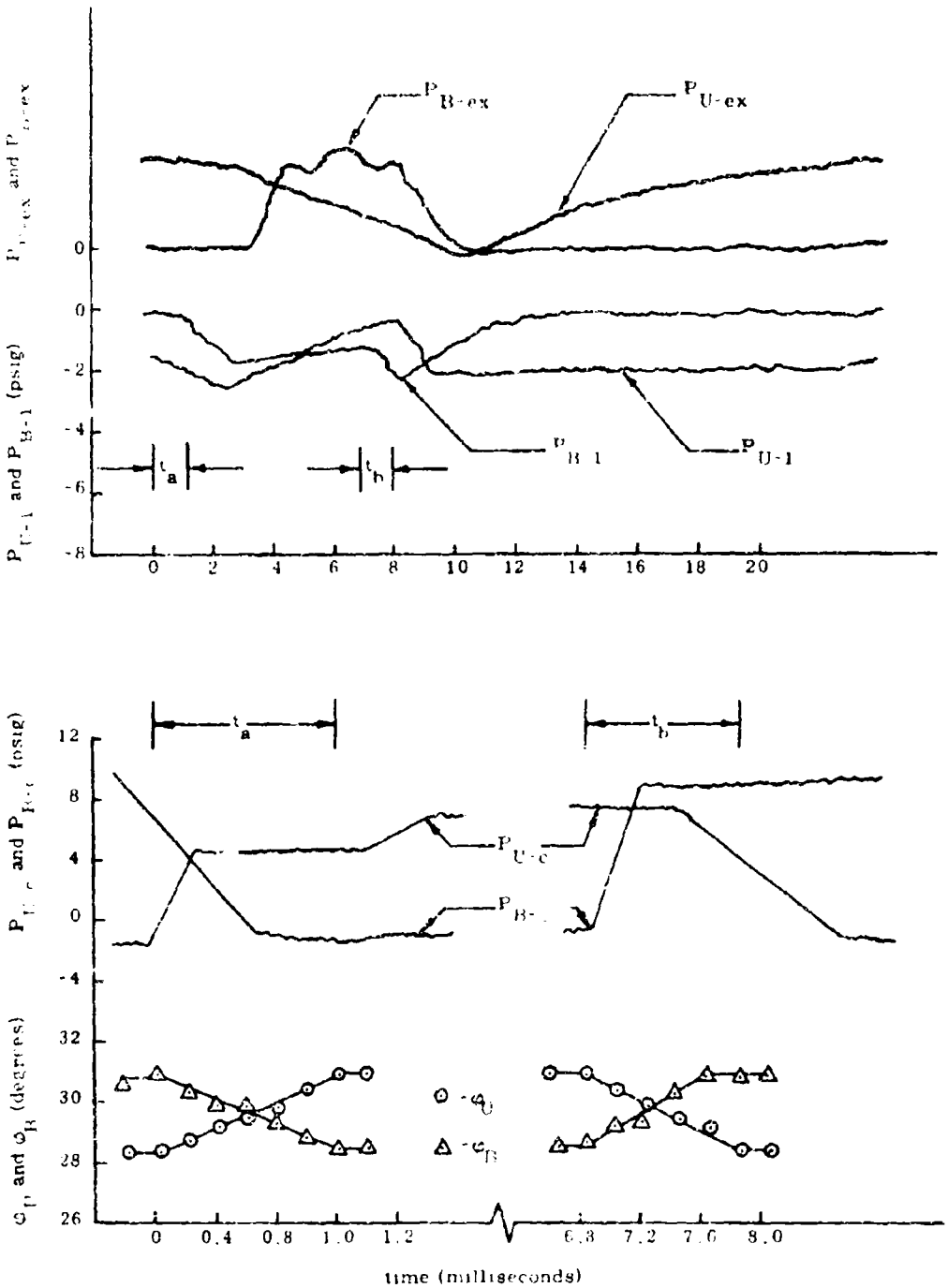

Figure IV-12. Pressures and Shock Angles Versus Time. P_o = 1000 psig, Power Gas - Hydrazine, Oscillator Control

shock angles must increase as control flow is initiated. The end of switching will be defined as the time when all shock angle change ceases.

Two time scales are utilized on Figures IV-10, IV-11, and IV-12. The scale for the shock angles and control pressures is four times greater than the scale for the exhaust pitots and wall pressures. Values of shock angles and control pressures are shown only for the part of the time cycle when the power stream is shifting from the upper to lower and from the lower to upper exits. Characteristics of the pressures from the oscillograph chart have been shown on these plots. These show, for example: control pressure rise versus time as nearly a straight line, pressure variations about the final maximum or minimum pressures, oscillator characteristics such as the partial rise of control pressure with a time lag at this pressure and then the final pressure rise and the nonuniform control pressures supplied by the oscillator.

A full cycle of pressures recorded by the exhaust pitot and wall pressure transducers at U-1 and B-1 are shown on the upper two graphs. Since the zero of time for all four curves on a graph are the same it can also be seen, as would be expected, that the pressure response recorded by the wall transducers and exhaust pitots lag the control pressures. It is noted at this point that the pitots were made of simple tubing. The positioning of the pitots over the exhaust exits was not rigidly fixed and the transducers sensing the exhaust

pressures were not calibrated since qualitative data only was required of them.

Positive and negative control will now be defined. When the amplifier exhibits positive control the power flow leaves the amplifier on the opposite side from which the control signal is applied. For example, if the lower control port supplies the control signal, then the power flow leaves the amplifier from the upper exhaust channel. Negative control is the reverse of positive control. When the lower control port supplies the control signal, the power fluid leaves the amplifier from the lower exhaust. Positive control is demonstrated in Figure IV-10, IV-11 and IV-14. Negative control is demonstrated in Figure IV-13 and IV-15. Figure IV-12 is an example of a case when the power stream was not fully controlled.

When φ_L is increasing the first bar from the time scale origin of Figure IV-10 indicates the time when control flow from the upper control port is first detected on the high speed schlieren film. From the film it can also be determined that the lower control flow begins to decrease at this time. The shock angles also indicate this. From Figure IV-10 it can be seen that φ_L for power flow out B-ex is greater than φ_L when power flow leaves the amplifier by L-ex. This is due to the control pressure at L-c being greater, when the power flow is out B-ex than the control pressure at B-c which the power fluid leaves by L-ex, and possibly to a slight bias in the model. The bias could be caused by a slight misalignment of the upper flow surface could

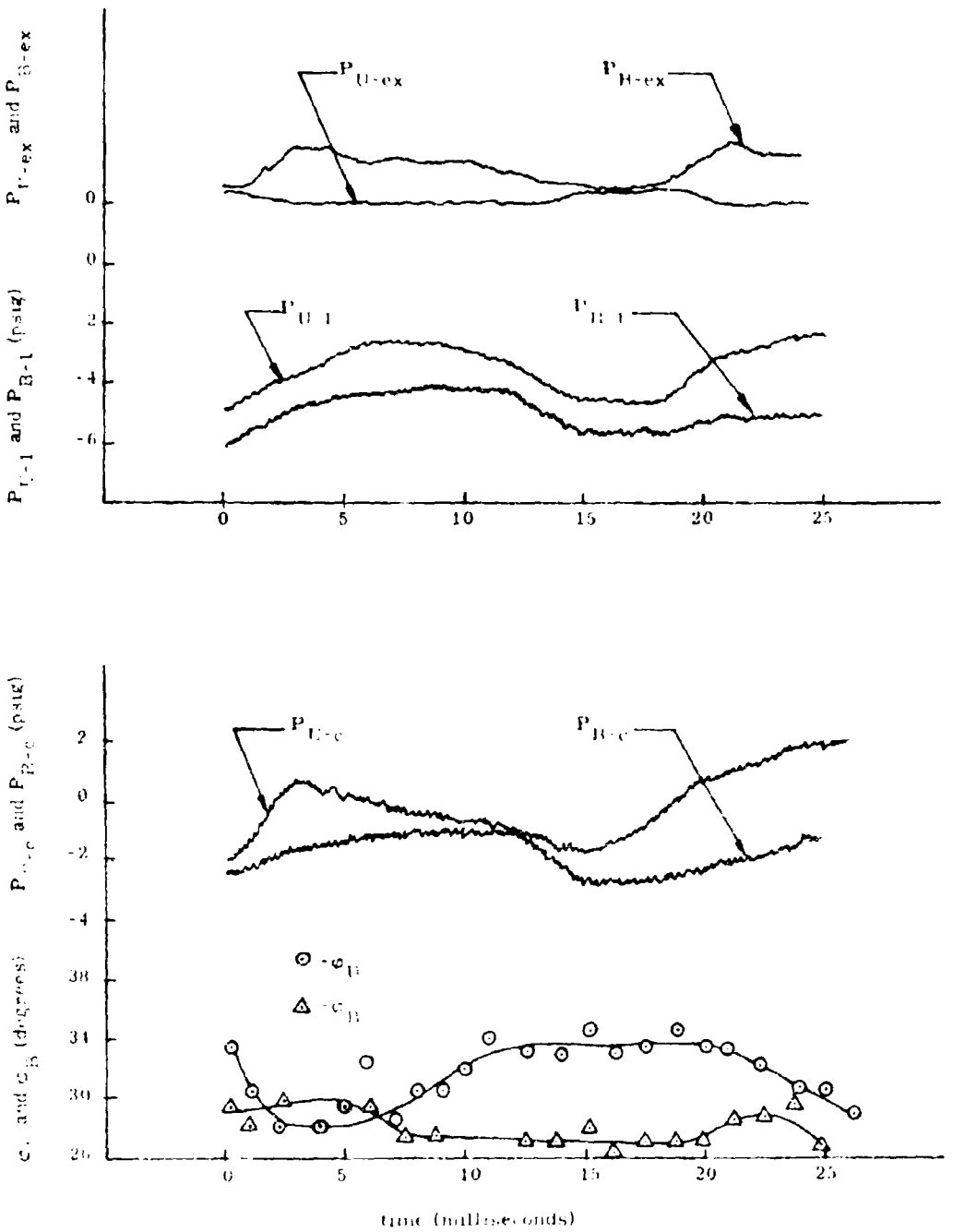

Figure IV-13. Pressures and Shock Angles Versus Time. P_o = 800 psig, Power Gas = Nitrogen, Oscillator Control

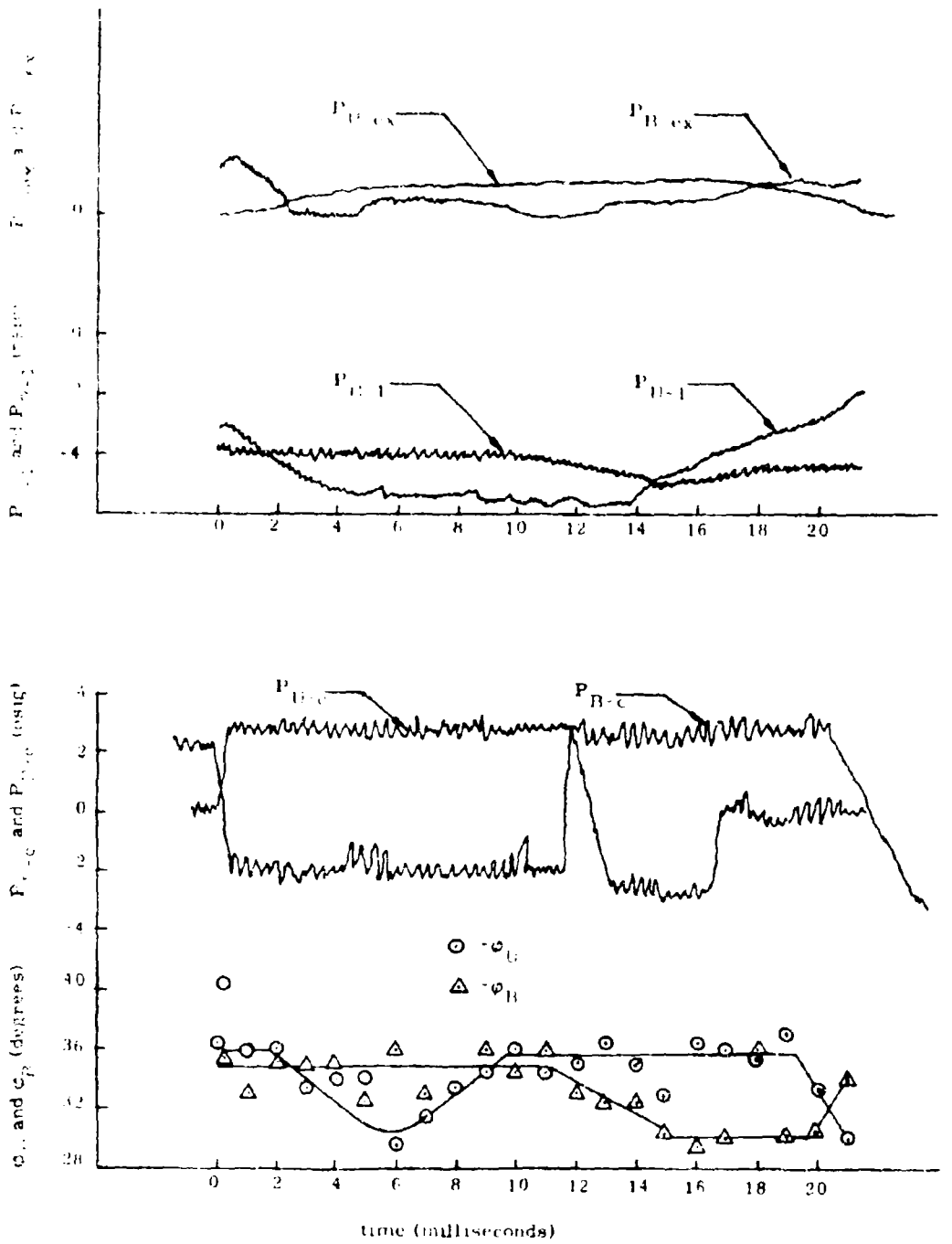

Figure IV-14. Pressures and Shock Angles Versus Time. P_o = 600 psig, Power Gas - Nitrogen, Oscillator Control

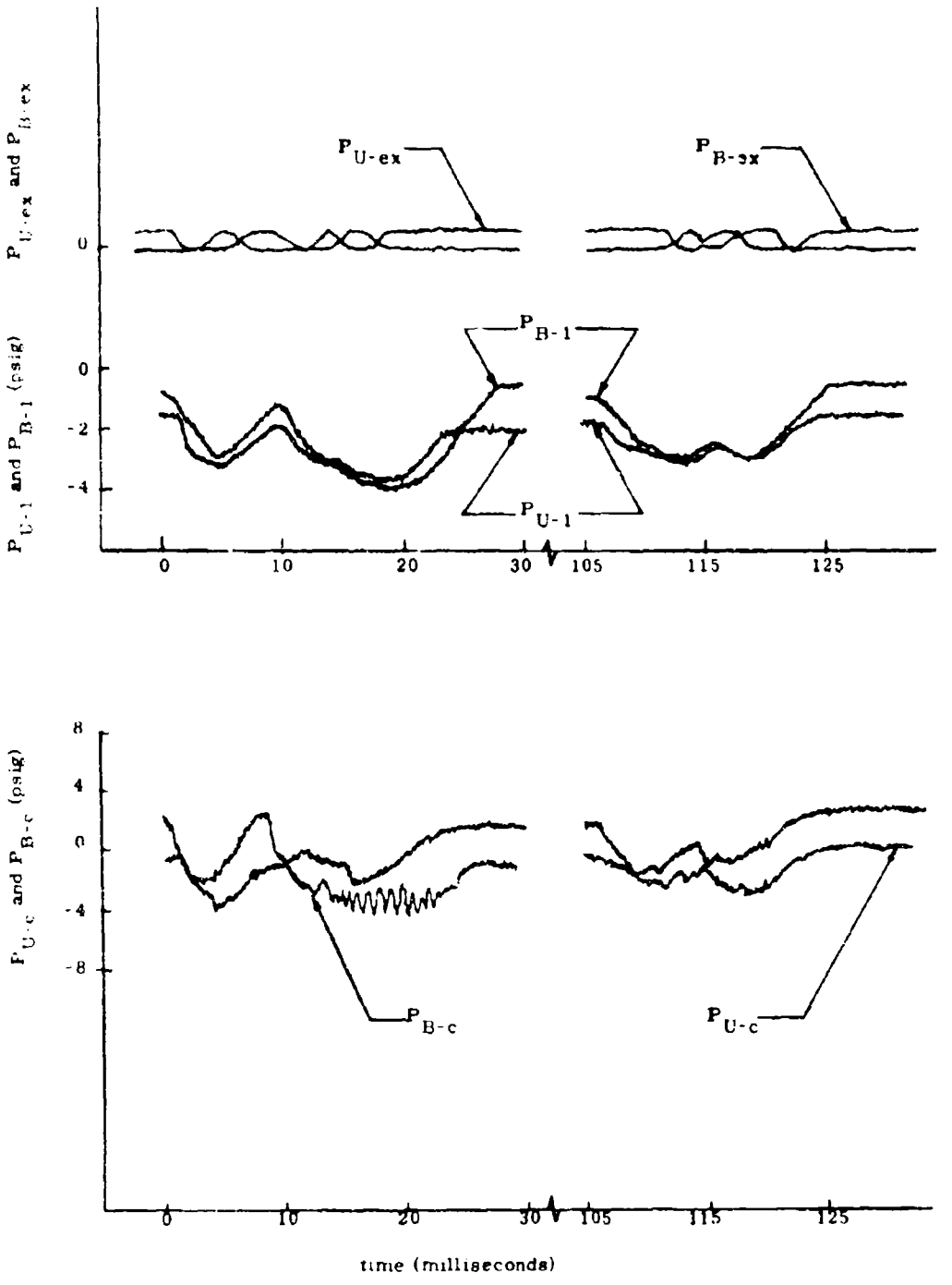

Figure IV-15. Pressures and Shock Angles Versus Time. P_o = 250 psig. Power Gas - Nitrogen, Solenoid Valves

possibly be a little rougher than the lower surface. If the upper surface were rougher this would cause an additional pressure disturbance in this overexpanded flow region that would affect the flow to a greater degree than if the stream were not overexpanded. The bias is more apparent in Figure IV-11 where the slight control pressure difference indicates that φ_B for flow out U-ex should be larger than φ_U when flow is out B-ex.

The second bar from the time scale origin of Figure IV-10 represents the time when the upper control flow can last be detected on the schlieren film. It can be seen that the upper control flow continues for approximately eight tenths of a millisecond after the lower control pressure begins. Because of this lag in upper control shut off, it can be determined from the φ-t graphs that the switching of the power fluid from B-ex to U-ex takes longer. This same control pressure lag can be seen in Figure IV-12. It may be noted in Figures IV-10 and IV-12 that the shock angles do not become equal or change appreciably, as might be expected, when the pressure in the on control port begins to decrease before positive control pressure is supplied from the other port. This is due to the reverse flow from the atmosphere which constrains the power stream to flow out the same exit until the pressure differential which exists between the upper and lower boundaries is destroyed. In reality the reduction of the control pressure after the power stream has switched would insure the ease of the next switch as can be seen from the φ vs t curves.

Figure IV-11 shows the same type data plots for a chamber pressure of P_o = 1000 psig and nitrogen as the power gas. Observations similar to those made about Figure IV-10 for which P_o = 1200 psig can also be made for the plot of data representing this test. Figure IV-12 is another plot of this type data for P_o = 1000 psig and hydrazine as the power gas. The first half cycle shown, when the power stream switches from the upper to lower exits, occurs normally except for the reduction of the bottom control pressure (P_{B-c}) before the upper control pressure (P_{U-ex}) begins to increase. Even if this occurs, as noted previously the angles do not change because of the reverse flow from the atmosphere until P_{U-c} begins to increase and destroy the low pressure region at the upper flow boundary. The second half cycle shows the reverse oscillator characteristic. P_{B-c} builds to its final value before P_{U-c} begins to decrease. Although the upper shock angle reaches a stable value two-tenths millisecond later than the lower shock angle there is little apparent affect on the shock angles which could not be explained by error in data reduction. The apparent delayed reduction in P_{U-c} should delay the reduction in φ_U. This does not happen. On the contrary the hydrazine power fluid was switched by the control flow smoothly, as is indicated by watching the high speed schlieren film and the plot of the shock angles taken from this film. There is six-tenths millisecond between the beginning of rise of P_{B-c} and fall of P_{U-c}, therefore it appears that there should be about a six-tenths millisecond delay between the

beginning of rise in φ_B and the beginning of fall of φ_U. In no other test does the oscillator display this characteristic in actuating the control signal, and as mentioned previously there was only one hot gas test performed with the oscillator used as the control signal actuator. Although it is possible to adjust the oscillator such that this type control signal is generated, no explanation is apparent to explain why the reduction in magnitude of φ_U is not delayed six-tenths millisecond by the delay in reduction of P_{U-c}.

Figure IV-13 shows a plot of shock angles, control signal pressures, wall pressures P_{U-1} and P_{B-1} and exhaust pitot pressures for P_o = 800 psig. As can be seen from observing the control pressure plot, the oscillator did not supply a good switching signal. Many attempts were made to make the amplifier switch when the supply pressure was 800 psig but at no time did the amplifier switch at this pressure when the oscillator was used as the control signal actuator. The control signal pressures shown in Figure IV-13 did not switch the power fluid and it was found experimentally that at this chamber pressure, control pressures up to approximately 10 psig would not cause switching.

The data plotted in Figure IV-14 is for a supply pressure of 600 psig, nitrogen power fluid and the switching signal actuated by the oscillator. Shock angle data appears haphazard in the plot. This is primarily due to the reduced clarity of angles when the power stream separates within the nozzle far from the nozzle exit (about

two-tenths of an inch as calculated using Figure IV-2 and assuming an atmospheric pressure of 14.5 psig). The amplifier operates with negative control for this P_o as is seen by observing the high speed schlieren film or by observing the time plots of φ and control pressure. From observing the film it is apparent that the power flow doesn't switch the power fluid completely to either exit, although this is not obvious from the exhaust pressure plot.

Figure IV-15 shows a complete cycle of pressure time curves obtained from the oscillograph pressure time record when solenoid valves were used as the control signal actuator, the chamber pressure was 250 psig and nitrogen was the power fluid. No shock angles could be obtained from the schlieren film but it is perfectly clear that the power stream switches negatively when the control pressure versus time curve is considered along with the exhaust pressure versus time curve. When a control flow is supplied at C-c the power flow leaves the amplifier from the upper exit, which is the definition of negative control.

Using the time lapse from the beginning to the end of all φ changes as the definition of switching time, and the φ vs t curves, a table of switching times can be compiled. The control signal was actuated by the oscillator for all switchings listed in Table IV-1. The control pressures listed in Table IV-1 are not necessarily the minimum pressures required to switch the power stream. They merely show the actual pressures which were used to switch the

Table IV-1. Switching Times for Different Chamber Pressures, Gases and Directions of Switch

Power Fluid	P_o (psig)	Direction of Switching	Δt (milliseconds)	P_c (psig)
Nitrogen	1200	U to B	1.12	6.0
Nitrogen	1200	B to U	1.70	5.0
Nitrogen	1000	U to B	1.60	5.0
Nitrogen	1000	B to U	2.50	5.0
Hydrazine	1000	U to B	1.20	4.2
Hydrazine	1000	B to U	1.04	9.0

power stream in these tests. From observing the times of switching, it appears that greater control pressures tend to decrease switching times, as is indicated by comparing the cases of nitrogen when the supply pressure is 1000 psig and hydrazine at the same supply pressure. This would normally be expected.

In order to obtain conclusive experimental evidence showing that smaller switching times will be obtained using larger control pressures, data from experiments should be examined in which variations of the other parameters are eliminated. For example, the time between the beginning of rise of P_{U-c} and fall of P_{B-c} and vice-versa should be the same in all cases. As can be seen from the φ vs t curves, Δt is greater when the control pressure on the side to which the stream is to switch does not begin to decrease at the same time the opposite control pressure begins to increase.

Figure IV-16 shows a sequence of enlarged frames taken from the 16 mm schlieren film. They show the amplifier's power stream switching from the upper to lower exit. Considerable change in the shock pattern can be detected between frames (a) and (b). A light spot shows at the upper control port entrance to the power flow channel in frame (b), which does not appear in frame (a). When this light spot can be detected at either control port entrance, a control flow is being supplied at that port.

Figures IV-16 through IV-19 show typical flow situations with nitrogen as the power fluid. They also illustrate the type of photographs from which shock angles (φ_U and φ_B) were recorded from each frame of a typical switching sequence in order to obtain Figures 10 through IV-15. Figures IV-16 and IV-17 illustrate well-defined switching sequences at chamber pressures of 1200 and 1000 ps respectively. As shown in Figure IV-18 at chamber pressure P_o = 800 psig the amplifier does not completely switch. It can be seen that the power stream partially switches but never splits evenly between the exit channels.

Figure IV-19 shows a negative switching sequence and also shows the lag in upper control cut off. In frame (a) it can be seen that the upper control port (U.C.P.) is supplying control flow. In frames (b), (c), and (d) the U.C.P. is still supplying flow but now the lower control port (L.C.P.) is supplying control flow also. In frame (e) the U.C.P. is off and L.C.P. on. In frame (f) the L.C.P. continues to

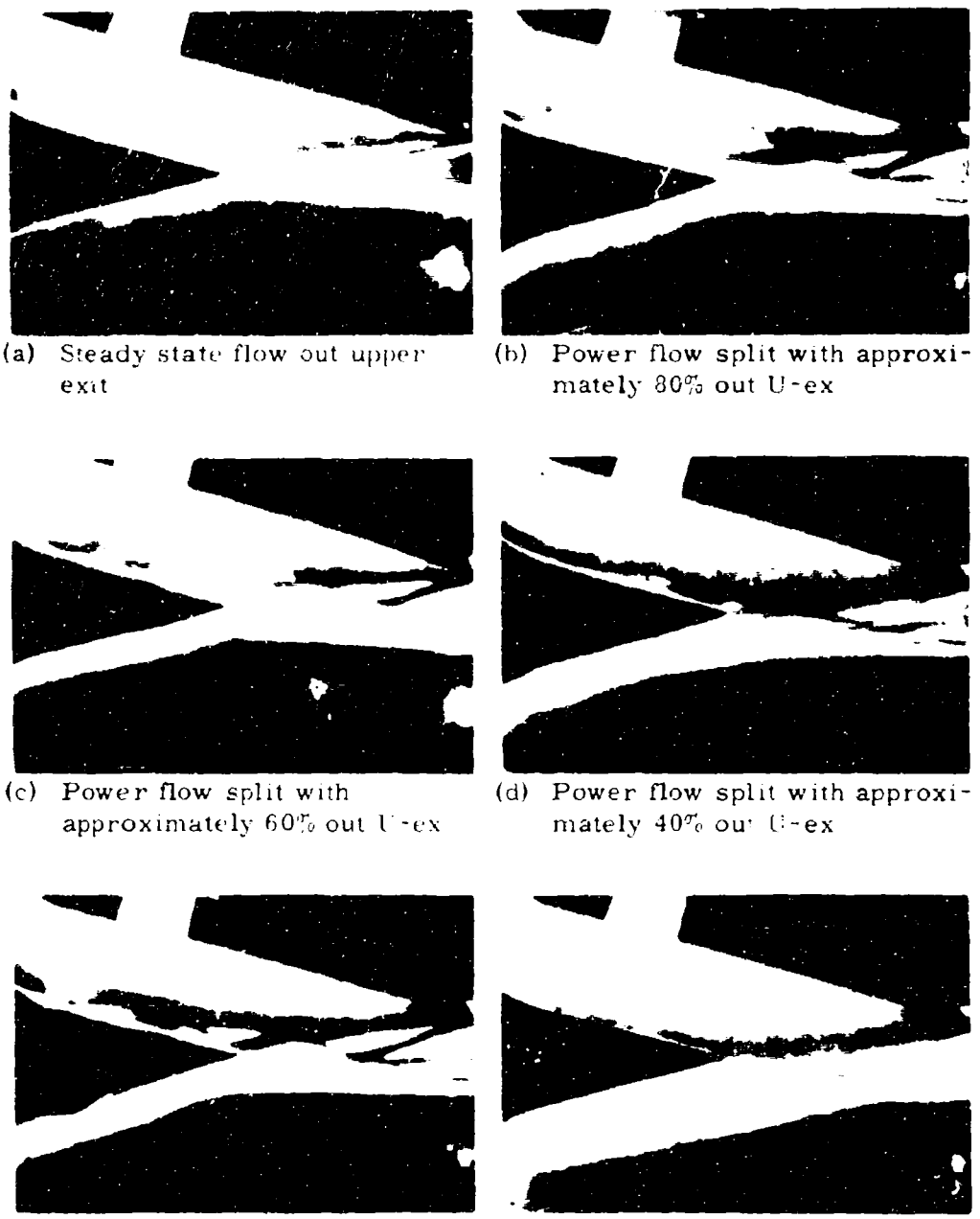

(a) Steady state flow out upper exit

(b) Power flow split with approximately 80% out U-ex

(c) Power flow split with approximately 60% out U-ex

(d) Power flow split with approximately 40% out U-ex

(e) Power flow split with approximately 20% out U-ex

(f) Steady state flow out bottom exit

Figure IV-16. Schlieren Photographs of Power Stream Switching. Power Fluid - Nitrogen, P_o = 1200 psig Oscillator Actuated Control Signal at 50 ± 5 cps.

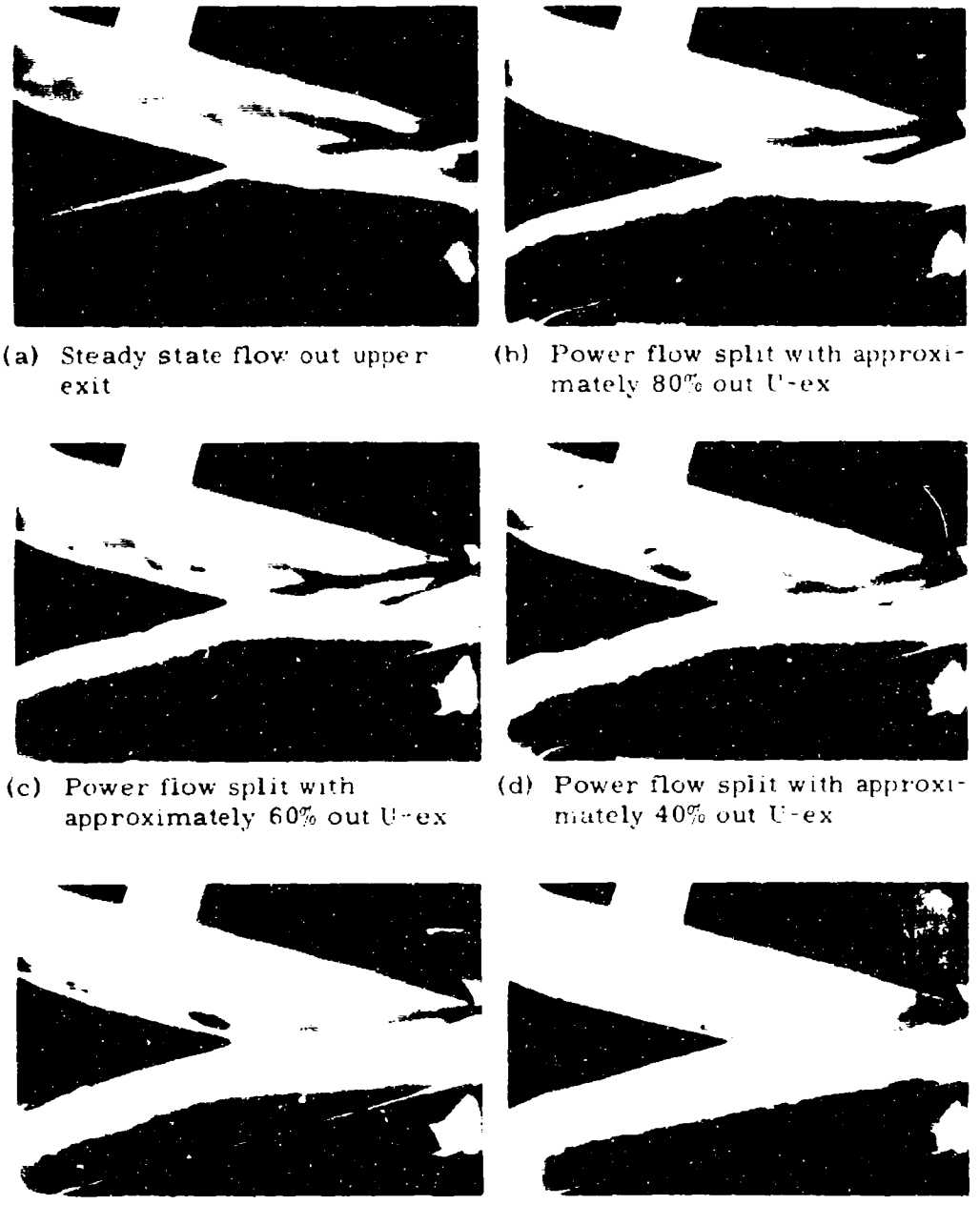

(a) Steady state flow out upper exit

(b) Power flow split with approximately 80% out U-ex

(c) Power flow split with approximately 60% out U-ex

(d) Power flow split with approximately 40% out U-ex

(e) Power flow split with approximately 20% out U-ex

(f) Steady state flow out bottom exit

Figure IV-17. Schlieren Photographs of Power Stream Switching. Power Fluid - Nitrogen, P_o = 1000 psig Oscillator Actuated Control Signal at 50 $\pm$ 5 cps.

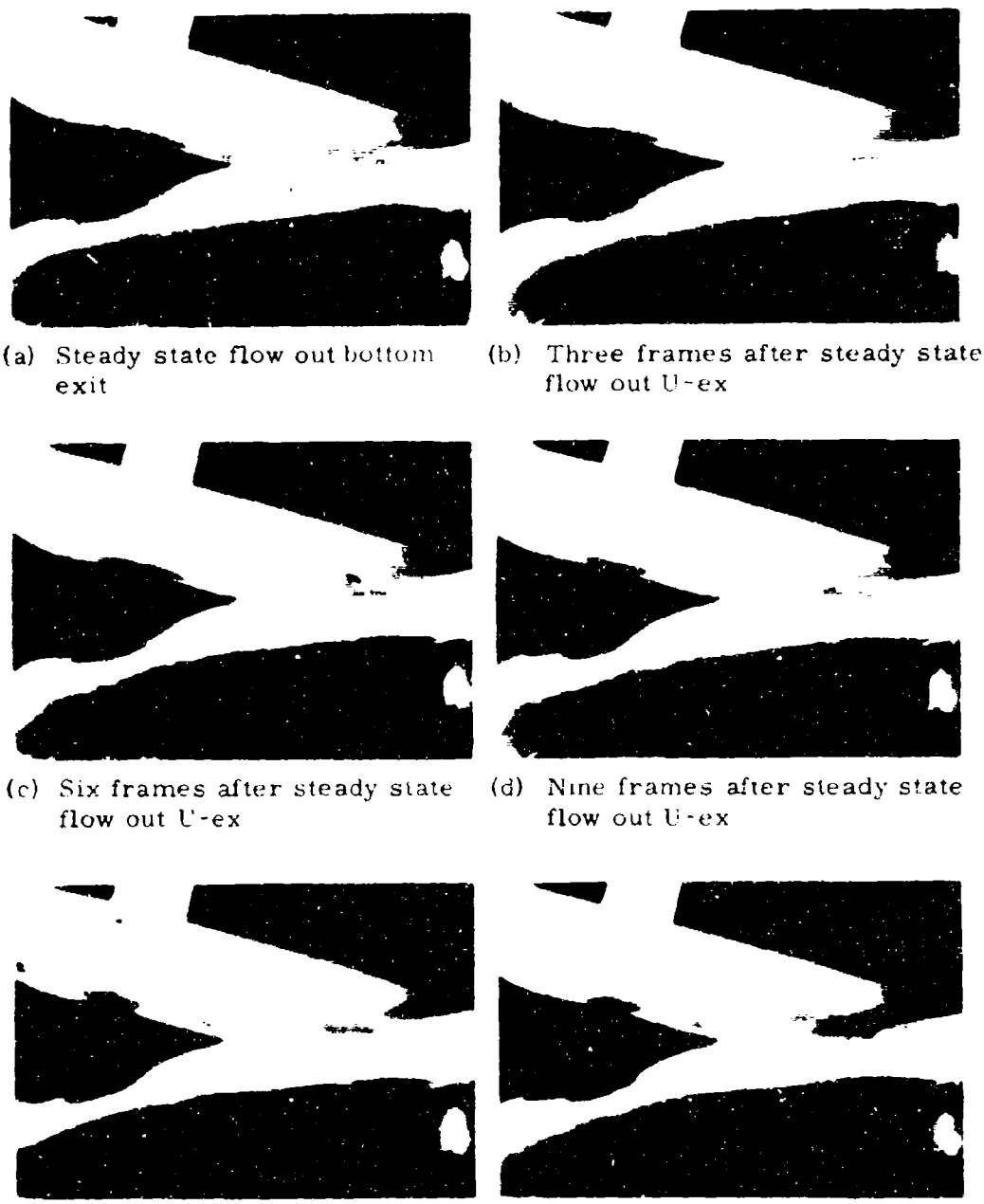

(a) Steady state flow out bottom exit

(b) Three frames after steady state flow out U-ex

(c) Six frames after steady state flow out U-ex

(d) Nine frames after steady state flow out U-ex

(e) Twelve frames after steady state flow out U-ex

(f) Steady state flow hanging on splitter

Figure IV-18. Schlieren Photographs of Power Stream Switching. Power Fluid - Nitrogen, P_o = 800 psig Oscillator Actuated Control Signal at 50 ± 5 cps.

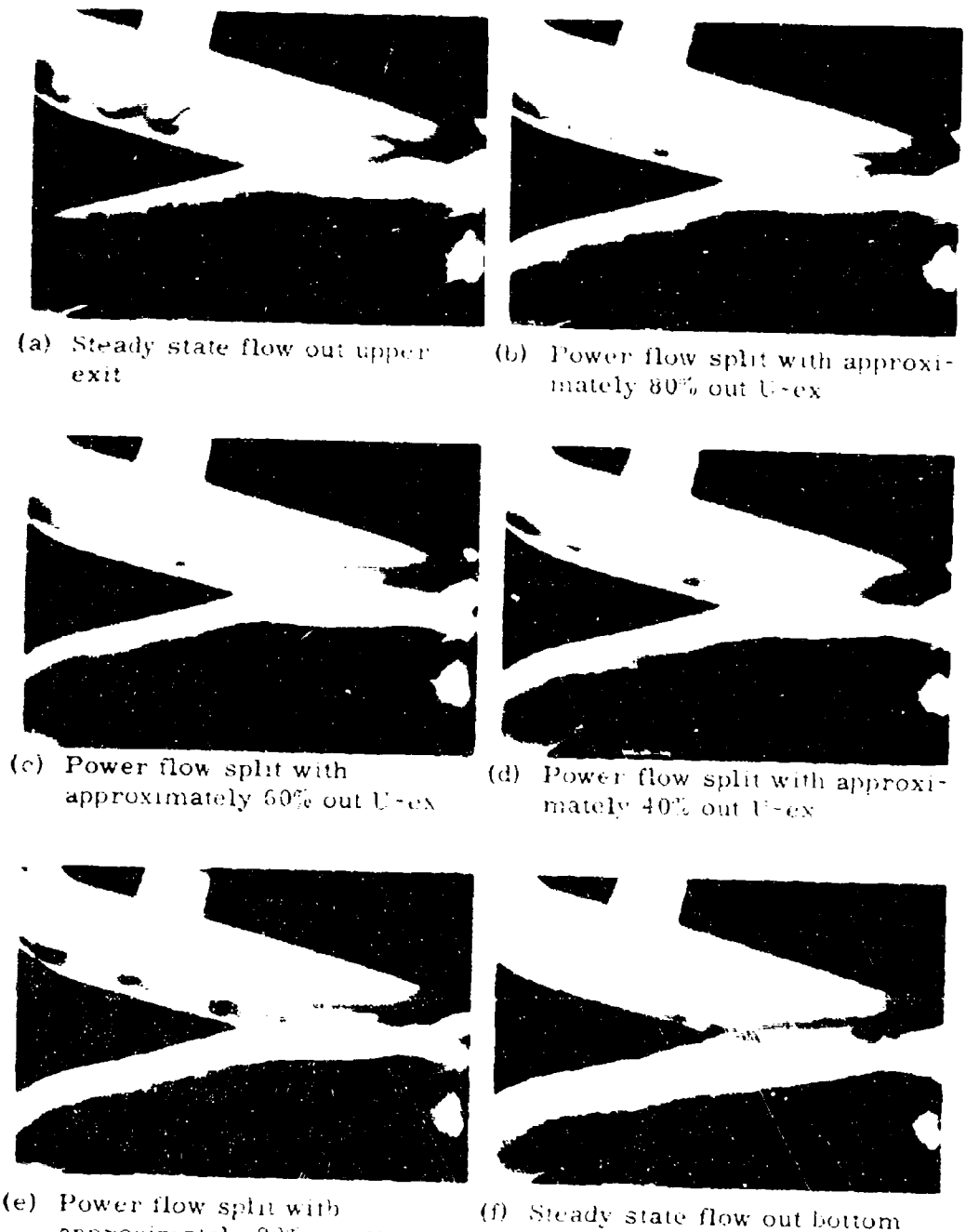

(a) Steady state flow out upper exit

(b) Power flow split with approximately 80% out U-ex

(c) Power flow split with approximately 60% out U-ex

(d) Power flow split with approximately 40% out U-ex

(e) Power flow split with approximately 20% out U-ex

(f) Steady state flow out bottom exit

Figure IV-19. Schlieren Photographs of Power Stream Switching. Power Fluid - Nitrogen, P_o = 600 psig Oscillator Actuated Control Signal at 50 ± 5 cps.

supply control fluid and the power stream leaves the amplifier from the lower exit channel.

Figure IV-20 shows the same negative switching phenomenon when solenoid valves actuate the control signal and P_o = 250 psig. Negative switching was not studied extensively but some of the characteristics of the power stream, when negative switching occurs, were noted and will be presented here. First, it is easy to see that the power stream does not fill the flow area at this chamber pressure. Second, when no control signal is supplied the flow splits between the upper and lower exits. Third, the power stream is just barely super sonic flowing past the splitter tip.

This negative control regime can be explained by considering Figure IV-21. Views (a) and (b) of Figure IV-21 illustrate the reduced size of the power jet in the control port region. Since the power flow does not fill the channel, the control fluid can flow around it. It is hypothesized that the control port serves as the critical throat of converging-diverging expanding flow. Thus when control flow enters as shown at C-c a high pressure region at B-c relative to C-c is produced because stagnation conditions in the control flow tend to exist on the side opposite the control inlet.

Figure IV-22 shows enlarged photographs from the film in which hydrazine was the power fluid, control flow was actuated by solenoid valves and P_o = 600 psig. As can be seen the power stream did not switch completely, and the lower control port is supplying the control

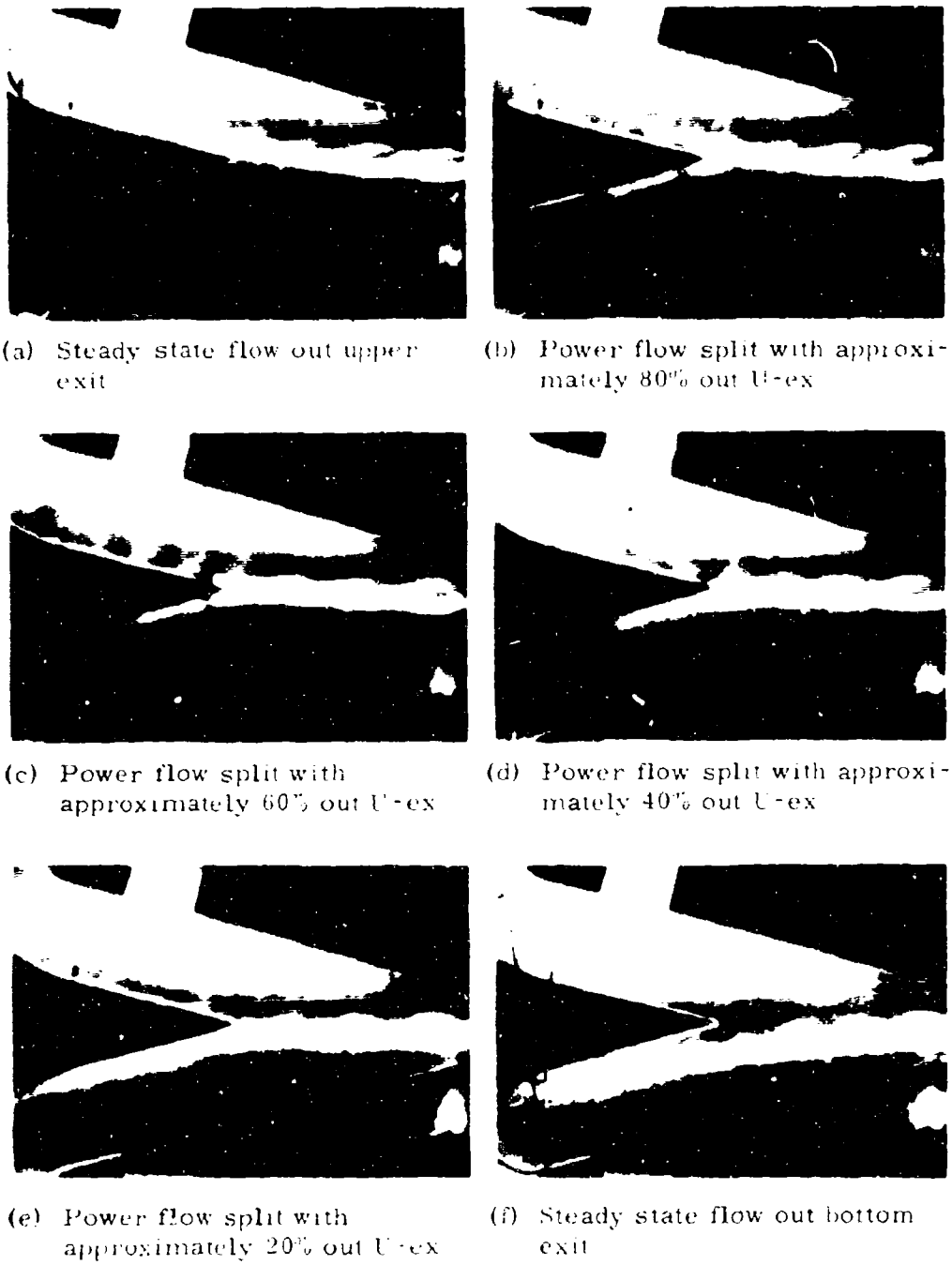

(a) Steady state flow out upper exit

(b) Power flow split with approximately 80% out U-ex

(c) Power flow split with approximately 60% out U-ex

(d) Power flow split with approximately 40% out U-ex

(e) Power flow split with approximately 20% out U-ex

(f) Steady state flow out bottom exit

Figure IV-20. Schlieren Photographs of Power Stream Switching Power Fluid - Nitrogen, P_o = 250 psig Solenoid Valves Actuated Control Signal.

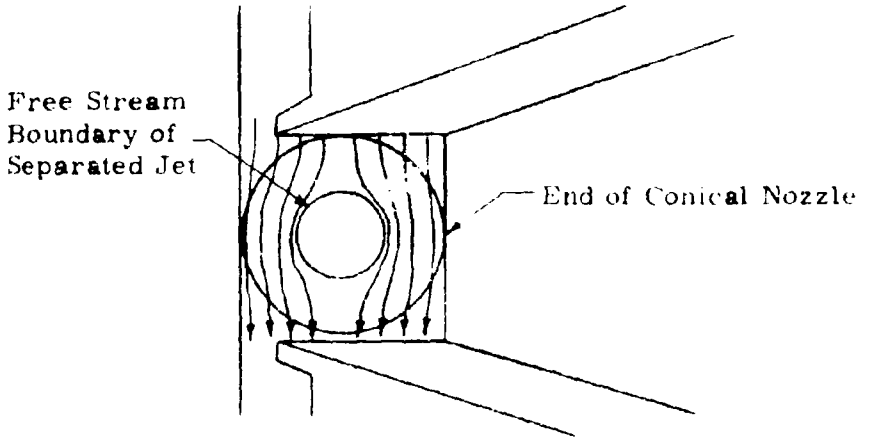

(a) Oblique View of Control Port Region

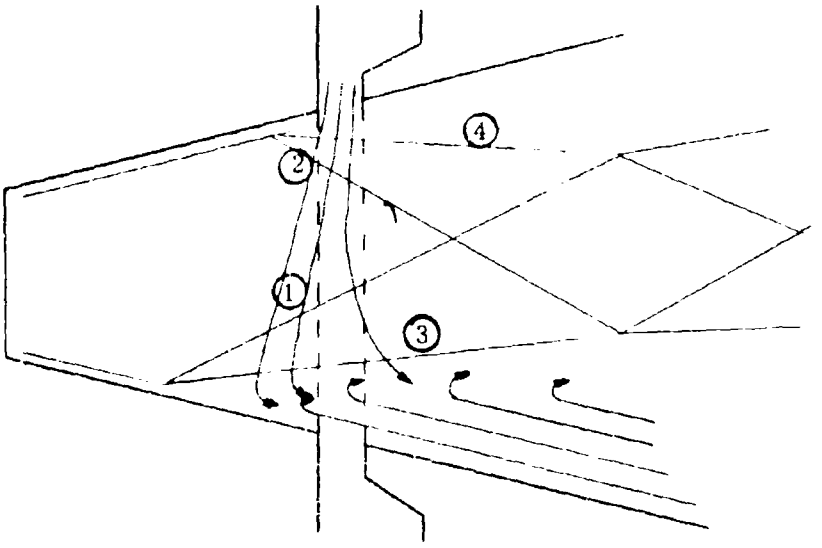

(b) Side View of Control Port Region

Figure IV-21. Flow Pattern of Control Gas in the Control Port Region

(a) Steady state flow out bottom exit

(b) Ten frames after steady state flow out B-ex

(c) Twenty frames after steady state flow out B-ex

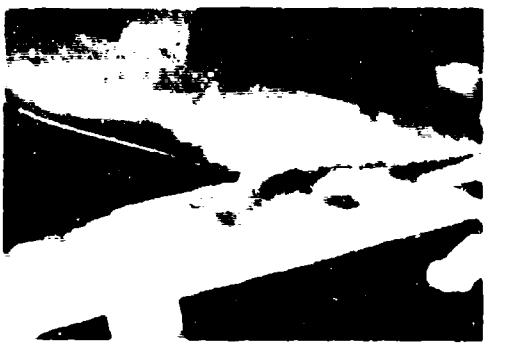

(d) Thirty frames after steady state flow out B-ex

(e) Forty frames after steady state flow out B-ex

(f) Steady state flow hanging on splitter

Figure IV-22. Schlieren Photographs of Power Stream Switching Power Fluid - Hydrazine, P_o = 600 psig Solenoid Valves Actuated Control Signal.

signal. These photographs were chosen for presentation here because they illustrate the best film clarity obtained when hydrazine was the power gas, and they also demonstrate the reduced clarity obtained because of external density currents and internal smudging of the glass side walls.

When the high speed schlieren film of the switching phenomenon is viewed using a motion picture projector, operating at 32 frames/second, it appears that the fluid stream rotates as a solid body for chamber pressures above 250 psig. This is not the case. The angle of the turning shocks changes smoothly with time. Thus the change of the flow directions of successive particles is smooth and should appear to have a wave shape during switching. Since the wave shape is not observed at high chamber pressures, and velocities are very high, it is reasonable to conclude that this is because the power fluid velocity is many times higher than the angular speed of the rotating shock. At the lower chamber pressures the apparent wave motion during switching is discernable. When the solenoid valves actuated the control signal, the wave motion was seen even at high chamber pressures because of the large dP_c/dt and consequent large rate of change of φ caused when the solenoid valves bounced off their seats during closing. This poor seating characteristic of the valves caused the large dP/dt, which resulted in the rapid change in φ with respect to time and the apparent wave motion.

Observing the high speed film of the switching, one also detects a momentary lag in the jet's rotation as it passes the splitter. This is probably due to the reverse flow from the atmosphere delaying the pressure reduction in the outlet channel to which the amplifier is to switch. As noted previously the power jet must be forced by the controlling signal into an asymmetrical shock and separation pattern such that the major portion of the flow is forced out the intended outlet channel. When this power flow begins to restrict the reverse atmospheric flow in the intended exit channel, the pressure falls in that channel and the deflecting shock's strength in the intended outlet channel decreases. Thus as the shock at the boundary to which the power stream is switching decreases in strength the power jet completes switching and a stable flow pattern is established, with or without the control signal.

At first glance it appears that there might be quite a difference between the mechanics of switching as a result of pressure forces and momentum forces. However, as stated previously in Section II, the important thing is to cause a disturbance and subsequent shock which deflects the flow. The deflecting mechanism in this case is an oblique shock. To establish the shock a minimum local pressure rise across the shock must be established. Whether one attributes the pressure downstream of the shock to the pressure or momentum of the signal is immaterial. Consider Bernoulli's one dimensional equation, $P + (1/2)(\rho v^2) = \text{Constant}$. The potential of the fluid before

flowing through the control port throat is primarily pressure. At, and immediately past the throat, this potential has changed primarily to kinetic potential. The control flow does not penetrate the power flow because the power flow acts like a rigid body when this type penetration is concerned. Thus when the control flow contacts the power flow, the control flow will be partially stagnated if the power stream fills the cross section and prevents flow around the power stream. This stagnation produces an effective local pressure rise which causes the shock and resulting direction of flow change. Thus pressure and momentum force switching are approximately the same when the control flow is directed normal to the power flow.

Due to the difficulty in evaluating some of the integrals of equation II-21, a lengthy numerical procedure will be required. At present a computer program is being written for an extremely simplified model to determine numerical switching times for different supply pressures, exhaust pressures and control pressures.

IV. CONCLUSIONS

An analysis has been developed which predicts the maximum P_o/P_f for which the power jet will flow out one exit. The analysis will be applicable to amplifiers which have similar geometries. The $(P_o/P_f)_{max}$ is corroborated by experimental data. The lower limit of P_o/P_f was also established by experiment.

For an amplifier with no geometrical bias and no control signals or restrictions applied to it, the power flow splits approximately evenly between the two exits even in the bistable flow regimes of supply pressures. Thus the flow separation and flow directing shocks are symmetrical since the flow splits evenly out the two exits.

Whenever all the power fluid flows out one exit then at some position in the amplifier the flow must separate from a model boundary. This separation is caused by the local pressure in that region, and the separation position can be predicted with the bistable analysis. Since all the power fluid flows out one exit and the flow is supersonic there must be an oblique shock which turns the flow. These separation shocks have been observed using the schlieren visualization technique.

The pressure ratio P_o/P_f determines the separation area ratio A_i/A_t and Mach Number M_i. If the power flow is to be stable and leave the model by one exit then different local ambient pressures must be maintained at the upper and lower flow boundaries. These

local ambient pressures establish shocks of different strengths which make it possible for the flow to be stable.

The filling of the exit flow channel to prevent unrestricted reverse flow from the atmosphere and thus cause a lower pressure in the intended exit channel is necessary for bistability. For the power flow to be bistable the flow channel in the control port region must also be sufficiently filled by the power jet to prevent control flow from the high to the low pressure region.

When the chamber pressure is 800 psig or less it is apparent from the high speed schlieren film that positive control is not achieved with the amplifier tested. For chamber pressures of 600 psig or less negative control effects are observed. The negative control phenomenon was not investigated closely. The reason that negative control occurs is very probably due to the separation of the power stream long before reaching the control port region. The separation and contraction of the power fluid allow the control signal to flow around the power jet, stagnate and create a higher pressure region at the opposite flow boundary. The higher pressure causes a stronger shock and the resulting negative control.

The separation area ratio A_i/A_t does not vary with the nozzle half angle α (2). Thus with the same expansion ratio and pressure ratio (P_o/P_f) and a larger nozzle half angle, the separation position will be closer to the nozzle exit. Therefore the fluid has less axial distance in which it can recompress and thereby decrease the diam-

eter of the stream. With the larger stream diameter the flow passage is more nearly filled and the control fluid has less space in which to flow around the power stream. It can also be seen that for a constant P_o/P_f the deflection angle of the free stream boundary is constant. Since the free stream boundary follows the model boundary approximately, if α is increased, some angle is reached for which the free stream boundary cannot be deflected into the desired outlet channel. Thus the half angle of expansion must be determined such that the free stream boundary can be deflected into the desired channel. For simple conical nozzles this fixes the angle α when the location of the splitter is fixed.

Extension of the range of chamber pressures which can be switched with the same amplifier and control signal would extend the usefulness of any amplifier. It is reasonable to assume that this can be accomplished by redirecting the control flow toward the nozzle throat. Consider Figures II-3 and IV-21. In the case of Figure II-3 the atmosphere effectively supplies the control flow that produces the bistable state. In switching the power stream to the second exit the control signal creates an initial temporary pressure. If the control signal were directed parallel to the model wall in a manner similar to the atmospheric reverse flow in Figure II-3 there would be less tendency for the control signal to flow around the power stream and the switching range would be extended to lower chamber pressures. Also at the higher chamber pressures the control signal

would be more effectively stagnated before being entrained by the power jet and swept downstream. Thus it is possible that both higher and lower values of chamber pressures may be controlled by directing the control signal input toward the power jet nozzle throat.

LIST OF REFERENCES

1. Ames Research Staff. 1953. Equations, Tables, and Charts for Compressible Flow. Report 1135. U. S. Government Printint Office. Washington 25, D. C.

2. Arens, M., Spiegler, E. March 1963. Shock Induced Boundary Layer Separation in Overexpanded Conical Exhaust Nozzles. Vol. 1. No. 3. AIAA Journal.

3. Bloomer, H. E., Antl, R. J., Renas, P. E. 1961. Experimental Study of Effects of Geometric Variables on Performance of Conical Rocket - Engine Exhaust Nozzles. Technical Note D-846. National Aeronautics and Space Administration.

4. Bogdonoff, S. M., Kepler, C. E. 1954. Separation of a Supersonic Turbulent Boundary Layer. pp. 414-424 J. Aeronaut Sci.

5. Broadwell, J. E. 1963. Analysis of the Fluid Mechanics of Secondary Injection for Thrust Vector Control. AIAA Journal.

6. Cerni, R. H., Foster, L. E. 1962. Instrumentation for Engineering Measurement. John Wiley and Sons, Inc., New York.

7. Duffy, R. E. 1965. Experimental Study of Nonequilibrium Expanding Flows. Vol. 3. No. 2. AIAA Journal.

8. Dunaway, J. C. 1965. Development of a Pure Fluid Missile Control System. U. S. Army Missile Command Report No. RG-TR-65-22.

9. Dunaway, J. D. 1965. The Development of a Hot Gas Reaction Control Valve for an Antitank Missile. U. S. Army Missile Command Report No. RG-TR-65-23.

10. Fraser, R. P., Eisenklam, P., Wilkie, D. 1959. Investigation of Supersonic Flow Separation in Nozzles. J. of Mech. Eng. Sci.

11. Foster, C. R. and Cowles, F. B. 1949. Experimental Study of Gas-Flow Separation in Overexpanded Exhaust Nozzles for Pocket Motors. Progress Report No. 4-103. Jet Propulsion Laboratory. Calif. Institute of Technology. California.

12. Gadd, G. E. 1953. Interactions Between Wholly Laminar or Wholly Turbulent Boundary Layers and Shock Waves Strong Enough to Cause Separation. pp. 729-739. J. Aeronaut. Sci.

13. Gadd, G. E., Holder, D. W., Regan, J. D. 1954. An Experimental Investigation of the Interaction Between Shock Waves and Boundary Layers. Proc. Roy. Soc. A226. 22-253. London.

14. Green, L. G. 1953. Flow Separation in Rocket Nozzles. Vol. 23. No. 81, pp. 34. J. American Rocket Soc.

15. Harry Diamond Laboratories. 1962. Proceedings of the Fluid Amplification Symposium. Vol. 1. Washington, D. C.

16. Holmes, A. B., Foxwell, J. E., Jr. May 1964. Supersonic Fluid Amplification With Various Expansion Ratio Nozzles. Vol. IV. Proceedings of Fluid Amplification Symposium.

17. Kalt, S., Badal, D. L. 1965. Conical Rocket Nozzle Performance Under Flow Separated Conditions. Vol. 2. No. 3. Spacecraft Journal. Engineering Notes.

18. Katz, S., Winston, E. T. 1964. The Response of A Bistable Fluid Amplifier to a Step Input. Proceedings of Fluid Amplification Symposium. Washington 25, D. C.

19. Keto, J. R. 1962. Flow Visualization - Compressible Fluids. TR-1041 Diamond Ordnance Fuze Laboratories. Department of the Army. Washington 25, D. C.

20. Liepmann, H. W., Roshko, A. 1957. Elements of Gasdynamics. John Wiley & Sons, Inc. New York.

21. Mager, A. 1956. On the Model of the Free, Shock-Separated, Turbulent Boundary Layer. Journal of Aeronautical Sciences.

22. McKenney, J. D. 1949. An Investigation of Flow Separation in an Overexpanded Supersonic Nozzle. Vol. 24. p. 320. Extract from Thesis at California Institute of Technology. Published as Appendix to Ref. 4. J. Amer. Rocket Soc.

23. Schardin, H. 1947. Toepler's Schlieren Method: Basic Principles for its Use and Quantitative Evaluation. Navy Department. David Taylor Model Basin. Washington, D. C.

24. Shapiro, A. H. 1953. The Dynamics and Thermodynamics of Compressible Fluid Flow. Vol. I. The Ronald Press Company. New York.

25. Shih, C. S. 1967. Flow Characteristics in a Supersonic Fluid Amplifier. The American Society of Mechanical Engineers. New York.

26. Summerfield, M. 1950. Fundamental Problems in Rocket Research. No. 81. J. Amer. Rocket Soc.

27. Summerfield, M., Foster, C. R., Swan, W. C. 1954. Flow Separation in Overexpanded Supersonic Exhaust Nozzles. Jet Propulsion 24. pp. 319-321.

28. Truitt, R. W. 1960. Fundamentals of Aerodynamics Heating. pp. 106. The Ronald Press Company. New York.

29. Warren, R. W. 1962. Some Parameters Affecting the Design of Bistable Fluid Amplifiers. ASME. Fluid Jet Control Devices. New York, N. Y.

30. Wood, O. L., Fox, H. L. November 1963. Fluid Computers. pp. 44-52. International Science and Technology.

31. Woodward, K., Mon, G., Joyce, J., Straub, H., Barilo, T. Four Fluid Amplifier Controlled Medical Devices. May 1964. Proceeding of the Fluid Amplification Symposium. Vol. IV. pp. 167-178. Washington, D. C.

32. Yalamanchili, J. 1966. Supersonic Fluid Amplifier Performance Characteristics. H neywell Document 6D-F502. Vol. A.

33. Yalamanchili, J. 1966. Flow Process in the Turbulent Mixing Region of a Supersonic Fluid Amplifier Using the Free Jet Analysis. Honeywell Document 6D-F-502. Vol. B.